Title
Novel Metabolites that Modulate Aging and Aging-related Symptoms

Author
Fu, Xudong

Publication Date
2017

Peer reviewed|Thesis/dissertation

UNIVERSITY OF CALIFORNIA

Los Angeles

Novel Metabolites that Modulate Aging and Aging-related Symptoms

A dissertation submitted in partial satisfaction of the

requirements for the degree Doctor of Philosophy

in Molecular and Medical Pharmacology

by

Xudong Fu

2017

ABSTRACT OF THE DISSERTATION

Novel Metabolites that Modulate Aging and Aging-related symptoms

by

Xudong Fu

Doctor of Philosophy in Molecular and Medical Pharmacology

University of California, Los Angeles, 2017

Professor Jing Huang, Chair

Aging is intimately related to health and disease. The incidence of major fatal pathological conditions, including cancer, is strongly associated with aging. The finding that aging is malleable by genetic or pharmacological perturbations has offered enormous hope for transforming our understanding and treatment of aging and age-related diseases. Yet few valid longevity drugs have been developed or translated for treating age-related diseases as target identification and a mechanistic understanding of their activity is largely missing.

Metabolism plays a pivotal role in aging. Metabolic interventions, such as dietary restriction, significantly modulate aging and aging-related symptoms. Recently, emerging evidences has shown that metabolites can directly modulate aging as well. Studies of these endogenous

“elixirs” provide insights on the biological regulatory networks acted upon by the metabolites as well as potential therapeutic interventions for aging and aging-related symptoms.

Our lab aims to discover novel longevity metabolites and explore their applications in aging-related symptoms. Here we present several novel longevity metabolites, which are α-ketoglutarate (α-KG), 2-hydroxyglutarate (2-HG), and α-ketobutyrate (α-KB). By combining target identification, epistasis, metabolomics, and bioenergetics analyses, we successfully uncover the molecular mechanisms of the longevity effects of these compounds. Specifically, we, for the first time, showed that α-KG and 2-HG extend lifespan of *C. elegans* by inhibiting ATP synthase and TOR, while α-KB delays aging through interruption of pyruvate oxidation and activation of AMPK. Interestingly, we discover an unexpected growth inhibitory effects of α-KG and 2-HG on tumor cells through targeting ATP synthase, and find that α-KG may confer beneficial effects for tumor treatment. In brief, our results identify novel potent longevity compounds and reveal their underlying mechanisms. More importantly, our work suggests a potential translational application of longevity metabolites in aging-related symptoms and provides novel directions for metabolic therapy.

The dissertation of Xudong Fu is approved.

Heather Christofk

Michael A. Teitell

Steven J. Bensinger

Steven M. Dubinett

Jing Huang, Committee Chair

University of California, Los Angeles

2017

To my family, for always standing in my back through good and bad times.

Table of Contents

LIST OF FIGURES AND TABLES

For Chapter 2 (reprint of previous publication):

ACKNOWLEDGEMENTS

First, I would like to thank my mentor, Jing Huang, for supporting and advising me during my Ph.D training. Join Jing Huang lab is one of the best decision I have made in these six years. Jing has given me tremendous support both in research and in my personal life. She is the most considerate, inspiring, and provocative mentor. She is the academic role model that inspires me to continue seek truth in my academia path. Without her help, I can never have achieved such a fruitful graduate training.

I would like to thank my committee members, Heather Christofk, Michael A. Teitell, Steven J. Bensinger, and Steven M. Dubinett. They have provided me the most helpful suggestions, abundant guidance, and expertise for my study. Their help greatly contributes to my research. I am also sincerely grateful for all the help and support from Heather Christofk and Michael A. Teitell with my postdoctoral position and fellowship application. In addition, I want to thank all the lab members from Jing Huang lab, including Randall M. Chin, Brett Lomenick, Heejun Hwang, Melody Pai, Chai Min, and Yin Xiang. They trained me scientific techniques, provided me support in my research, and sharing my joy and sorrow during my graduate training.

During my graduate training, I am very honored to receive finical support from China Scholarship Council scholarship and UCLA graduate division dissertation year fellowship.

Chapter 2 is a reprint of a previous publication published in *Nature* (Chin, R. M. *et al*. The metabolite alpha-ketoglutarate extends lifespan by inhibiting ATP synthase and TOR. *Nature*, doi:10.1038/nature13264 (2014)) that has been modified to meet the specifications in the UCLA graduate division thesis and dissertation formatting and filing guide. I would like to acknowledge contributions from the following co-authors: R. M. Chin, M.Y. Pai, L. Vergnes, H. Hwang, G. Deng, S. Diep, B. Lomenick, V.S. Meli, G.C. Monsalve, E. Hu, S.A. Whelan, J.X.

Wang, G. Jung, G.M. Solis, F. Fazlollahi, C. Kaweeteerawat, A. Quach, M. Nili, A.S. Krall, H.A. Godwin, H.R. Chang, K.F. Faull, F. Guo, M. Jiang, S.A. Trauger, A. Saghatelian, D. Braas, H.R. Christofk, C.F. Clarke, M.A. Teitell, M. Petrascheck, K. Reue, M.E. Jung, A.R. Frand, and J. Huang. J. Huang is the principle investigator of the work presented in Chapter 2; she provided ideas, helped design experiments and analyze result. J. Huang and R.M. Chin wrote the manuscript. As an author of this paper, I retain the copyrights to reprint and reuse without permission from *Nature*.

Chapter 3 is a reprint of a previous publication published in *Cell Metabolism* (Xudong F. *et al*. 2-Hydroxyglutarate Inhibits ATP Synthase and mTOR Signaling. *Cell metabolism.* 2015; 22: 508-515.) that has been modified to meet the specifications in the UCLA graduate division thesis and dissertation formatting and filing guide. I would like to acknowledge contributions from the following co-authors: R.M. Chin, L. Vergnes, H. Hwang, G. Deng, Y. Xing, M.Y. Pai, S. Li, L. Ta, F. Fazlollahi, C. Chen, R.M. Prins, M.A. Teitell, D.A. Nathanson, A. Lai, K.F. Faull, M. Jiang, S.G. Clarke, T.F. Cloughesy, T.G. Graeber, D. Braas, H.R. Christofk, M.E. Jung , K. Reue and J. Huang. J. Huang is the principle investigator of the work presented in Chapter 3; she provided ideas, helped design experiments and analyze results. J. Huang, X. Fu, and K. Reue wrote the manuscript. As an author of this paper, I retain the copyrights to reprint and reuse without permission from *Cell Metabolism*.

For the study in Chapter 4, I would like to acknowledge contribution from: M. Chai, B. Lomenick, H. Hwang, L. Vergnes, K. Reue, D. Brass, Z. Quan, S.J. Bensinger, N.H. Kim, M.A. Teitell, M. Jiang, A.S. Divakaruni, and J. Huang. M. Chai performed and analyze all the *C. elegans* experiment. B. Lomenick and H. Hwang performed the target identification assays. L. Vergenes and K. Reue contributed to mitochondrial respiration study design and analyses. D. Brass, Z. Quan, and S.J Bensinger contributed to metabolomics analyses. M. Chai, B. Lomenick, H. Hwang, L. Vergnes, K. Reue, D. Brass, Z. Quan, S.J. Bensinger, N.H. Kim, M.A.

Teitell, M. Jiang, A.S. Divakaruni, and J. Huang provided guidance, specialized reagents, and expertise. J. Huang is the principle investigator of the work presented in Chapter 4; she provided ideas, helped design experiments and analyze results. J. Huang, X. Fu, and M. Chai wrote the manuscript.

VITA

EDUCATION

07/2007-06/2011 B.S., Biological Sciences,
College of Life Sciences and Chu Kochen Honors College,
Zhejiang University, Hangzhou, China

PUBLICATIONS

RESEARCH PAPERS

Fu X, Chin RM, Vergnes L et al., 2-Hydroxyglutarate inhibits ATP synthase and mTOR signaling. *Cell metabolism*. 2015; 22: 508-515.

Chin RM, **Fu X**, Pai MY et al., The metabolite alpha-ketoglutarate extends lifespan by inhibiting the ATP synthase and TOR. *Nature*. 2014; 510: 397-401.

Feng J, Gong D, **Fu X** et al., M1 of Murine Gamma-Herpesvirus 68 Induces Endoplasmic Reticulum Chaperone Production. *Scientific Reports*. 2015; 5:17228.

PATENTS AND PATENT APPLICATIONS

Jing Huang, Randall Chin, Simon Diep, Melody Y. Pai, Brett E. Lomenick, **Xudong Fu**, Karen Reue, Laurent Vergnes, Michael E. Jung, Gang Deng, Heejun Hwang, Meisheng Jiang. “Compositions and Methods for Treating Aging and Age Related Diseases and Symptoms.” PCT/US2015/015304, filed February 11, 2015.

Jing Huang, Randall Chin, **Xudong Fu**, Heejun Hwang, Karen Reue, Laurent Vergnes, Meisheng Jiang, Brett E. Lomenick, Xiang Yin, Mansoureh Eghbali, Jingyuan Li, Samuel Wheeler French, Ronik Khachatoorian. “Compounds and Compositions for Treating

Age-Related Symptoms and Diseases." International Application No. PCT/US2015/038227, filed June 29, 2015.

AWARDS AND HONORS

2016	UCLA Dissertation Year Fellowship
2011-2015	China Scholarship Council Scholarship
2014	Speaker, International TSC-LAM Research Conference
2014	Department of Molecular and Medical Pharmacology Travel Award
2014	International TSC-LAM Research Conference Travel Award
2007-2010	First Prize Academic Scholarship, Zhejiang University
2010	Excellent Student Leadership Prize, Zhejiang University
2010	Cross-disciplinary Scholars in Science and Technology Fellowship, UCLA
2010	Chinese Academy of Sciences Scholarship

PRESENTATIONS

Talks

Fu X, Huang J, Endogenous regulators of aging pathways to longevity. Invited talk for 2014 International TSC-LAM Research Conference, October 10-13 2014, Beijing, China

Fu X, Growth inhibitory effects of the oncometabolite 2-hydroxyglutarate by modulation of mitochondrial energy metabolism. Invited talk for Metabolism Interest Group, November 9 2015, UCLA

Posters

Fu X, Chin, RM, Hwang H et al., Growth inhibitory effects of the oncometabolite 2-HG by modulation of mitochondrial energy metabolism. “Multifaceted Mitochondria” Conference, 19-21 July 2015, Chicago, IL, USA

Fu X, Chin RM, Hwang H et al., TOR-modulating metabolites and their mechanisms in aging and TOR-related disease models. 2014 International TSC-LAM Research Conference, October 10-13 2014, Beijing, China

Fu X, Chin RM, Hwang H et al., Novel dietary restriction-related TOR modulation by metabolites. 2014 International TSC-LAM Research Conference, October 10-13 2014, Beijing, China

CHAPTER 1

Introduction

Long considered an inevitable process of living, aging is characterized as the progressive decline in physiological integrity. The hallmarks of aging include genome instability, loss of proteostasis, dysregulation of metabolism, and mitochondrial malfunction[1]. Aging is intimately linked to health. According to the WHO report, the occurrence of major fatal pathological conditions, including cancer, diabetes, and neuronal degeneration, is strongly associated with aging[2]. Therefore, aging research is important to not only reveal molecular basis of aging, but also provide insights on interventions for aging-related symptoms.

Aging studies exploit the short lifespan of animal models, such as *Caenorhabditis elegans* (*C. elegans)* and *Drosophila*. Similar to other biological processes, aging is tightly controlled by intrinsic signaling, transcription factors, and metabolism[3]. Highly conserved pathways, including the insulin/insulin like growth factor (IGF1) pathway, the target of rapamycin (TOR), and AMP kinase (AMPK) pathways, have been identified as crucial aging mediators[3,4]. These and most other aging-related pathways are involved in nutrition sensing or stress response, and are intimately connected to metabolism. Modulation of these pathways can shift the organisms from a growth and proliferative state to a self-maintenance status, protecting the organisms from environmental stresses, and increasing their lifespan.

Metabolism plays a vital role in aging. In 1993, Cynthia Kenyon *et al.* identified the first metabolic aging-modulatory pathway, the Insulin/IGF-1 pathway[5]. This finding sparked, an

intense interest in aging, and subsequently led to the identification of an increasing number of aging-related metabolic pathways. Additionally, many reports have shown that endogenous small molecules can also modulate aging via metabolism and/or signaling. For instance, the TOR pathway is a sensor for macronutrients, and several studies have shown that metabolites can modulate aging through direct or indirect regulation of TOR[6-8]. Studies focusing on metabolites and aging have provided novel insights of aging mechanisms, and have open a new avenue for aging interventions. With the ongoing studies of metabolism and aging, additional endogenous regulators of longevity will be discovered.

TOR and dietary restriction (DR)

TOR is a pivotal nutrition sensor that is directly regulated by cellular energy status, amino acid levels, mitogens, and the insulin/IGF-1 pathway[9]. Downregulation of TOR signaling changes the organism from growth promotion into a self-maintenance state through inhibition of protein translation and activation autophagy. In *C. elegans*, TOR signaling modulates lifespan in a manner dependent on the transcription factor PHA-4/FOXA. More specifically, PHA-4/FOXA is activated upon inhibition of TOR, and this activation induces autophagy and extends lifespan[10]. Interestingly, TOR itself can also negatively regulate autophagy through ULK-1 phosphorylation[11]. On the other hand, the TOR signaling activate protein synthesis through phosphorylation of S6K and 4E-BP1. In worms, flies, and mice, the anti-aging effect of TOR pathway inhibition requires S6K or 4E-BP1[3,12-14].

Dietary restriction (DR) regulates lifespan across many diverse species, spanning from yeast to primates[15]. Although multiple pathways contribute to the DR-induced lifespan extension, TOR is the most validated signaling pathway involved in dietary restriction-mediated longevity. Indeed, chronic shortage of food regulates aging through TOR inhibition in *C. elegans*, *Drosophila*, and mice[4]. Pharmacological inhibition of TOR is an accepted strategy for disease therapy as well as for aging intervention. Inhibition of TOR by rapamycin can extend

lifespan in mice[7]. Metabolites, such as branch chain amino acids and Δ7-dafachronic acid, which regulate TOR signaling, modulate lifespan as well[8,16]. These results support the inhibition of TOR is a potential strategy for aging intervention.

Mitochondria

Mitochondria are the crucial organelle for energy metabolism. It is therefore intuitive to assume that mitochondria biogenesis would be beneficial for longevity. Indeed, mitochondrial function decreases with age[17] and increases of mitochondria biogenesis and respiration are associated with lifespan extension[18,19].

Interestingly, mild interruption of the mitochondrial electron transport chain (ETC), has also been shown to extend lifespan in yeast, worms, flies, and mice[20-22]. However, the detailed mechanism of mitochondrial interruption induced lifespan is not fully understood.

One proposed model for mitochondrial interruption induced lifespan extension involves is reactive oxygen species(ROS) and hormesis. Hormesis refers to an adaptive induction of responsive and repair mechanisms in an organism upon mild exposure to toxins or stresses[23]. It has been reported that mild oxidative stress, induced by perturbations on electron transport chain, can extend the lifespan of *C. elegans*[24].

Recently, the mitochondrial unfolded protein response (UPR^{mt}) has also been proposed to play a crucial role in the extension of lifespan by ETC inhibition[25,26]. The UPR^{mt} is a stress response machinery which responds to mitochondrial proteostasis imbalance[27]. A stoichiometric imbalance between the levels of nuclear-encoded and mitochondrial-encoded mitochondrial proteins activates the UPR^{mt} [25]. The UPR^{mt} has been shown to be activated by RNAi knockdown of certain ETC genes, but whether the UPR^{mt} serves as a unifying mechanism for the lifespan extension by ETC interruption, especially by pharmacological inhibition of the ETC, is debatable[25,26,28].

Insulin/IGF-1 pathway

The Insulin/IGF-1 pathway is highly conserved across metazoans and serves as a central pathway to regulate glycaemia. Insulin/IGF-1 receptors transduce the signaling from insulin/IGF-1 to downstream kinases, including phosphatidylinositol 3-kinase (PI3K) and AKT, and prevent the transcription factor FOXO/DAF-16 from being translocated to nucleus, thereby inhibiting the transcription of target genes[29]. The Insulin/IGF-1 pathway was the very first metabolic pathway to be g reported as an aging mediator. Specific *daf-2* (the homologue of insulin and IGF-1 receptor in *C. elegans*) mutations were found to double the lifespan of *C. elegans*[5]. Consistently, activation of the Insulin/IGF-1 pathway inhibitor, PTEN/DAF-18, extends the lifespan of *C. elegans*[30]. Downregulation of the Insulin/IGF-1 pathway leads to the induction of FOXO/DAF-16, which activates the transcription of stress-response genes such as catalases, glutathione S-transferases, as well as genes encoding chaperones, apolipoproteins, and lipases[4]. The activation of these “maintenance genes” contributes to the anti-aging effects arising from the inhibition of Insulin/IGF-1 signaling. Other than FOXO/DAF-16, the transcription factor heat-shock factor-1 (HSF-1) and Nrf2/SKN-1 (an Nrf-like xenobiotic-response factor) are also involved in the Insulin/IGF-1-mediated longevity. HSF-1 and SKN-1 can each activate the transcription of heat-stress response machineries and oxidative-stress responsive machineries respectively[31,32], protecting the organism from stress-induced damage, and extending its lifespan.

Glucose is the primary energy source for multiple organisms. In yeast, glucose deprivation may confer benefits on lifespan[33]. Similarly, in *C. elegans* and in humans, high glucose accelerates aging and jeopardizes health. High glycemic index (GI) food may cause diabetes, obesity, and cardiovascular diseases potentially through activation of the insulin/IGF-1 pathway[34]. Lee and colleagues have reported that glucose treatment shortens the lifespan of *C. elegans* by activating insulin pathway[35]. This report is theoretically consistent with the studies on high GI food. It is therefore plausible that a diet with low GI food can confer beneficial effects

on human health. It is also likely that the effects may be modified by genetics, depending on both the individual's genotype and epigenetics.

AMPK

AMPK is a nutrient sensor that tis regulated by the endogenous AMP/ATP ratio. It serves as a switch for catabolism and anabolism through its regulation of multiple cellular proteins/pathways including TOR, ULK1, and ACC1[36]. It has been shown that in *C. elegans*, AAK-2 (homologue of AMPK in *C. elegans*) overexpression is sufficient to extend lifespan. AAK-2/AMPK also serves as an upstream regulator of DAF-16[37]. Metformin, a well-known AMPK activator, has been reported to extend lifespan in mice[38]. Consistently, Weimer and colleagues reported that an endogenous glycolysis inhibitor, glucosamine, can extend the lifespan of *C. elegans* in an AMPK- and ROS-dependent manner[39]. In addition, this study found that Nrf2/SKN-1 is a downstream mediator of AMPK. Humans can tolerate high dose of glucosamine. In fact, glucosamine has been widely used as a health supplement. Together these raise the possibility of utilizing glucosamine as a potential aging intervention in humans.

Current evidence clearly indicates that specific metabolites can serve as aging regulator. However, research in this area is exceptional challenging, and there is likely much more to discover regarding metabolic regulation of aging. First, metabolites are endogenous small molecules that typically interact with multiple targets, and many of these interactions remain to be discovered. Identification of the protein-metabolite interaction networks of these longevity metabolites is a crucial yet difficult undertaking that will be necessary to uncover the vast molecular mechanisms by which they are able to affect longevity. Secondly, metabolites are easily transformed to other small molecules through enzymatic reactions, making it imperative to validate whether the longevity effects are directly induced by a given metabolites itself or via a secondary metabolic effect. Finally, the biological significance of these anti-aging metabolites needs to be considered as the functions of metabolites have been shaped by evolution. It is

possible that the longevity effects of metabolites represent an unappreciated endogenous machinery that defends against aging-promoting factors to help maintain the long-term health of the organism.

In this dissertation, I present the identification of several novel longevity metabolites, including alpha-ketoglutarate (α-KG)[6], 2-hydroxyglutartae (2-HG)[40], and alpha-ketobutyrate (α-KB). We used a label-free drug-target identification strategy[41] to identify the functional targets of these anti-aging metabolites. We further combined metabolomics, epistasis, and bioenergetics analyses to validate these targets and determine the anti-aging molecular mechanisms of each compound. Finally, we explored the roles that these anti-aging compounds play in aging-related symptoms, including cancer and neurodegeneration, and present the potential application of longevity metabolites for the prevention and treatment of aging-related symptoms.

References

1 Lopez-Otin, C., Blasco, M. A., Partridge, L., Serrano, M. & Kroemer, G. The hallmarks of aging. *Cell* **153**, 1194-1217, doi:10.1016/j.cell.2013.05.039 (2013).

2 de Cabo, R., Carmona-Gutierrez, D., Bernier, M., Hall, M. N. & Madeo, F. The search for antiaging interventions: from elixirs to fasting regimens. *Cell* **157**, 1515-1526, doi:10.1016/j.cell.2014.05.031 (2014).

3 Lapierre, L. R. & Hansen, M. Lessons from C. elegans: signaling pathways for longevity. *Trends Endocrinol Metab* **23**, 637-644, doi:10.1016/j.tem.2012.07.007 (2012).

4 Kenyon, C. J. The genetics of ageing. *Nature* **464**, 504-512, doi:10.1038/nature08980 (2010).

5 Kenyon, C., Chang, J., Gensch, E., Rudner, A. & Tabtiang, R. A C-Elegans Mutant That Lives Twice as Long as Wild-Type. *Nature* **366**, 461-464, doi:DOI 10.1038/366461a0 (1993).

6 Chin, R. M. *et al.* The metabolite alpha-ketoglutarate extends lifespan by inhibiting ATP synthase and TOR. *Nature* **510**, 397-401, doi:10.1038/nature13264 (2014).

7 Harrison, D. E. *et al.* Rapamycin fed late in life extends lifespan in genetically heterogeneous mice. *Nature* **460**, 392-395, doi:10.1038/nature08221 (2009).

8 Thondamal, M., Witting, M., Schmitt-Kopplin, P. & Aguilaniu, H. Steroid hormone signalling links reproduction to lifespan in dietary-restricted Caenorhabditis elegans. *Nat Commun* **5**, 4879, doi:10.1038/ncomms5879 (2014).

9 Wullschleger, S., Loewith, R. & Hall, M. N. TOR signaling in growth and metabolism. *Cell* **124**, 471-484, doi:10.1016/j.cell.2006.01.016 (2006).

10 Vellai, T. *et al.* Genetics: influence of TOR kinase on lifespan in C. elegans. *Nature* **426**, 620, doi:10.1038/426620a (2003).

11 Kim, J., Kundu, M., Viollet, B. & Guan, K. L. AMPK and mTOR regulate autophagy through direct phosphorylation of Ulk1. *Nat Cell Biol* **13**, 132-141, doi:10.1038/ncb2152 (2011).

12 Bonawitz, N. D., Chatenay-Lapointe, M., Pan, Y. & Shadel, G. S. Reduced TOR signaling extends chronological life span via increased respiration and upregulation of mitochondrial gene expression. *Cell Metab* **5**, 265-277, doi:10.1016/j.cmet.2007.02.009 (2007).

13 Kapahi, P. & Vijg, J. Aging--lost in translation? *N Engl J Med* **361**, 2669-2670, doi:10.1056/NEJMcibr0909815 (2009).

14 Hansen, M. *et al.* Lifespan extension by conditions that inhibit translation in Caenorhabditis elegans. *Aging Cell* **6**, 95-110, doi:10.1111/j.1474-9726.2006.00267.x (2007).

15 Mair, W. & Dillin, A. Aging and survival: the genetics of life span extension by dietary restriction. *Annu Rev Biochem* **77**, 727-754, doi:10.1146/annurev.biochem.77.061206.171059 (2008).

16 Solon-Biet, S. M. *et al.* The ratio of macronutrients, not caloric intake, dictates cardiometabolic health, aging, and longevity in ad libitum-fed mice. *Cell Metab* **19**, 418-430, doi:10.1016/j.cmet.2014.02.009 (2014).

17 Lin, M. T. & Beal, M. F. Mitochondrial dysfunction and oxidative stress in neurodegenerative diseases. *Nature* **443**, 787-795, doi:10.1038/nature05292 (2006).

18 Guarente, L. Mitochondria--a nexus for aging, calorie restriction, and sirtuins? *Cell* **132**, 171-176, doi:10.1016/j.cell.2008.01.007 (2008).

19 Civitarese, A. E. *et al.* Calorie restriction increases muscle mitochondrial biogenesis in healthy humans. *PLoS Med* **4**, e76, doi:10.1371/journal.pmed.0040076 (2007).

20 Liu, X. *et al.* Evolutionary conservation of the clk-1-dependent mechanism of longevity: loss of mclk1 increases cellular fitness and lifespan in mice. *Genes Dev* **19**, 2424-2434, doi:10.1101/gad.1352905 (2005).

21 Copeland, J. M. *et al.* Extension of Drosophila life span by RNAi of the mitochondrial respiratory chain. *Curr Biol* **19**, 1591-1598, doi:10.1016/j.cub.2009.08.016 (2009).

22 Kirchman, P. A., Kim, S., Lai, C. Y. & Jazwinski, S. M. Interorganelle signaling is a determinant of longevity in Saccharomyces cerevisiae. *Genetics* **152**, 179-190 (1999).

23 Calabrese, E. J., McCarthy, M. E. & Kenyon, E. The occurrence of chemically induced hormesis. *Health Phys* **52**, 531-541 (1987).

24 Lee, S. J., Hwang, A. B. & Kenyon, C. Inhibition of respiration extends C. elegans life span via reactive oxygen species that increase HIF-1 activity. *Curr Biol* **20**, 2131-2136, doi:10.1016/j.cub.2010.10.057 (2010).

25 Houtkooper, R. H. *et al.* Mitonuclear protein imbalance as a conserved longevity mechanism. *Nature* **497**, 451-457, doi:10.1038/nature12188 (2013).

26 Durieux, J., Wolff, S. & Dillin, A. The cell-non-autonomous nature of electron transport chain-mediated longevity. *Cell* **144**, 79-91, doi:10.1016/j.cell.2010.12.016 (2011).

27 Yoneda, T. *et al.* Compartment-specific perturbation of protein handling activates genes encoding mitochondrial chaperones. *J Cell Sci* **117**, 4055-4066, doi:10.1242/jcs.01275 (2004).

28 Bennett, C. F. *et al.* Activation of the mitochondrial unfolded protein response does not predict longevity in Caenorhabditis elegans. *Nature Communications* **5**, doi:ARTN 348310.1038/ncomms4483 (2014).

29 Wolff, S. & Dillin, A. The trifecta of aging in Caenorhabditis elegans. *Exp Gerontol* **41**, 894-903, doi:10.1016/j.exger.2006.06.054 (2006).

30 Mihaylova, V. T., Borland, C. Z., Manjarrez, L., Stern, M. J. & Sun, H. The PTEN tumor suppressor homolog in Caenorhabditis elegans regulates longevity and dauer formation in an insulin receptor-like signaling pathway. *P Natl Acad Sci USA* **96**, 7427-7432, doi:DOI 10.1073/pnas.96.13.7427 (1999).

31 Tullet, J. M. A. *et al.* Direct inhibition of the longevity-promoting factor SKN-1 by insulin-like signaling in C. elegans. *Cell* **132**, 1025-1038, doi:10.1016/j.cell.2008.01.030 (2008).

32 Hsu, A. L., Murphy, C. T. & Kenyon, C. Regulation of aging and age-related disease by DAF-16 and heat-shock factor. *Science* **300**, 1142-1145, doi:DOI 10.1126/science.1083701 (2003).

33 Orlandi, I., Ronzulli, R., Casatta, N. & Vai, M. Ethanol and Acetate Acting as Carbon/Energy Sources Negatively Affect Yeast Chronological Aging. *Oxid Med Cell Longev*, doi:Unsp 80287010.1155/2013/802870 (2013).

34 Aston, L. M. Glycaemic index and metabolic disease risk. *P Nutr Soc* **65**, 125-134, doi:10.1079/Pns2005485 (2006).

35 Lee, S. J., Murphy, C. T. & Kenyon, C. Glucose Shortens the Life Span of C. elegans by Downregulating DAF-16/FOXO Activity and Aquaporin Gene Expression. *Cell Metabolism* **10**, 379-391, doi:10.1016/j.cmet.2009.10.003 (2009).

36 Hardie, D. G., Ross, F. A. & Hawley, S. A. AMPK: a nutrient and energy sensor that maintains energy homeostasis. *Nat Rev Mol Cell Bio* **13**, 251-262, doi:10.1038/nrm3311 (2012).

37 Greer, E. L., Banko, M. R. & Brunet, A. AMP-activated Protein Kinase and FoxO Transcription Factors in Dietary Restriction-induced Longevity. *Ann Ny Acad Sci* **1170**, 688-692, doi:10.1111/j.1749-6632.2009.04019.x (2009).

38 Martin-Montalvo, A. *et al.* Metformin improves healthspan and lifespan in mice. *Nature Communications* **4**, doi:ARTN 219210.1038/ncomms3192 (2013).

39 Weimer, S. *et al.* D-Glucosamine supplementation extends life span of nematodes and of ageing mice. *Nature Communications* **5**, doi:ARTN 356310.1038/ncomms4563 (2014).

40 Fu, X. *et al.* 2-Hydroxyglutarate Inhibits ATP Synthase and mTOR Signaling. *Cell Metab* **22**, 508-515, doi:10.1016/j.cmet.2015.06.009 (2015).

41 Lomenick, B. *et al.* Target identification using drug affinity responsive target stability (DARTS). *P Natl Acad Sci USA* **106**, 21984-21989, doi:10.1073/pnas.0910040106 (2009).

CHAPTER 2

The Metabolite Alpha-Ketoglutarate Extends Lifespan by Inhibiting ATP Synthase and TOR

(A reprint of “The metabolite α-ketoglutarate extends lifespan by inhibiting ATP synthase and TOR,” which was previously published in Nature (doi:10.1038/nature13264), is provided here as Chapter 2)

LETTER

doi:10.1038/nature13264

The metabolite α-ketoglutarate extends lifespan by inhibiting ATP synthase and TOR

Randall M. Chin[1], Xudong Fu[2], Melody Y. Pai[1]*, Laurent Vergnes[3]*, Heejun Hwang[2]*, Gang Deng[4], Simon Diep[2], Brett Lomenick[2], Vijaykumar S. Meli[5], Gabriela C. Monsalve[5], Eileen Hu[2], Stephen A. Whelan[6], Jennifer X. Wang[7], Gwanghyun Jung[2], Gregory M. Solis[8], Farbod Fazlollahi[9], Chitrada Kaweeteerawat[10], Austin Quach[2], Mahta Nili[11], Abby S. Krall[2], Hilary A. Godwin[10], Helena R. Chang[6], Kym F. Faull[9], Feng Guo[5], Meisheng Jiang[2], Sunia A. Trauger[7], Alan Saghatelian[12], Daniel Braas[2,13], Heather R. Christofk[2,13], Catherine F. Clarke[1,4], Michael A. Teitell[1,11], Michael Petrascheck[8], Karen Reue[1,3], Michael E. Jung[1,4], Alison R. Frand[5] & Jing Huang[1,2]

Metabolism and ageing are intimately linked. Compared with *ad libitum* feeding, dietary restriction consistently extends lifespan and delays age-related diseases in evolutionarily diverse organisms[1,2]. Similar conditions of nutrient limitation and genetic or pharmacological perturbations of nutrient or energy metabolism also have longevity benefits[3,4]. Recently, several metabolites have been identified that modulate ageing[5,6]; however, the molecular mechanisms underlying this are largely undefined. Here we show that α-ketoglutarate (α-KG), a tricarboxylic acid cycle intermediate, extends the lifespan of adult *Caenorhabditis elegans*. ATP synthase subunit β is identified as a novel binding protein of α-KG using a small-molecule target identification strategy termed drug affinity responsive target stability (DARTS)[7]. The ATP synthase, also known as complex V of the mitochondrial electron transport chain, is the main cellular energy-generating machinery and is highly conserved throughout evolution[8,9]. Although complete loss of mitochondrial function is detrimental, partial suppression of the electron transport chain has been shown to extend *C. elegans* lifespan[10–13]. We show that α-KG inhibits ATP synthase and, similar to ATP synthase knockdown, inhibition by α-KG leads to reduced ATP content, decreased oxygen consumption, and increased autophagy in both *C. elegans* and mammalian cells. We provide evidence that the lifespan increase by α-KG requires ATP synthase subunit β and is dependent on target of rapamycin (TOR) downstream. Endogenous α-KG levels are increased on starvation and α-KG does not extend the lifespan of dietary-restricted animals, indicating that α-KG is a key metabolite that mediates longevity by dietary restriction. Our analyses uncover new molecular links between a common metabolite, a universal cellular energy generator and dietary restriction in the regulation of organismal lifespan, thus suggesting new strategies for the prevention and treatment of ageing and age-related diseases.

To gain insight into the regulation of ageing by endogenous small molecules, we screened normal metabolites and aberrant disease-associated metabolites for their effects on adult lifespan using the *C. elegans* model. We discovered that the tricarboxylic acid (TCA) cycle intermediate α-KG (but not isocitrate or citrate) delays ageing and extends the lifespan of *C. elegans* by ~50% (Fig. 1a and Extended Data Fig. 1a). In the cell, α-KG (or 2-oxoglutarate; Fig. 1b) is produced from isocitrate by oxidative decarboxylation catalysed by isocitrate dehydrogenase (IDH). α-KG can also be produced anaplerotically from glutamate by oxidative deamination using glutamate dehydrogenase, and as a product of pyridoxal phosphate-dependent transamination reactions in which glutamate is a common amino donor. α-KG extended the lifespan of wild-type N2 worms in a concentration-dependent manner, with 8 mM α-KG producing the maximal lifespan extension (Fig. 1c); 8 mM was the concentration used in all subsequent *C. elegans* experiments. There is a ~50% increase in α-KG concentration in worms on 8 mM α-KG plates compared with those on vehicle plates (Extended Data Fig. 1b), or ~160 μM versus ~110 μM assuming homogenous distribution (Methods). α-KG not only extends lifespan, but also delays age-related phenotypes, such as the decline in rapid, coordinated body movement (Supplementary Videos 1 and 2). α-KG supplementation in the adult stage is sufficient for longevity (Extended Data Fig. 1c).

The dilution or killing of the *C. elegans* bacterial food source has been shown to extend worm lifespan[14], but the lifespan increase by α-KG is not due to altered bacterial proliferation or metabolism (Fig. 1d, e and Extended Data Fig. 1d). Animals also did not view α-KG-treated food as less favourable (Extended Data Fig. 1e, f), and there was no significant change in food intake, pharyngeal pumping, foraging behaviour, body size or brood size in the presence of α-KG (Extended Data Fig. 1e–h; data not shown).

In the cell, α-KG is decarboxylated to succinyl-CoA and CO_2 by α-KG dehydrogenase (encoded by *ogdh-1*), a key control point in the TCA cycle. Increasing α-KG levels by *ogdh-1* RNA interference (RNAi) (Extended Data Fig. 1b) also extends worm lifespan (Fig. 1f and Supplementary Notes), consistent with a direct effect of α-KG on longevity independent of bacterial food.

To investigate the molecular mechanism(s) of longevity by α-KG, we took advantage of an unbiased biochemical approach, DARTS[7]. As we proposed that key target(s) of α-KG are likely to be conserved and ubiquitously expressed, we used a human cell line (Jurkat) that is easy to culture as the protein source for DARTS (Fig. 2a). Mass spectrometry identified ATP5B, the β subunit of the catalytic core of the ATP synthase, among the most abundant and enriched proteins present in the α-KG-treated sample (Extended Data Table 1); the homologous α subunit ATP5A was also enriched but to a lesser extent. The interaction between α-KG and ATP5B was verified using additional cell lines (Fig. 2b; data not shown), and corroborated for the *C. elegans* orthologue ATP-2 (Extended Data Fig. 2a).

α-KG inhibits the activity of complex V, but not complex IV, from bovine heart mitochondria (Fig. 2c and Extended Data Fig. 2b; data not

[1]Molecular Biology Institute, University of California Los Angeles, Los Angeles, California 90095, USA. [2]Department of Molecular and Medical Pharmacology, University of California Los Angeles, Los Angeles, California 90095, USA. [3]Department of Human Genetics, University of California Los Angeles, Los Angeles, California 90095, USA. [4]Department of Chemistry and Biochemistry, University of California Los Angeles, Los Angeles, California 90095, USA. [5]Department of Biological Chemistry, University of California Los Angeles, Los Angeles, California 90095, USA. [6]Department of Surgery, University of California Los Angeles, Los Angeles, California 90095, USA. [7]Small Molecule Mass Spectrometry Facility, FAS Division of Science, Harvard University, Cambridge, Massachusetts 02138, USA. [8]Department of Chemical Physiology, The Scripps Research Institute, La Jolla, California 92037, USA. [9]Pasarow Mass Spectrometry Laboratory, Department of Psychiatry and Biobehavioral Sciences and Semel Institute for Neuroscience and Human Behavior, University of California Los Angeles, Los Angeles, California 90095, USA. [10]Department of Environmental Health Sciences, University of California Los Angeles, Los Angeles, California 90095, USA. [11]Department of Pathology and Laboratory Medicine, University of California Los Angeles, Los Angeles, California 90095, USA. [12]Department of Chemistry and Chemical Biology, Harvard University, Cambridge, Massachusetts 02138, USA. [13]UCLA Metabolomics Center, University of California Los Angeles, Los Angeles, California 90095, USA.
*These authors contributed equally to this work.

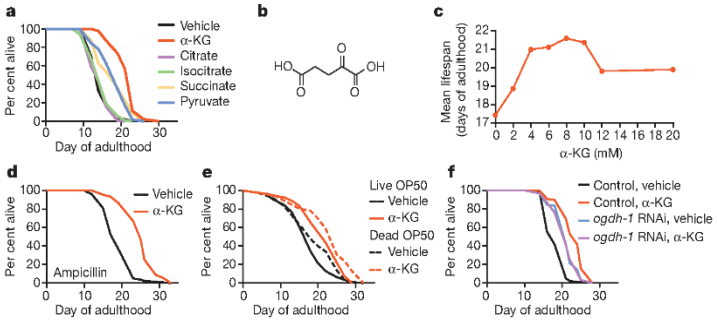

Figure 1 | α-KG extends the adult lifespan of *C. elegans*. **a**, α-KG extends the lifespan of adult worms in the metabolite longevity screen. All metabolites were given at a concentration of 8 mM. **b**, Structure of α-KG. **c**, Dose–response curve of the α-KG effect on longevity. **d**, **e**, α-KG extends the lifespan of worms fed bacteria that have been ampicillin arrested, mean lifespan (days of adulthood) with vehicle treatment (m_{veh}) = 19.4 (n = 80 animals tested), $m_{\alpha\text{-KG}}$ = 25.1 (n = 91), $P < 0.0001$ (log-rank test) (**d**); or γ-irradiation-killed, m_{veh} = 19.0 (n = 88), $m_{\alpha\text{-KG}}$ = 23.0 (n = 46), $P < 0.0001$ (log-rank test) (**e**). OP50, *E. coli* OP50 strain. **f**, α-KG does not further extend the lifespan of *ogdh-1* RNAi worms, m_{veh} = 21.2 (n = 98), $m_{\alpha\text{-KG}}$ = 21.1 (n = 100), P = 0.65 (log-rank test).

shown). This inhibition is also readily detected in live mammalian cells (Fig. 2d; data not shown) and in live nematodes (Fig. 2e), as evidenced by reduced ATP levels. Concomitantly, oxygen consumption rates are lowered (Fig. 2f, g), similar to with *atp-2* knockdown (Extended Data Fig. 2c). Specific inhibition of complex V—but not the other electron transport chain (ETC) complexes—by α-KG is further confirmed by respiratory control analysis[15] (Fig. 2h and Extended Data Fig. 2d–h). To understand the mechanism of inhibition by α-KG, we studied the enzyme inhibition kinetics of ATP synthase. α-KG (released from octyl α-KG) decreases both the effective velocity of the enzyme-catalysed reaction at an infinite concentration of the substrate (V_{max}) and the Michaelis constant (K_m) of ATP synthase, indicative of uncompetitive inhibition (Fig. 2i and Supplementary Notes).

To determine the significance of ATP-2 to the longevity by α-KG, we measured the lifespan of *atp-2* RNAi adults given α-KG. As reported previously[13], *atp-2* RNAi animals live longer than control RNAi animals (Fig. 3a). However, their lifespan is not further extended by α-KG (Fig. 3a), indicating that ATP-2 is required for the longevity benefit of

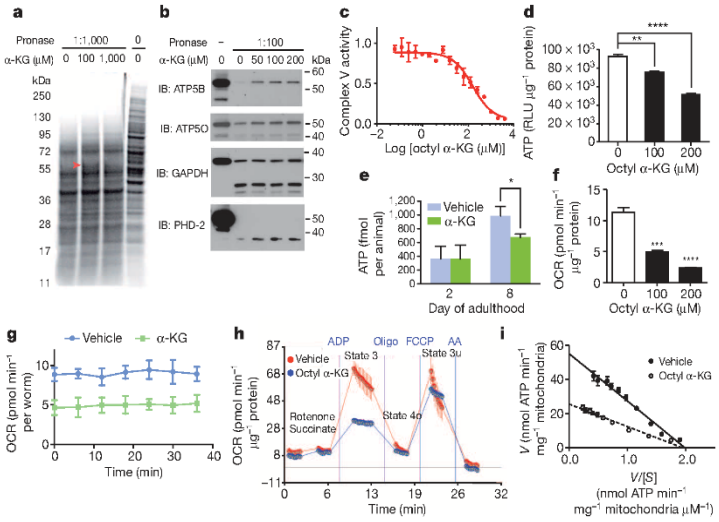

Figure 2 | α-KG binds and inhibits ATP synthase. **a**, DARTS identifies ATP5B as an α-KG-binding protein. Red arrowhead, protected band. **b**, DARTS confirms α-KG binding specifically to ATP5B. IB, immunoblot. **c**, Inhibition of ATP synthase by α-KG (released from octyl α-KG; Supplementary Notes). This inhibition was reversible (data not shown). **d**, **e**, Reduced ATP levels in octyl α-KG-treated normal human fibroblasts (**P = 0.0016, ****$P < 0.0001$; by t-test, two-tailed, two-sample unequal variance) (**d**) and α-KG-treated worms (day 2, P = 0.969; day 8, *P = 0.012; by t-test, two-tailed, two-sample unequal variance) (**e**). RLU, relative luminescence units. **f**, **g**, Decreased oxygen consumption rate (OCR) in octyl α-KG-treated cells (***P = 0.0004, ****$P < 0.0001$; by t-test, two-tailed, two-sample unequal variance) (**f**) and α-KG-treated worms ($P < 0.0001$; by t-test, two-tailed, two-sample unequal variance) (**g**). **h**, α-KG, released from octyl α-KG (800 μM), decreases state 3, but not state 4o or 3u (P = 0.997), respiration in mitochondria isolated from mouse liver. The respiratory control ratio is decreased in the octyl α-KG- (3.1 ± 0.6) versus vehicle-treated mitochondria (5.2 ± 1.0) (*P = 0.015; by t-test, two-tailed, two-sample unequal variance). Oligo, oligomycin; FCCP, carbonyl cyanide-4-(trifluoromethoxy)phenylhydrazone; AA, antimycin A. **i**, Eadie–Hofstee plot of steady-state inhibition kinetics of ATP synthase by α-KG (produced by *in situ* hydrolysis of octyl α-KG). [S] is the substrate (ADP) concentration, and V is the initial velocity of ATP synthesis in the presence of 200 μM octanol (vehicle control) or octyl α-KG. α-KG (produced from octyl α-KG) decreases the apparent V_{max} (53.9 to 26.7) and K_m (25.9 to 15.4), by nonlinear regression least-squares fit. **c**–**i**, Results were replicated in two independent experiments. Mean ± standard deviation (s.d.) is plotted in all cases.

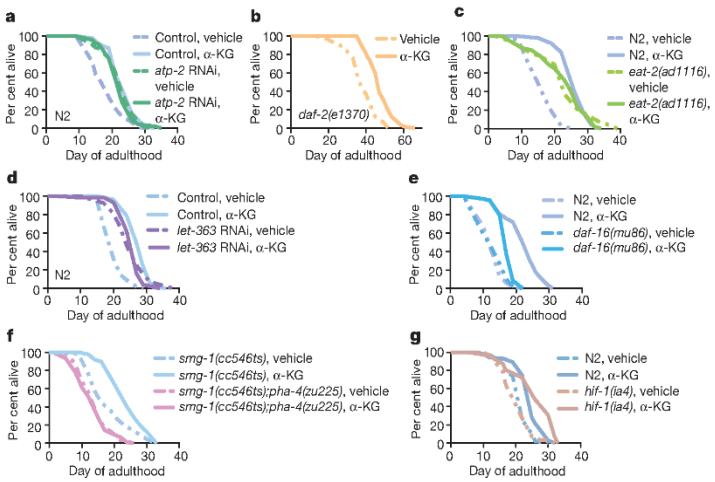

Figure 3 | α-KG longevity is mediated through ATP synthase and the dietary restriction/TOR axis. a–g, Effect of α-KG on the lifespan of mutant or RNAi worms. **a**, *atp-2* RNAi, $m_{veh} = 22.8$ ($n = 97$), $m_{\alpha\text{-}KG} = 22.5$ ($n = 94$), $P = 0.35$; or RNAi control, $m_{veh} = 18.6$ ($n = 94$), $m_{\alpha\text{-}KG} = 23.4$ ($n = 91$), $P < 0.0001$. **b**, *daf-2(e1370)*, $m_{veh} = 38.0$ ($n = 72$), $m_{\alpha\text{-}KG} = 47.6$ ($n = 69$), $P < 0.0001$. **c**, *eat-2(ad1116)*, $m_{veh} = 22.8$ ($n = 59$), $m_{\alpha\text{-}KG} = 22.9$ ($n = 40$), $P = 0.79$. **d**, *let-363* RNAi, $m_{veh} = 25.1$ ($n = 96$), $m_{\alpha\text{-}KG} = 25.7$ ($n = 74$), $P = 0.95$; or *gfp* RNAi control, $m_{veh} = 20.2$ ($n = 99$), $m_{\alpha\text{-}KG} = 27.7$ ($n = 81$), $P < 0.0001$. **e**, *daf-16(mu86)*, $m_{veh} = 13.4$ ($n = 71$), $m_{\alpha\text{-}KG} = 17.4$ ($n = 72$), $P < 0.0001$; or N2, $m_{veh} = 13.2$ ($n = 100$), $m_{\alpha\text{-}KG} = 22.3$ ($n = 104$), $P < 0.0001$. **f**, *pha-4(zu225)*, $m_{veh} = 14.2$ ($n = 94$), $m_{\alpha\text{-}KG} = 13.5$ ($n = 109$), $P = 0.55$. **g**, *hif-1(ia4)*, $m_{veh} = 20.5$ ($n = 85$), $m_{\alpha\text{-}KG} = 26.0$ ($n = 71$), $P < 0.0001$; or N2, $m_{veh} = 21.5$ ($n = 101$), $m_{\alpha\text{-}KG} = 24.6$ ($n = 102$), $P < 0.0001$. *P* values were determined by the log-rank test. Number of independent experiments: RNAi control (6), *atp-2* (2), *let-363* (3), *N2* (5), *daf-2* (2), *eat-2* (2), *pha-4* (2), *daf-16* (2), *hif-1* (5).

α-KG. This requirement is specific because, in contrast, the lifespan of the even longer-lived insulin/IGF-1 receptor *daf-2(e1370)* mutant worms[3] is further increased by α-KG (Fig. 3b). Remarkably, oligomycin, an inhibitor of ATP synthase, also extends the lifespan of adult worms (Extended Data Fig. 3a). Together, the direct binding of ATP-2 by α-KG, the related enzymatic inhibition, reduction in ATP levels and oxygen consumption, lifespan analysis, and other similarities (see also Supplementary Notes, Extended Data Fig. 4) to *atp-2* knockdown or oligomycin treatment demonstrate that α-KG probably extends lifespan primarily by targeting ATP-2.

The lower ATP content in α-KG-treated animals suggests that increased longevity by α-KG may involve a state similar to that induced by dietary restriction. Consistent with this idea, we found that α-KG does not extend the lifespan of *eat-2(ad1116)* animals (Fig. 3c), which is a model of dietary restriction with impaired pharyngeal pumping and therefore reduced food intake[16]. The longevity of *eat-2* mutants requires TOR (encoded by the *C. elegans* orthologue *let-363*)[17], an important mediator of the effects of dietary restriction on longevity[18]. Likewise, α-KG fails to increase the lifespan of *let-363* RNAi animals (Fig. 3d). The AMP-activated protein kinase (AMPK) is another conserved major sensor of cellular energy status[19]. Both AMPK (*C. elegans* orthologue *aak-2*) and the FoxO transcription factor DAF-16 mediate dietary-restriction-induced longevity in *C. elegans* fed diluted bacteria[20], but neither is required for lifespan extension in the *eat-2* model[16,20]. We found that in *aak-2* (Extended Data Fig. 5a) and *daf-16* (Fig. 3e) mutants the longevity effect of α-KG is smaller than in N2 animals ($P < 0.0001$), suggesting that α-KG longevity partially depends on AMPK and FoxO; nonetheless, lifespan is significantly increased by α-KG in *aak-2* (24.3%, $P < 0.0001$) and *daf-16* (29.5%, $P < 0.0001$) mutant or RNAi animals (Fig. 3e and Extended Data Fig. 5a, b; data not shown), indicating an AMPK- and FoxO-independent effect of α-KG in increasing longevity.

The inability of α-KG to extend further the lifespan of *let-363* RNAi animals suggests that α-KG treatment and TOR inactivation extend lifespan either through the same pathway (with α-KG acting on or upstream of TOR), or through independent mechanisms or parallel pathways that converge on a downstream effector. The first model predicts that the TOR pathway will be less active upon α-KG treatment, whereas if the latter model were true then TOR would be unaffected by α-KG treatment. In support of the first model, we found that TOR pathway activity is decreased in human cells treated with octyl α-KG (Fig. 4a and Extended Data Fig. 6a, b). However, α-KG does not interact with TOR directly (Extended Data Fig. 6d, e). Consistent with the involvement of TOR in α-KG longevity, the FoxA transcription factor PHA-4, which is required to extend adult lifespan in response to reduced TOR signalling[21] and for dietary-restriction-induced longevity in *C. elegans*[22], is likewise required for α-KG-induced longevity (Fig. 3f). Moreover, autophagy, which is activated both by TOR inhibition[18,23] and by dietary restriction[24], is markedly increased in worms treated with α-KG (or *ogdh-1* RNAi) and in *atp-2* RNAi animals (Fig. 4b, c, Extended Data Figs 6c, 7 and Supplementary Notes), as indicated by the prevalence of green fluorescent protein GFP::LGG-1 puncta (Methods). Autophagy was also induced in mammalian cells treated with octyl α-KG (Extended Data Fig. 6f). Furthermore, α-KG does not result in significantly more autophagy in either *atp-2* RNAi or *let-363* RNAi worms (Fig. 4b, c). The data provide further evidence that α-KG decreases TOR pathway activity through the inhibition of ATP synthase. Similarly, autophagy is induced by oligomycin, and oligomycin does not augment autophagy in *let-363* RNAi worms (Extended Data Fig. 3b, c).

α-KG is not only a metabolite, but also a co-substrate for a large family of dioxygenases[25]. The hypoxia inducible factor (HIF-1) is modified by one of these enzymes, the prolyl 4-hydroxylase (PHD) EGL-9, and thereafter degraded by the von Hippel–Lindau (VHL) protein[26,27]. α-KG extends the lifespan of animals with loss-of-function mutations in *hif-1*, *egl-9* and *vhl-1* (Fig. 3g and Extended Data Fig. 5c), suggesting that this pathway does not play a major part in lifespan extension by α-KG. However, it is prudent to acknowledge that the formal possibility of other α-KG-binding targets having an additional role in the extension of lifespan by α-KG cannot be eliminated at this time.

We show that ageing in *C. elegans* is delayed by α-KG supplementation in adult animals. The
synthase, which we identified as a direct target of α-KG, and TOR, a major effector of dietary restriction. Identification of new protein targets

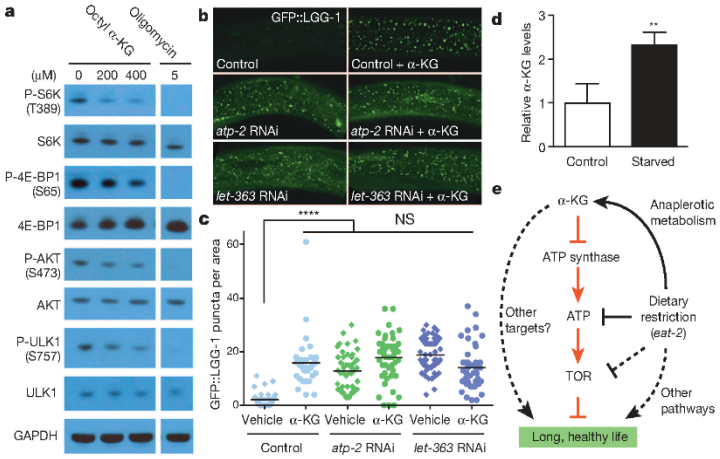

Figure 4 | Inhibition of ATP synthase by α-KG causes a conserved decrease in TOR pathway activity. **a**, Decreased phosphorylation of mammalian TOR substrates in U87 cells treated with octyl α-KG or oligomycin. Similar results were obtained in HEK-293 cells, normal human fibroblasts and mouse embryonic fibroblasts (data not shown). P, phospho. **b**, Increased autophagy in animals treated with α-KG or RNAi for *atp-2* or *let-363*. Photographs were taken at ×100 magnification. **c**, GFP::LGG-1 puncta quantified using ImageJ (Methods). Data show results of 2–3 independent experiments. Bars indicate the mean. $^{****}P < 0.0001$; NS, not significant (*t*-test, two-tailed, two-sample unequal variance). **d**, α-KG levels are increased in starved worms. $^{**}P < 0.01$ (*t*-test, two-tailed, two-sample unequal variance). Mean ± s.d. is plotted. **e**, Model of α-KG-mediated longevity.

of α-KG illustrates that regulatory networks acted upon by metabolites are probably more complex than appreciated at present, and that DARTS is a useful method for discovering new protein targets and regulatory functions of metabolites. Our findings demonstrate a novel mechanism for extending lifespan that is mediated by the regulation of cellular energy metabolism by a key metabolite. Such moderation of ATP synthesis by metabolite(s) has probably evolved to ensure energy efficiency by the organism in response to nutrient availability. We suggest that this system may be exploited to confer a dietary-restriction-like state that favours maintenance over growth, and thereby delays ageing and prevents age-related diseases. In fact, the TOR pathway is often hyperactivated in human cancer; inhibition of TOR function by α-KG in normal human cells suggests an exciting role for α-KG as an endogenous tumour suppressor metabolite. Interestingly, physiological increases in α-KG levels have been reported in starved yeast and bacteria[28], in the liver of starved pigeons[29], and in humans after physical exercise[30]. The biochemical basis for this increase of α-KG is explained by starvation-based anaplerotic gluconeogenesis, which activates glutamate-linked transaminases in the liver to provide carbon derived from amino acid catabolism. Consistent with this idea, α-KG levels are elevated in starved *C. elegans* (Fig. 4d). These findings suggest a model in which α-KG is a key metabolite mediating lifespan extension by starvation/dietary restriction (Fig. 4e).

Longevity molecules that delay ageing and extend lifespan have long been a dream of humanity. Endogenous metabolites such as α-KG that can alter *C. elegans* lifespan suggest that an internal mechanism may exist that is accessible to intervention; whether this can translate into manipulating the ageing process in humans remains to be seen.

METHODS SUMMARY

Lifespan analysis. All lifespan assays were conducted at 20 °C on solid nematode growth media (NGM) and were replicated in at least two independent experiments. *P* values were determined by the log-rank (Mantel–Cox) test; survival curves were generated using GraphPad Prism. All lifespan data are available in Extended Data Table 2.

DARTS. Human Jurkat cell lysates were incubated with α-KG and digested using Pronase. Proteins protected from proteolysis by α-KG binding were analysed by liquid chromatography-tandem mass spectrometry (LC-MS/MS) as described previously[7], and identified by searching against the human Swissprot database (release 57.15) using Mascot with all peptides meeting a significance threshold of $P < 0.05$.

Online Content Any additional Methods, Extended Data display items and Source Data are available in the online version of the paper; references unique to these sections appear only in the online paper.

Received 3 October 2012; accepted 17 March 2014.
Published online 14 May 2014.

1. Colman, R. J. *et al.* Caloric restriction delays disease onset and mortality in rhesus monkeys. *Science* **325,** 201–204 (2009).
2. Mattison, J. A. *et al.* Impact of caloric restriction on health and survival in rhesus monkeys from the NIA study. *Nature* **489,** 318–321 (2012).
3. Kenyon, C. J. The genetics of ageing. *Nature* **464,** 504–512 (2010).
4. Harrison, D. E. *et al.* Rapamycin fed late in life extends lifespan in genetically heterogeneous mice. *Nature* **460,** 392–395 (2009).
5. Williams, D. S., Cash, A., Hamadani, L. & Diemer, T. Oxaloacetate supplementation increases lifespan in *Caenorhabditis elegans* through an AMPK/FOXO-dependent pathway. *Aging Cell* **8,** 765–768 (2009).
6. Lucanic, M. *et al.* N-acylethanolamine signalling mediates the effect of diet on lifespan in *Caenorhabditis elegans*. *Nature* **473,** 226–229 (2011).
7. Lomenick, B. *et al.* Target identification using drug affinity responsive target stability (DARTS). *Proc. Natl Acad. Sci. USA* **106,** 21984–21989 (2009).
8. Abrahams, J. P., Leslie, A. G., Lutter, R. & Walker, J. E. Structure at 2.8 Å resolution of F1-ATPase from bovine heart mitochondria. *Nature* **370,** 621–628 (1994).
9. Boyer, P. D. The ATP synthase—a splendid molecular machine. *Annu. Rev. Biochem.* **66,** 717–749 (1997).
10. Tsang, W. Y., Sayles, L. C., Grad, L. I., Pilgrim, D. B. & Lemire, B. D. Mitochondrial respiratory chain deficiency in *Caenorhabditis elegans* results in developmental arrest and increased life span. *J. Biol. Chem.* **276,** 32240–32246 (2001).
11. Dillin, A. *et al.* Rates of behavior and aging specified by mitochondrial function during development. *Science* **298,** 2398–2401 (2002).
12. Lee, S. S. *et al.* A systematic RNAi screen identifies a critical role for mitochondria in *C. elegans* longevity. *Nature Genet.* **33,** 40–48 (2002).
13. Curran, S. P. & Ruvkun, G. Lifespan regulation by evolutionarily conserved genes essential for viability. *PLoS Genet.* **3,** e56 (2007).
14. Gems, D. & Riddle, D. L. Genetic, behavioral and environmental determinants of male longevity in *Caenorhabditis elegans*. *Genetics* **154,** 1597–1610 (2000).
15. Brand, M. D. & Nicholls, D. G. Assessing mitochondrial dysfunction in cells. *Biochem. J.* **435,** 297–312 (2011).
16. Lakowski, B. & Hekimi, S. The genetics of caloric restriction in *Caenorhabditis elegans*. *Proc. Natl Acad. Sci. USA* **95,** 13091–13096 (1998).
17. Hansen, M. *et al.* Lifespan extension by conditions that inhibit translation in *Caenorhabditis elegans*. *Aging Cell* **6,** 95–110 (2007).
18. Stanfel, M. N., Shamieh, L. S., Kaeberlein, M. & Kennedy, B. K. The TOR pathway comes of age. *Biochim. Biophys. Acta* **1790,** 1067–1074 (2009).
19. Hardie, D. G., Scott, J. W., Pan, D. A. & Hudson, E. R. Management of cellular energy by the AMP-activated protein kinase system. *FEBS Lett.* **546,** 113–120 (2003).

20. Greer, E. L. & Brunet, A. Different dietary restriction regimens extend lifespan by both independent and overlapping genetic pathways in *C. elegans*. *Aging Cell* **8,** 113–127 (2009).
21. Sheaffer, K. L., Updike, D. L. & Mango, S. E. The target of rapamycin pathway antagonizes *pha-4/FoxA* to control development and aging. *Curr. Biol.* **18,** 1355–1364 (2008).
22. Panowski, S. H., Wolff, S., Aguilaniu, H., Durieux, J. & Dillin, A. PHA-4/Foxa mediates diet-restriction-induced longevity of *C. elegans*. *Nature* **447,** 550–555 (2007).
23. Wullschleger, S., Loewith, R. & Hall, M. N. TOR signaling in growth and metabolism. *Cell* **124,** 471–484 (2006).
24. Meléndez, A. *et al.* Autophagy genes are essential for dauer development and life-span extension in *C. elegans*. *Science* **301,** 1387–1391 (2003).
25. Loenarz, C. & Schofield, C. J. Expanding chemical biology of 2-oxoglutarate oxygenases. *Nature Chem. Biol.* **4,** 152–156 (2008).
26. Epstein, A. C. *et al. C. elegans* EGL-9 and mammalian homologs define a family of dioxygenases that regulate HIF by prolyl hydroxylation. *Cell* **107,** 43–54 (2001).
27. Zhang, Y., Shao, Z., Zhai, Z., Shen, C. & Powell-Coffman, J. A. The HIF-1 hypoxia-inducible factor modulates lifespan in *C. elegans*. *PLoS ONE* **4,** e6348 (2009).
28. Brauer, M. J. *et al.* Conservation of the metabolomic response to starvation across two divergent microbes. *Proc. Natl Acad. Sci. USA* **103,** 19302–19307 (2006).
29. Kaminsky, Y. G., Kosenko, E. A. & Kondrashova, M. N. Metabolites of citric acid cycle, carbohydrate and phosphorus metabolism, and related reactions, redox and phosphorylating states of hepatic tissue, liver mitochondria and cytosol of the pigeon, under normal feeding and natural nocturnal fasting conditions. *Comp. Biochem. Physiol. B* **73,** 957–963 (1982).
30. Brugnara, L. *et al.* Metabolomics approach for analyzing the effects of exercise in subjects with type 1 diabetes mellitus. *PLoS ONE* **7,** e40600 (2012).

Supplementary Information is available in the online version of the paper.

Acknowledgements We thank S. Lee, M. Hansen, B. Lemire, A. van der Bliek, S. Clarke, T. K. Blackwell, R. Johnson, J. E. Walker, A. G. W. Leslie, K. N. Houk, B. Martin, J. Lusis, J. Gober, Y. Wang and H. Sun for advice and discussions. J. Avruch for the *let-363* RNAi vector; J. Powell-Coffman for strains and advice; and K. Yan for technical assistance. Worm strains were provided by the *Caenorhabditis* Genetics Center, which is funded by the National Institutes of Health (NIH) Office of Research Infrastructure Programs (P40 OD010440). We thank the NIH for traineeship support of R.M.C. (T32 GM007104), M.Y.P. (T32 GM007185), B.L. (T32 GM008496) and M.N. (T32 CA009120). X.F. is a recipient of the China Scholarship Council Scholarship. G.C.M. was supported by Ford Foundation and National Science Foundation Graduate Research Fellowships.

Author Contributions Lifespan assays were performed by R.M.C., M.P. and E.H.; DARTS-mass spectrometry by S.D. and B.L.; DARTS-western blots by M.Y.P., H.H. and R.M.C.; mammalian cell experiments by X.F. and H.H.; mitochondrial respiration study design and analyses by L.V. and K.R.; enzyme kinetics and analyses by R.M.C. and J.H.; confocal microscopy by V.S.M., G.C.M. and A.R.F.; ultra-high-performance liquid chromatography-electrospray ionization-tandem mass spectrometry (UHPLC-ESI/MS/MS) by J.X.W. and S.A.T.; compound syntheses by G.D. and M.E.J.; other analyses by H.H., X.F., M.Y.P., D.B., R.M.C., E.H., G.J., G.M.S., C.K. and A.Q. S.A.W., F.F., M.N., A.S.K., H.A.G., H.R. Chang, K.F.F., F.G., M.J., S.A.T., A.S., D.B., H.R. Christofk, C.F.C., M.A.T., M.E.J., L.V., K.R., A.R.F. and M.P. provided guidance, specialized reagents and expertise. J.H. conceived the study. R.M.C. and J.H. wrote the paper. R.M.C., X.F. and J.H. analysed data. All authors discussed the results, commented on the studies and contributed to aspects of preparing the manuscript.

Author Information Reprints and permissions information is available at www.nature.com/reprints. The authors declare no competing financial interests. Readers are welcome to comment on the online version of the paper. Correspondence and requests for materials should be addressed to J.H. (jinghuang@mednet.ucla.edu).

METHODS

Nematode strains and maintenance. *C. elegans* strains were maintained using standard methods[31]. The following strains were used (strain, genotype): Bristol N2, wild type; DA1116, *eat-2(ad1116)*II; CB1370, *daf-2(e1370)*III; CF1038, *daf-16(mu86)*I; PD8120, *smg-1(cc546ts)*I; SM190, *smg-1(cc546ts)*I;*pha-4(zu225)*V; RB754, *aak-2(ok524)*X; ZG31, *hif-1(ia4)*V; ZG596, *hif-1(ia7)*V; JT307, *egl-9(sa307)*V; CB5602, *vhl-1(ok161)*X; DA2123, *adIs2122[lgg-1::GFP + rol-6(su1006)]*. They were all obtained from the *Caenorhabditis* Genetics Center (CGC).

RNAi in *C. elegans*. RNAi in *C. elegans* was accomplished by feeding worms HT115 (DE3) bacteria expressing target-gene double-stranded RNA (dsRNA) from the pL4440 vector[32]. dsRNA production was induced overnight on plates containing 1 mM isopropyl-β-D-thiogalactoside (IPTG). All RNAi feeding clones were obtained from the *C. elegans* ORF-RNAi Library (Thermo Scientific/Open Biosystems) unless otherwise stated. The *C. elegans* TOR (*let-363*) RNAi clone[33] was obtained from Joseph Avruch (MGH/Harvard). Efficient knockdown was confirmed by western blotting of the corresponding protein or by qRT–PCR of the mRNA. The primer sequences used for qRT–PCR are as follows. *atp-2* forward: TGACAACATTTTC CGTTTCACC; *atp-2* reverse: AAATAGCCTGGACGGATGTGAT; *let-363* forward: GATCCGAGACAAGATGAACGTG; *let-363* reverse: ACAATTTGGAAC CCAACCAATC; *ogdh-1* forward: TGATTTGGACCGAGAATTCCTT; *ogdh-1* reverse: GGATCAGACGTTTGAACAGCAC.

We validated the RNAi knockdown of both *ogdh-1* and *atp-2* by quantitative RT–PCR and also of *atp-2* by western blotting. Transcripts of *ogdh-1* were reduced by 85%, and transcripts and protein levels of *atp-2* were reduced by 52% and 83%, respectively, in larvae that were cultivated on bacteria that expressed the corresponding dsRNAs. In addition, RNAi of *atp-2* in this study was associated with delayed post-embryonic development and larval arrest, consistent with the phenotypes of *atp-2(ua2)* animals. Analysis by qRT–PCR indicated a modest but significant decrease by 26% in transcripts of *let-363* in larvae undergoing RNAi; moreover, molecular markers for autophagy were induced in these animals, and the lifespan of adults was extended, consistent with partial inactivation of the kinase.

In lifespan experiments, we used RNAi to inactivate *atp-2*, *ogdh-1* and *let-363* in mature animals in the presence or absence of exogenous α-KG. The concentration of α-KG used in these experiments (8 mM) was empirically determined to be most beneficial for wild-type animals (Fig. 1c). This approach enabled us to evaluate the contribution of essential proteins and pathways to the longevity conferred by supplementary α-KG. Specifically, we were able to substantially but not fully inactivate *atp-2* in adult animals that had completed embryonic and larval development. As described earlier, supplementation with 8 mM α-KG did not further extend (and in fact, on one occasion, even decreased) the lifespan of *atp-2* RNAi animals (Extended Data Table 2), indicating that *atp-2* is required for α-KG to promote longevity. On the other hand, a complete inactivation of *atp-2* would be lethal, and thereby mask the benefit of ATP synthase inhibition by α-KG.

Lifespan analysis. Lifespan assays were conducted at 20 °C on solid nematode growth media (NGM) using standard protocols and were replicated in at least two independent experiments. *C. elegans* were synchronized by performing either a timed egg lay[34] or an egg preparation (lysing ~100 gravid worms in 70 µl M9 buffer[31], 25 µl bleach (10% sodium hypochlorite solution) and 5 µl 10 N NaOH). Young adult animals were picked onto NGM assay plates containing 1.5% dimethyl sulfoxide (DMSO; Sigma, D8418), 49.5 µM 5-fluoro-2′-deoxyuridine[34] (FUDR; Sigma, F0503), and α-KG (Sigma, K1128) or vehicle control (H_2O). FUDR was included to prevent progeny production. Media containing α-KG were adjusted to pH 6.0 (that is, the same pH as the control plates) by the addition of NaOH. All compounds were mixed into the NGM media after autoclaving and before solidification of the media. Assay plates were seeded with OP50 (or a designated RNAi feeding clone, see later). Worms were moved to new assay plates every 4 days (to ensure sufficient food was present at all times and to reduce the risk of mould contamination). To assess the survival of the worms, the animals were prodded with a platinum wire every 2–3 days, and those that failed to respond were scored as dead. For analysis concerning mutant strains, the corresponding parent strain was used as a control in the same experiment.

For lifespan experiments involving RNAi, the plates also contained 1 mM IPTG (Acros, CAS 367-93-1) and 50 µg ml^{-1} ampicillin (Fisher, BP1760-25). RNAi was accomplished by feeding N2 worms HT115(DE3) bacteria expressing target-gene dsRNA from pL4440 (ref. 32); control RNAi was done in parallel for every experiment by feeding N2 worms HT115(DE3) bacteria expressing either GFP dsRNA or empty vector (which gave identical lifespan results).

Lifespan experiments with oligomycin (Cell Signaling, 9996) were performed as described for α-KG (that is, NGM plates with 1.5% DMSO and 49.5 µM FUDR; N2 worms; OP50 bacteria).

For lifespan experiments concerning *smg-1(cc546ts);pha-4(zu225)* and *smg-1(cc546ts)*[32,35], from egg to L4 stage the strains were grown at 24 °C, which inactivates the *smg-1* temperature-sensitive allele, preventing mRNA surveillance-mediated degradation of the *pha-4(zu225)* mRNA, which contains a premature stop codon, and thus produces a truncated but fully functional PHA-4 transcription factor[35]. Then at the L4 stage the temperature was shifted to 20 °C, which restores *smg-1* function and thereby results in the degradation of *pha-4(zu225)* mRNA. Treatment with α-KG began at the L4 stage.

All lifespan data are available in Extended Data Table 2, including sample sizes. The sample size was chosen on the basis of standards done in the field in published manuscripts. No statistical method was used to predetermine the sample size. Animals were assigned randomly to the experimental groups. Worms that ruptured, bagged (that is, exhibited internal progeny hatching), or crawled off the plates were censored. Lifespan data were analysed using GraphPad Prism; *P* values were calculated using the log-rank (Mantel–Cox) test.

Statistical analyses. All experiments were repeated at least two times with identical or similar results. Data represent biological replicates. Appropriate statistical tests were used for every figure. Data meet the assumptions of the statistical tests described for each figure. Mean ± s.d. is plotted in all figures unless stated otherwise.

Food preference assay. Protocol adapted from Abada *et al.*[36]. A 10 cm NGM plate was seeded with two spots of OP50 as shown in Extended Data Fig. 1e. After letting the OP50 lawns dry over 2 days at room temperature, vehicle (H_2O) or α-KG (8 mM) was added to the top of the lawn and allowed to dry over 2 days at room temperature. Approximately 50–100 synchronized adult day 1 worms were placed onto the centre of the plate and their preference for either bacterial lawn was recorded after 3 h at room temperature.

Target identification using DARTS. For unbiased target identification (Fig. 2a), human Jurkat cells were lysed using M-PER (Thermo Scientific, 78501) with the addition of protease inhibitors (Roche, 11836153001) and phosphatase inhibitors[37]. TNC buffer (50 mM Tris-HCl pH 8.0, 50 mM NaCl, 10 mM $CaCl_2$) was added to the lysate and protein concentration was then determined using the BCA Protein Assay kit (Pierce, 23227). Cell lysates were incubated with either vehicle (H_2O) or α-KG for 1 h on ice followed by an additional 20 min at room temperature. Digestion was performed using Pronase (Roche, 10165921001) at room temperature for 30 min and stopped using excess protease inhibitors with immediate transfer to ice. The resulting digests were separated by SDS–PAGE and visualized using SYPRO Ruby Protein Gel Stain (Invitrogen, S12000). The band with increased staining from the α-KG lane (corresponding to potential protein targets that are protected from proteolysis by the binding of α-KG) and the matching area of the control lane were excised, in-gel trypsin digested, and subjected to liquid chromatography–tandem mass spectrometry (LC-MS/MS) analysis as described previously[7,38]. Mass spectrometry results were searched against the human Swissprot database (release 57.15) using Mascot version 2.3.0, with all peptides meeting a significance threshold of $P < 0.05$.

For target verification by DARTS with western blotting (Fig. 2b), HeLa cells were lysed in M-PER buffer (Thermo Scientific, 78501) with the addition of protease inhibitors (Roche, 11836153001) and phosphatase inhibitors (50 mM NaF, 10 mM β-glycerophosphate, 5 mM sodium pyrophosphate, 2 mM Na_3VO_4). Chilled TNC buffer (50 mM Tris-HCl pH 8.0, 50 mM NaCl, 10 mM $CaCl_2$) was added to the protein lysate, and protein concentration of the lysate was measured by the BCA Protein Assay kit (Pierce, 23227). The protein lysate was then incubated with vehicle control (H_2O) or varying concentrations of α-KG for 3 h at room temperature with shaking at 600 r.p.m. in an Eppendorf Thermomixer. Pronase (Roche, 10165921001) digestions were performed for 20 min at room temperature, and stopped by adding SDS loading buffer and immediately heating at 70 °C for 10 min. Samples were subjected to SDS–PAGE on 4–12% Bis-Tris gradient gel (Invitrogen, NP0322BOX) and western blotted for ATP synthase subunits ATP5B (Sigma, AV48185), ATP5O (Abcam, ab91400) and ATP5A (Abcam, ab110273). Binding between α-KG and PHD-2 (encoded by *EGLN1*) (Cell Signaling, 4835), for which α-KG is a co-substrate[39], was confirmed by DARTS. GAPDH (Ambion, AM4300) was used as a negative control.

For DARTS using *C. elegans* (Extended Data Fig. 2a), wild-type animals of various ages were grown on NGM/OP50 plates, washed four times with M9 buffer, and immediately placed in the −80 °C freezer. Animals were lysed in HEPES buffer (40 mM HEPES pH 8.0, 120 mM NaCl, 10% glycerol, 0.5% Triton X-100, 10 mM β-glycerophosphate, 50 mM NaF, 0.2 mM Na_3VO_4, protease inhibitors (Roche, 11836153001)) using Lysing Matrix C tubes (MP Biomedicals, 6912-100) and the FastPrep-24 (MP Biomedicals) high-speed bench-top homogenizer in the 4 °C room (disrupt worms for 20 s at 6.5 m s^{-1}, rest on ice for 1 min; repeat twice). Lysed animals were centrifuged at 14,000 r.p.m. for 10 min at 4 °C to pellet worm debris, and supernatant was collected for DARTS. Protein concentration was determined by BCA Protein Assay kit (Pierce, 23223). A worm lysate concentration of 1.13 µg µl^{-1} was used for the DARTS experiment. All steps were performed on ice or at 4 °C to help prevent premature protein degradation. TNC buffer (50 mM Tris-HCl pH 8.0, 50 mM NaCl, 10 mM $CaCl_2$) was added to the worm lysates. Worm lysates were incubated with vehicle control (H_2O) or α-KG for 1 h on ice and then 50 min at room temperature. Pronase (Roche, 10165921001) digestions were performed for

30 min at room temperature and stopped by adding SDS loading buffer and heating at 70 °C for 10 min. Samples were then subjected to SDS–PAGE on NuPAGE Novex 4–12% Bis-Tris gradient gels (Invitrogen, NP0322BOX), and western blotting was carried out with an antibody against ATP5B (Sigma, AV48185) that also recognizes ATP-2.

Complex V activity assay. Complex V activity was assayed using the MitoTox OXPHOS Complex V Activity Kit (Abcam, ab109907). Vehicle (H_2O) or α-KG was mixed with the enzyme before the addition of phospholipids. In experiments using octyl α-KG, vehicle (1% DMSO) or octyl α-KG was added with the phospholipids. Relative complex V activity was compared to vehicle. Oligomycin (Sigma, O4876) was used as a positive control for the assay.

Isolation of mitochondria from mouse liver. Animal studies were performed under approved University of California, Los Angeles animal research protocols. Mitochondria from 3-month-old C57BL/6 mice were isolated as described[40]. Briefly, livers were extracted, minced at 4 °C in MSHE plus BSA (70 mM sucrose, 210 mM mannitol, 5 mM HEPES, 1 mM EGTA, and 0.5% fatty acid free BSA, pH 7.2), and rinsed several times to remove blood. All subsequent steps were performed on ice or at 4 °C. The tissue was disrupted in ten volumes of MSHE plus BSA with a glass Dounce homogenizer (5–6 strokes) and the homogenate was centrifuged at 800*g* for 10 min to remove tissue debris and nuclei. The supernatant was decanted through a cell strainer and centrifuged at 8,000*g* for 10 min. The dark mitochondrial pellet was resuspended in MSHE plus BSA and re-centrifuged at 8,000*g* for 10 min. The final mitochondrial pellets were used for various assays as described later.

Submitochondrial particle ATPase assay. ATP hydrolysis by ATP synthase was measured using submitochondrial particles (see ref. 41 and references therein). Mitochondria were isolated from mouse liver as described earlier. The final mitochondrial pellet was resuspended in buffer A (250 mM sucrose, 10 mM Tris-HCl, 1 mM ATP, 5 mM $MgCl_2$ and 0.1 mM EGTA, pH 7.4) at 10 μg μl^{-1}, subjected to sonication on ice (Fisher Scientific Model 550 Sonic Dismembrator; medium power, alternating between 10 s intervals of sonication and resting on ice for a total of 60 s of sonication), and then centrifuged at 18,000*g* for 10 min at 4 °C. The supernatant was collected and centrifuged at 100,000*g* for 45 min at 4 °C. The final pellet (submitochondrial particles) was resuspended in buffer B (250 mM sucrose, 10 mM Tris-HCl and 0.02 mM EGTA, pH 7.4).

The SMP ATPase activity was assayed using the Complex V Activity Buffer as described eariler. The production of ADP is coupled to the oxidation of NADH to NAD^+ through pyruvate kinase and lactate dehydrogenase. The addition of α-KG (up to 10 mM) did not affect the activity of pyruvate kinase or lactate dehydrogenase when external ADP was added. The absorbance decrease of NADH at 340 nm correlates to ATPase activity. Submitochondrial particles (2.18 ng μl^{-1}) were incubated with vehicle or α-KG for 90 min at room temperature before the addition of activity buffer, and then the absorbance decrease of NADH at 340 nm was measured every 1 min for 1 h. Oligomycin (Cell signaling, 9996) was used as a positive control for the assay.

Assay for ATP levels. Normal human diploid fibroblast WI-38 (ATCC, CCL-75) cells were seeded in 96-well plates at 2×10^4 cells per well. Cells were treated with either DMSO (vehicle control) or octyl α-KG at varying concentrations for 2 h in triplicate. ATP levels were measured using the CellTiter-Glo luminescent ATP assay (Promega, G7572); luminescence was read using Analyst HT (Molecular Devices). In parallel, identically treated cells were lysed in M-PER (Thermo Scientific, 78501) to obtain protein concentration by BCA Protein Assay kit (Pierce, 23223). ATP levels were normalized to protein content. Statistical analysis was performed using GraphPad Prism (unpaired *t*-test).

The assay for ATP levels in *C. elegans* was carried out as follows. Synchronized day 1 adult wild type *C. elegans* were placed on NGM plates containing either vehicle or 8 mM α-KG. On day 2 and 8 of adulthood, 9 replicates and 4 replicates, respectively, of about 100 worms were collected from α-KG or vehicle control plates, washed 4 times in M9 buffer, and frozen in −80 °C. Animals were lysed using Lysing Matrix C tubes (MP Biomedicals, 6912-100) and the FastPrep-24 (MP Biomedicals) high-speed bench-top homogenizer (disrupt worms for 20 s at 6.5 m s^{-1}, rest on ice for 1 min; repeat twice). Lysed animals were centrifuged at 14,000 r.p.m. for 10 min at 4 °C to pellet worm debris, and supernatant was saved for ATP quantification using the Kinase-Glo Luminescent Kinase Assay Platform (Promega, V6713) according to the manufacturer's instructions. The assay was performed in white opaque 96-well tissue culture plates (Falcon, 353296), and luminescence was measured using Analyst HT (Molecular Devices). ATP levels were normalized to the number of worms. Statistical analysis was performed using Microsoft Excel (*t*-test, two-tailed, two-sample unequal variance).

Measurement of oxygen consumption rates. Oxygen consumption rate (OCR) measurements were made using a Seahorse XF-24 analyser (Seahorse Bioscience)[42]. Cells were seeded in Seahorse XF-24 cell culture microplates at 50,000 cells per well in DMEM media supplemented with 10% FBS and 10 mM glucose, and incubated at 37 °C and 5% CO_2 overnight. Treatment with octyl α-KG or DMSO (vehicle control) was for 1 h. Cells were washed in unbuffered DMEM medium (pH 7.4, 10 mM glucose) just before measurement, and maintained in this buffer with indicated concentrations of octyl α-KG. OCR was measured three times under basal conditions and normalized to protein concentration per well. Statistical analysis was performed using GraphPad Prism.

Measurement of OCR in living *C. elegans* was carried out as follows. The protocol was adapted from those previously described[43,44]. Wild-type day 1 adult N2 worms were placed on NGM plates containing 8 mM α-KG or H_2O (vehicle control) seeded with OP50 or HT115 *E. coli*. OCR was assessed on day 2 of adulthood. On day 2 of adulthood, worms were collected and washed four times with M9 to rid the samples of bacteria (we further verified that α-KG does not affect oxygen consumption of the bacteria—therefore, even if there were any leftover bacteria after the washes, the changes in OCR observed would still be worm specific), and then the animals were seeded in quadruplicates in Seahorse XF-24 cell culture microplates (Seahorse Bioscience, V7-PS) in 200 μl M9 at ~200 worms per well. Oxygen consumption rates were measured seven times under basal conditions and normalized to the number of worms counted per well. The experiment was repeated twice. Statistical analysis was performed using Microsoft Excel (*t*-test, two-tailed, two-sample unequal variance).

Measurement of mitochondrial respiratory control ratio. Mitochondrial respiratory control ratio (RCR) was analysed using isolated mouse liver mitochondria (see ref. 15 and references therein). Mitochondria were isolated from mouse liver as described earlier. The final mitochondrial pellet was resuspended in 30 μl of MAS buffer (70 mM sucrose, 220 mM mannitol, 10 mM KH_2PO_4, 5 mM $MgCl_2$, 2 mM HEPES, 1 mM EGTA, and 0.2% fatty acid free BSA, pH 7.2).

Isolated mitochondrial respiration was measured by running coupling and electron flow assays as described[40]. For the coupling assay, 20 μg of mitochondria in complete MAS buffer (MAS buffer supplemented with 10 mM succinate and 2 μM rotenone) were seeded into a XF24 Seahorse plate by centrifugation at 2,000*g* for 20 min at 4 °C. Just before the assay, the mitochondria were supplemented with complete MAS buffer for a total of 500 μl (with 1% DMSO or octyl α-KG), and warmed at 37 °C for 30 min before starting the OCR measurements. Mitochondrial respiration begins in a coupled state 2; state 3 is initiated by 2 mM ADP; state 4o (oligomycin insensitive, that is, complex V independent) is induced by 2.5 μM oligomycin; and state 3u (FCCP-uncoupled maximal respiratory capacity) by 4 μM FCCP. Finally, 1.5 μg ml^{-1} antimycin A was injected at the end of the assay. The state 3/state 4o ratio gives the RCR.

For the electron flow assay, the MAS buffer was supplemented with 10 mM sodium pyruvate (complex I substrate), 2 mM malate (complex II inhibitor) and 4 μM FCCP, and the mitochondria are seeded the same way as described for the coupling assay. After basal readings, the sequential injections were as follows: 2 μM rotenone (complex I inhibitor), 10 mM succinate (complex II substrate), 4 μM antimycin A (complex III inhibitor) and 10 mM/100 μM ascorbate/tetramethylphenylenediamine (complex IV substrate).

ATP synthase enzyme inhibition kinetics. ATP synthesis enzyme inhibition kinetic analysis was performed using isolated mitochondria. Mitochondria were isolated from mouse liver as described earlier. The final mitochondrial pellet was resuspended in MAS buffer supplemented with 5 mM sodium ascorbate (Sigma, A7631) and 5 mM TMPD (Sigma, T7394).

The reaction was carried out in MAS buffer containing 5 mM sodium ascorbate, 5 mM TMPD, luciferase reagent (Roche, 11699695001), octanol or octyl α-KG, variable amounts of ADP (Sigma, A2754), and 3.75 ng μl^{-1} mitochondria. ATP synthesis was monitored by the increase in luminescence over time by a luminometer (Analyst HT, Molecular Devices). ATP-synthase-independent ATP formation, derived from the oligomycin-insensitive luminescence, was subtracted as background. The initial velocity of ATP synthesis was calculated from the slope of the first 3 min of the reaction, before the velocity begins to decrease. Enzyme inhibition kinetics was analysed by nonlinear regression least-squares fit using GraphPad Prism.

Assay for mammalian TOR pathway activity. Mammalian (m)TOR pathway activity in cells treated with octyl α-KG or oligomycin was determined by the levels of phosphorylation of known mTOR substrates, including S6K (T389), 4E-BP1 (S65), AKT (S473) and ULK1 (S757)[45–49]. Specific antibodies used: phospho (P)-S6K T389 (Cell Signaling, 9234), S6K (Cell Signaling, 9202S), P-4E-BP1 S65 (Cell Signaling, 9451S), 4E-BP1 (Cell Signaling, 9452S), P-AKT S473 (Cell Signaling, 4060S), AKT (Cell Signaling, 4691S), P-ULK1 S757 (Cell Signaling, 6888), ULK1 (Cell Signaling, 4773S) and GAPDH (Santa Cruz Biotechnology, 25778).

Assay for autophagy. DA2123 animals carrying an integrated GFP::LGG-1 translational fusion gene[50–52], were used to quantify levels of autophagy. To obtain a synchronized population of DA2123, we performed an egg preparation of gravid adults (by lysing ~100 gravid worms in 70 μl M9 buffer, 25 μl bleach and 5 μl 10 N NaOH) and allowed the eggs to hatch overnight in M9, causing starvation-induced L1 diapause. L1 larvae were deposited onto NGM treatment plates containing vehicle,

8 mM α-KG or 40 μM oligomycin, and seeded with either *E. coli* OP50, HT115(DE3) with an empty vector, or HT115(DE3)-expressing dsRNAs targeting *atp-2*, *let-363* or *ogdh-1* as indicated. When the majority of animals in a given sample first reached the mid-L3 stage, individual L3 larvae were mounted onto microscope slides and anaesthetized with 1.6 mM levamisole (Sigma, 31742). Nematodes were observed using an Axiovert 200M Zeiss confocal microscope with a LSM5 Pascal laser, and images were captured using the LSM Image Examiner (Zeiss). For each specimen, GFP::LGG-1 puncta (autophagosomes) in the epidermis, including the lateral seam cells and Hyp7, were counted in three separate regions of 140.97 μm^2 using 'analyze particles' in ImageJ[53]. Measurements were made blind to both the genotype and supplement. Statistical analysis was performed using Microsoft Excel (*t*-test, two-tailed, two-sample unequal variance).

The assay for autophagy in mammalian cells was carried out as follows. HEK-293 cells were seeded in 6-well plates at 2.5×10^5 cells per well in DMEM media supplemented with 10% FBS and 10 mM glucose, and incubated overnight before treatment with either octanol (vehicle control) or octyl α-KG for 72 h. Cells were lysed in M-PER buffer with protease and phosphatase inhibitors. Lysates were subjected to SDS–PAGE on a 4–12% Bis-Tris gradient gel with MES running buffer and western blotted for LC3 (Novus, NB100-2220). LC3 is the mammalian homologue of worm LGG-1, and conversion of the soluble LC3-I to the lipidated LC3-II is activated in autophagy, for example, upon starvation[54].

Pharyngeal pumping rates of *C. elegans* treated with 8 mM α-KG. The pharyngeal pumping rates of 20 wild-type N2 worms per condition were assessed. Pharyngeal contractions were recorded for 1 min using a Zeiss M2 BioDiscovery microscope and an attached Sony NDR-XR500V video camera at 12-fold optical zoom. The resulting videos were played back at 0.3× speed using MPlayerX and pharyngeal pumps were counted. Statistical analysis was performed using Microsoft Excel (*t*-test, two-tailed, two-sample unequal variance).

Assay for α-KG levels in *C. elegans*. Synchronized adult worms were collected from plates with vehicle (H_2O) or 8 mM α-KG, washed three times with M9 buffer, and flash frozen. Worms were lysed in M9 using Lysing Matrix C tubes (MP Biomedicals, 6912-100) and the FastPrep-24 (MP Biomedicals) high-speed bench-top homogenizer in the 4 °C room (disrupt worms for 20 s at 6.5 m s^{-1}, rest on ice for 1 min; repeat three times). Lysed animals were centrifuged at 14,000 r.p.m. for 10 min at 4 °C to pellet worm debris, and the supernatant was saved. The protein concentration of the supernatant was determined by the BCA Protein Assay kit (Pierce, 23223); there was no difference in protein level per worm in α-KG-treated and vehicle-treated animals (data not shown). α-KG content was assessed as described previously[55] with modifications. Worm lysates were incubated at 37 °C in 100 mM KH_2PO_4 (pH 7.2), 10 mM NH_4Cl, 5 mM $MgCl_2$ and 0.3 mM NADH for 10 min. Glutamate dehydrogenase (Sigma, G2501) was then added to reach a final concentration of 1.83 units ml^{-1}. Under these conditions, glutamate dehydrogenase uses α-KG and NADH to make glutamate. The absorbance decrease was monitored at 340 nm. The intracellular level of α-KG was determined from the absorbance decrease in NADH. The approximate molarity of α-KG present inside the animals was estimated using average protein content (~245 ng per worm, from BCA assay) and volume (~3 nl for adult worms 1.1 mm in length and 60 μm in diameter (http://www.wormatlas.org/hermaphrodite/introduction/Introframeset.html)).

For quantitative analysis of α-KG in worms using ultra-high-performance liquid chromatography-electrospray ionization-tandem mass spectrometry (UHPLC-ESI/MS/MS), synchronized day 1 adult worms were placed on vehicle plates with or without bacteria for 24 h, and then collected and lysed in the same manner as described earlier. α-KG analysis by LC/MS/MS was carried out on an Agilent 1290 Infinity UHPLC system and 6460 Triple Quadrupole mass spectrometer (Agilent Technologies) using an electrospray ionization (ESI) source with Agilent Jet Stream technology. Data were acquired with Agilent MassHunter Data Acquisition software version B.06.00, and processed for precursor and product ions selection with MassHunter Qualitative Analysis software version B.06.00 and for calibration and quantification with MassHunter Quantitative Analysis for QQQ software version B.06.00.

For UHPLC, 3 μl calibration standards and samples were injected onto the UHPLC system including a G4220A binary pump with a built-in vacuum degasser and a thermostatted G4226A high performance autosampler. An ACQUITY UPLC BEH Amide analytical column (2.1 × 50 mm, 1.7 μm) and a VanGuard BEH Amide Pre-column (2.1 × 5 mm, 1.7 μm) from Waters Corporation were used at the flow rate of 0.6 ml min^{-1} using 50/50/0.04 acetonitrile/water/ammonium hydroxide with 10 mM ammonium acetate as mobile phase A and 95/5/0.04 acetonitrile/water/ammonium hydroxide with 10 mM ammonium acetate as mobile phase B. The column was maintained at room temperature. The following gradient was applied: 0–0.41 min: 100% B isocratic; 0.41–5.30 min: 100–30% B; 5.30–5.35 min: 30–0% B; 5.35–7.35 min: 0% B isocratic; 7.35–7.55 min: 0–100% B; 7.55–9.55 min: 100% B isocratic.

For the MS detection, the ESI mass spectra data were recorded on a negative ionization mode by MRM. MRM transitions of α-KG and its ISTD $^{13}C_4$-α-KG (Cambridge Isotope Laboratories) were determined using a 1 min 37% B isocratic UHPLC method through the column at a flow rate of 0.6 ml min^{-1}. The precursor ion of $[M-H]^-$ and the product ion of $[M-CO_2-H]^-$ were observed to have the highest signal-to-noise ratios. The precursor and product ions are respectively 145.0 and 100.9 for α-KG, and 149.0 and 104.9 for ISTD $^{13}C_4$-α-KG. Nitrogen was used as the drying, sheath and collision gas. All the source and analyser parameters were optimized using Agilent MassHunter Source and iFunnel Optimizer and Optimizer software, respectively. The source parameters are as follows: drying gas temperature 120 °C, drying gas flow 13 l min^{-1}, nebulizer pressure 55 psi, sheath gas temperature 400 °C, sheath gas flow 12 l min^{-1}, capillary voltage 2,000 V, and nozzle voltage 0 V. The analyser parameters are as follows: fragmentor voltage 55 V, collision energy 2 V and cell accelerator voltage 1 V. The UHPLC eluants before 1 min and after 5.3 min were diverted to waste.

Membrane-permeable esters of α-KG. Octyl α-KG, a commonly used membrane-permeable ester of α-KG[55–58], was used to deliver α-KG across lipid membranes in experiments using cells and mitochondria. Upon hydrolysis by cellular esterases, octyl α-KG yields α-KG and the by-product octanol. We showed that, whereas octanol control has no effect (Extended Data Fig. 2e, f and Extended Data Fig. 6a), α-KG alone can bind and inhibit ATP synthase (Fig. 2a, b and Extended Data Fig. 2a, b; data not shown), decrease ATP and OCR (Fig. 2e, g), induce autophagy (Fig. 4b) and increase *C. elegans* lifespan (Figs 1, 3, Extended Data Figs 1, 5 and Extended Data Table 2). The existence and activity of esterases in our mitochondrial and cell culture experiments have been confirmed using calcein AM (C1430, Molecular Probes), an esterase substrate that fluoresces upon hydrolysis, and also by mass spectrometry (data not shown). The hydrolysis by esterases explains why distinct esters of α-KG, such as 1-octyl α-KG, 5-octyl α-KG, and dimethyl α-KG, have similar effects to α-KG (Extended Data Fig. 2g, h and Extended Data Table 2).

Synthesis of octyl α-KG. Synthesis of 1-octyl α-KG has been previously described[59]. Briefly, 1-octanol (0.95 ml, 6.0 mmol), DMAP (37 mg, 0.3 mmol) and DCC (0.743 g, 3.6 mmol) were added to a solution of 1-cyclobutene-1-carboxylic acid (0.295 g, 3.0 mmol) in dry CH_2Cl_2 (6.0 ml) at 0 °C. After it had been stirred for 1 h, the solution was allowed to warm to room temperature and stirred for another 8 h. The precipitate was filtered and washed with ethyl acetate (3 × 100 ml). The combined organic phases were washed with water and brine, and dried over anhydrous Na_2SO_4. Flash column chromatography on silica gel eluting with 80/1 hexane/ethyl acetate gave octyl cyclobut-1-enecarboxylate as a clear oil (0.604 g, 96%). To a −78 °C solution of this oil (0.211 g, 1.0 mmol) in CH_2Cl_2 (10 ml) was bubbled O_3/O_2 until the solution turned blue. The residual ozone was discharged by bubbling with O_2 and the reaction was warmed to room temperature and stirred for another 1 h. Dimethyl sulphide (Me_2S, 0.11 ml, 1.5 mmol) was added to the mixture and it was stirred for another 2 h. The CH_2Cl_2 was removed *in vacuo* and the crude product was dissolved in a solution of 2-methyl-2-butene (0.8 ml) in *t*-BuOH (3.0 ml). To this was added dropwise a solution containing sodium chlorite (0.147 g, 1.3 mmol) and sodium dihydrogen phosphate monohydrate (0.179 g, 1.3 mmol) in H_2O (1.0 ml). The mixture was stirred at room temperature overnight, and then extracted with ethyl acetate (3 × 50 ml). The combined organic phases were washed with water and brine, and dried over anhydrous Na_2SO_4. Flash column chromatography on silica gel eluting with 5/1 hexane/ethyl acetate gave octyl α-KG, which became a pale solid when stored in the refrigerator (0.216 g, 84%).

Synthesis of 5-octyl L-glutamate. L-Glutamic acid (0.147 g, 1.0 mmol) and anhydrous sodium sulphate (0.1 g) was dissolved in octanol (2.0 ml), and then tetrafluoroboric acid–dimethyl ether complex (0.17 ml) was added. The suspended mixture was stirred at 21 °C overnight. Anhydrous THF (5 ml) was added to the mixture and it was filtered through a thick pad of activated charcoal. Anhydrous triethylamine (0.4 ml) was added to the clear filtrate to obtain a milky white slurry. Upon trituration with ethyl acetate (10 ml), the monoester monoacid precipitated. The precipitate was collected, washed with additional ethyl acetate (2 × 5 ml), and dried *in vacuo* to give the desired product, 5-octyl L-glutamate (0.249 g, 96%) as a white solid. ^1H NMR (500 MHz, acetic acid-d_4): δ 4.12 (dd, $J = 6.6, 6.6$ Hz, 1H), 4.11 (t, $J = 6.8$ Hz, 2H), 2.64 (m, 2H), 2.26 (m, 2H), 1.64 (m, 2H), 1.30 (m, 10H), 0.89 (t, $J = 7.0$ Hz, 3H). ^{13}C NMR (125 MHz, acetic acid-d_4): δ 175.0, 174.3, 66.3, 55.0, 32.7, 30.9, 30.11, 30.08, 29.3, 26.7, 26.3, 23.4, 14.4.

Synthesis of 5-octyl D-glutamate. The synthesis of the opposite enantiomer, that is, 5-octyl D-glutamate, was carried out by the exact same procedure starting with D-glutamic acid. The spectroscopic data was identical to that of the enantiomeric compound.

Synthesis of 5-octyl α-KG. 1-Benzyl 5-octyl 2-oxopentanedioate was obtained as follows. To a solution of 5-octyl L-glutamate (0.249 g) in H_2O (6.0 ml) and acetic acid (2.0 ml) cooled to 0 °C was added slowly a solution of aqueous sodium nitrite (0.207 g, 3.0 mmol in 4 ml H_2O). The reaction mixture was allowed to warm slowly to room temperature and was stirred overnight. The mixture was concentrated.

The resulting residue was dissolved in DMF (10 ml) and $NaHCO_3$ (0.42 g, 5.0 mmol) and benzyl bromide (0.242 ml, 2.0 mmol) were added to the mixture. The mixture was stirred at 21 °C overnight and then extracted with ethyl acetate (3 × 30 ml). The combined organic phase was washed with water and brine and dried over anhydrous $MgSO_4$. Flash column chromatography on silica gel eluting with 7/1 hexanes/ethyl acetate gave the mixed diester 1-benzyl 5-octyl (*S*)-2-hydroxypentanedioate as a colourless oil. To this oil, dissolved in dichloromethane (10.0 ml), were added $NaHCO_3$ (0.42 g, 5.0 mmol) and Dess–Martin periodinane (0.509 g, 1.2 mmol), and the mixture was stirred at room temperature for 1 h and then extracted with ethyl acetate (3 × 30 ml). The combined organic phase was washed with water and brine and dried over anhydrous $MgSO_4$. Flash column chromatography on silica gel eluting with 5/1 hexanes/ethyl acetate gave the desired 1-benzyl 5-octyl 2-oxopentanedioate (0.22 g, 66%) as a white solid. ^{1}H NMR (500 MHz, $CDCl_3$): δ 7.38 (m, 5H), 5.27 (s, 2H), 4.05 (t, J = 6.5 Hz, 2H), 3.14 (t, J = 6.5 Hz, 2H), 2.64 (t, J = 6.5 Hz, 2H), 1.59 (m, 2H), 1.28 (m, 10H), 0.87 (t, J = 7.0 Hz, 3H). ^{13}C NMR (125 MHz, $CDCl_3$): δ 192.2, 171.9, 160.1, 134.3, 128.7, 128.6, 128.5, 67.9, 65.0, 34.2, 31.7, 29.07, 29.05, 28.4, 27.5, 25.7, 22.5, 14.0.

5-Octyl α-KG (5-(octyloxy)-2,5-dioxopentanoic acid) was obtained as follows. To a solution of 1-benzyl 5-octyl 2-oxopentanedioate (0.12 g, 0.344 mmol) in ethyl acetate (15 ml) was added 5% Pd/C (80 mg). Over the mixture was passed a stream of argon and then the argon was replaced with hydrogen gas and the mixture was stirred vigorously for 15 min. The mixture was filtered through a thick pad of Celite to give the desired product 5-octyl α-KG (0.088 g, 99%) as white solid. ^{1}H NMR (500 MHz, $CDCl_3$): δ 8.16 (br s, 1H), 4.06 (t, J = 6.5 Hz, 2H), 3.18 (t, J = 6.5 Hz, 2H), 2.69 (t, J = 6.0 Hz, 2H), 1.59 (m, 2H), 1.26 (m, 10H), 0.85 (t, J = 7.0 Hz, 3H). ^{13}C NMR (125 MHz, $CDCl_3$): δ 193.8, 172.7, 160.5, 65.5, 33.0, 31.7, 29.08, 29.06, 28.4, 27.8, 25.8, 22.5, 14.0.

31. Brenner, S. The genetics of *Caenorhabditis elegans*. *Genetics* **77,** 71–94 (1974).
32. Timmons, L. & Fire, A. Specific interference by ingested dsRNA. *Nature* **395,** 854 (1998).
33. Long, X. *et al.* TOR deficiency in *C. elegans* causes developmental arrest and intestinal atrophy by inhibition of mRNA translation. *Curr. Biol.* **12,** 1448–1461 (2002).
34. Sutphin, G. L. & Kaeberlein, M. Measuring *Caenorhabditis elegans* life span on solid media. *J. Vis. Exp.* **27,** 1152 (2009).
35. Gaudet, J. & Mango, S. E. Regulation of organogenesis by the *Caenorhabditis elegans* FoxA protein PHA-4. *Science* **295,** 821–825 (2002).
36. Abada, E. A. *et al. C. elegans* behavior of preference choice on bacterial food. *Mol. Cells* **28,** 209–213 (2009).
37. Lomenick, B., Jung, G., Wohlschlegel, J. A. & Huang, J. Target identification using drug affinity responsive target stability (DARTS). *Curr. Protoc. Chem. Biol.* **3,** 163–180 (2011).
38. Lomenick, B., Olsen, R. W. & Huang, J. Identification of direct protein targets of small molecules. *ACS Chem. Biol.* **6,** 34–46 (2011).
39. Stubbs, C. J. *et al.* Application of a proteolysis/mass spectrometry method for investigating the effects of inhibitors on hydroxylase structure. *J. Med. Chem.* **52,** 2799–2805 (2009).
40. Rogers, G. W. *et al.* High throughput microplate respiratory measurements using minimal quantities of isolated mitochondria. *PLoS ONE* **6,** e21746 (2011).
41. Alberts, B. *Molecular Biology of the Cell* 3rd edn (Garland, 1994).
42. Wu, M. *et al.* Multiparameter metabolic analysis reveals a close link between attenuated mitochondrial bioenergetic function and enhanced glycolysis dependency in human tumor cells. *Am. J. Physiol. Cell Physiol.* **292,** C125–C136 (2007).
43. Yamamoto, H. *et al.* NCoR1 is a conserved physiological modulator of muscle mass and oxidative function. *Cell* **147,** 827–839 (2011).
44. Pathare, P. P., Lin, A., Bornfeldt, K. E., Taubert, S. & Van Gilst, M. R. Coordinate regulation of lipid metabolism by novel nuclear receptor partnerships. *PLoS Genet.* **8,** e1002645 (2012).
45. Pullen, N. & Thomas, G. The modular phosphorylation and activation of p70s6k. *FEBS Lett.* **410,** 78–82 (1997).
46. Burnett, P. E., Barrow, R. K., Cohen, N. A., Snyder, S. H. & Sabatini, D. M. RAFT1 phosphorylation of the translational regulators p70 S6 kinase and 4E-BP1. *Proc. Natl Acad. Sci. USA* **95,** 1432–1437 (1998).
47. Gingras, A. C. *et al.* Hierarchical phosphorylation of the translation inhibitor 4E-BP1. *Genes Dev.* **15,** 2852–2864 (2001).
48. Sarbassov, D. D., Guertin, D. A., Ali, S. M. & Sabatini, D. M. Phosphorylation and regulation of Akt/PKB by the rictor-mTOR complex. *Science* **307,** 1098–1101 (2005).
49. Kim, J., Kundu, M., Viollet, B. & Guan, K. L. AMPK and mTOR regulate autophagy through direct phosphorylation of Ulk1. *Nature Cell Biol.* **13,** 132–141 (2011).
50. Kang, C., You, Y. J. & Avery, L. Dual roles of autophagy in the survival of *Caenorhabditis elegans* during starvation. *Genes Dev.* **21,** 2161–2171 (2007).
51. Hansen, M. *et al.* A role for autophagy in the extension of lifespan by dietary restriction in *C. elegans*. *PLoS Genet.* **4,** e24 (2008).
52. Alberti, A., Michelet, X., Djeddi, A. & Legouis, R. The autophagosomal protein LGG-2 acts synergistically with LGG-1 in dauer formation and longevity in *C. elegans*. *Autophagy* **6,** 622–633 (2010).
53. Schneider, C. A., Rasband, W. S. & Eliceiri, K. W. NIH Image to ImageJ: 25 years of image analysis. *Nature Methods* **9,** 671–675 (2012).
54. Kabeya, Y. *et al.* LC3, a mammalian homologue of yeast Apg8p, is localized in autophagosome membranes after processing. *EMBO J.* **19,** 5720–5728 (2000).
55. MacKenzie, E. D. *et al.* Cell-permeating α-ketoglutarate derivatives alleviate pseudohypoxia in succinate dehydrogenase-deficient cells. *Mol. Cell. Biol.* **27,** 3282–3289 (2007).
56. Zhao, S. *et al.* Glioma-derived mutations in IDH1 dominantly inhibit IDH1 catalytic activity and induce HIF-1α. *Science* **324,** 261–265 (2009).
57. Xu, W. *et al.* Oncometabolite 2-hydroxyglutarate is a competitive inhibitor of α-ketoglutarate-dependent dioxygenases. *Cancer Cell* **19,** 17–30 (2011).
58. Jin, G. *et al.* Disruption of wild-type IDH1 suppresses D-2-hydroxyglutarate production in IDH1-mutated gliomas. *Cancer Res.* **73,** 496–501 (2013).
59. Jung, M. E. & Deng, G. Synthesis of the 1-monoester of 2-ketoalkanedioic acids, for example, octyl α-ketoglutarate. *J. Org. Chem.* **77,** 11002–11005 (2012).

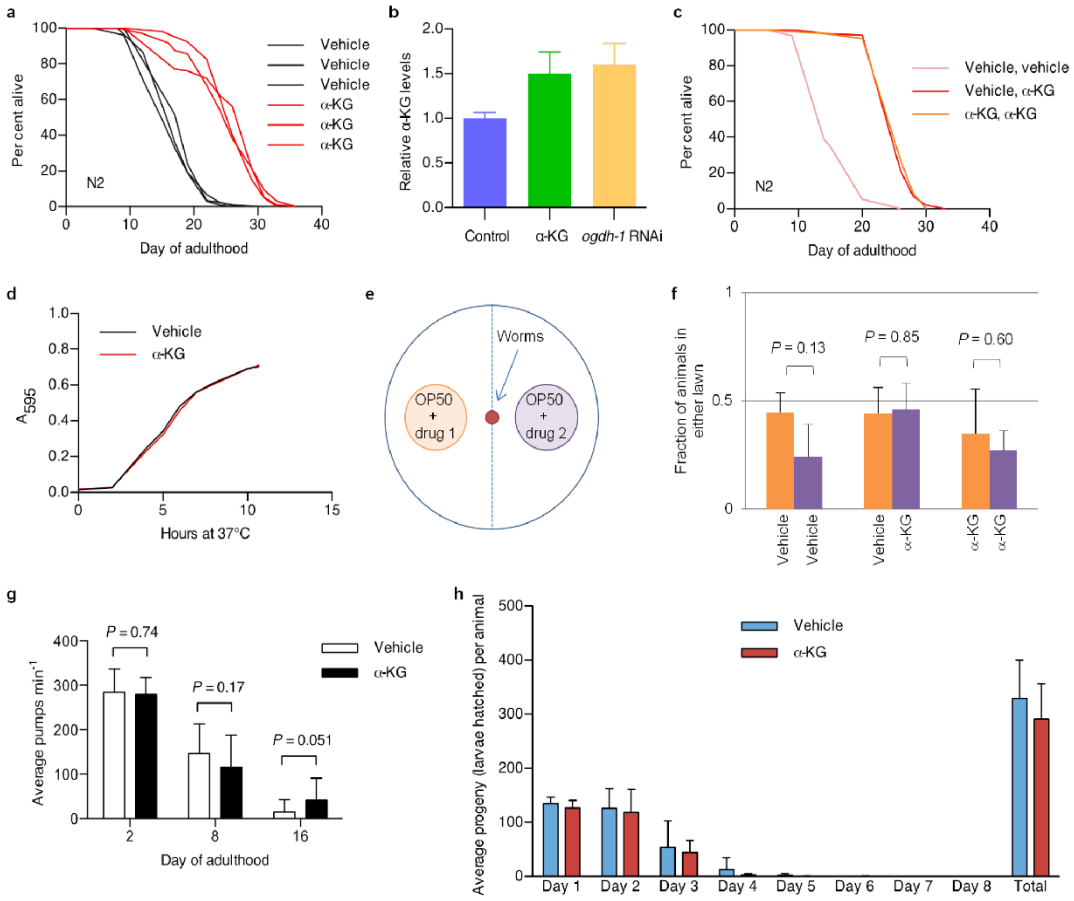

Extended Data Figure 1 | Supplementation with α-KG extends *C. elegans* adult lifespan but does not change the growth rate of bacteria, or food intake, pharyngeal pumping rate or brood size of the worms. **a**, Robust lifespan extension in adult *C. elegans* by α-KG. 8 mM α-KG increased the mean lifespan of N2 by an average of 47.3% in three independent experiments ($P < 0.0001$ for every experiment, by log-rank test). Experiment 1, mean lifespan (days of adulthood) with vehicle treatment (m_{veh}) = 18.9 ($n = 87$ animals tested), $m_{\alpha\text{-KG}} = 25.8$ ($n = 96$); experiment 2, $m_{veh} = 17.5$ ($n = 119$), $m_{\alpha\text{-KG}} = 25.4$ ($n = 97$); experiment 3, $m_{veh} = 16.3$ ($n = 100$), $m_{\alpha\text{-KG}} = 26.1$ ($n = 104$). **b**, Worms supplemented with 8 mM α-KG and worms with RNAi knockdown of α-KGDH (encoded by *ogdh-1*) have increased α-KG levels. Young adult worms were placed on treatment plates seeded with control HT115 *E. coli* or HT115-expressing *ogdh-1* dsRNA, and α-KG content was assayed after 24 h (see Methods). **c**, α-KG treatment beginning at the egg stage and that beginning in adulthood produced identical lifespan increases. Light red, treatment with vehicle control throughout larval and adult stages ($m = 15.6$, $n = 95$); dark red, treatment with vehicle during larval stages and with 8 mM α-KG at adulthood ($m = 26.3$, $n = 102$), $P < 0.0001$ (log-rank test); orange, treatment with 8 mM α-KG throughout larval and adult stages ($m = 26.3$, $n = 102$), $P < 0.0001$ (log-rank test). **d**, α-KG does not alter the growth rate of the OP50 *E. coli*, which is the standard laboratory food source for nematodes. α-KG (8 mM) or vehicle (H_2O) was added to standard LB media and the pH was adjusted to 6.6 by the addition of NaOH. Bacterial cells from the same overnight OP50 culture were added to the LB ± α-KG mixture at a 1:40 dilution, and then placed in the 37 °C incubator shaker at 300 r.p.m. The absorbance at 595 nm was read at 1 h time intervals to generate the growth curve. **e**, Schematic representation of food preference assay. **f**, N2 worms show no preference between OP50 *E. coli* food treated with vehicle or α-KG ($P = 0.85$, by *t*-test, two-tailed, two-sample unequal variance), nor preference between identically treated OP50 *E. coli*. **g**, Pharyngeal pumping rate of *C. elegans* on 8 mM α-KG is not significantly altered (by *t*-test, two-tailed, two-sample unequal variance). **h**, Brood size of *C. elegans* treated with 8 mM α-KG. Brood size analysis was conducted at 20 °C. Ten L4 wild-type worms were each singly placed onto an NGM plate containing vehicle or 8 mM α-KG. Worms were transferred one per plate onto a new plate every day, and the eggs laid were allowed to hatch and develop on the previous plate. Hatchlings were counted as a vacuum was used to remove them from the plate. Animals on 8 mM α-KG showed no significant difference in brood size compared with animals on vehicle plates ($P = 0.223$, by *t*-test, two-tailed, two-sample unequal variance). Mean ± s.d. is plotted in all cases.

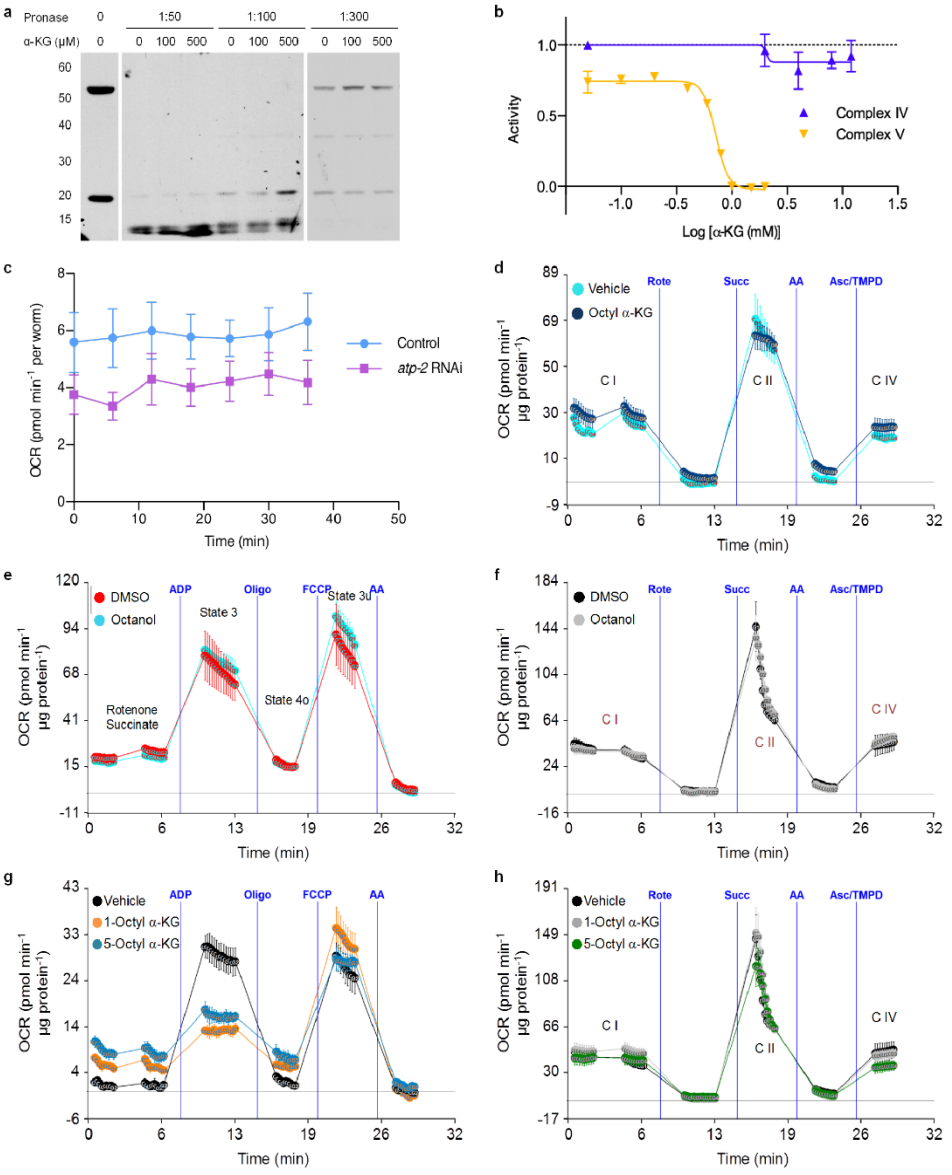

Extended Data Figure 2 | α-KG binds to the β subunit of ATP synthase and inhibits the activity of complex V but not the other ETC complexes. **a**, Western blot showing protection of the ATP-2 protein from Pronase digestion upon α-KG binding in the DARTS assay. The antibody for human ATP5B (Sigma, AV48185) recognizes the epitope $_{144}$IMNVIGEPIDERGPIKT KQFAPIHAEAPEFMEMSVEQEILVTGIKVVDLL$_{193}$ that has 90% identity to the *C. elegans* ATP-2. The lower molecular weight band near 20 kDa is a proteolytic fragment of the full-length protein corresponding to the domain directly bound by α-KG. **b**, α-KG does not affect complex IV activity. Complex IV activity was assayed using the MitoTox OXPHOS Complex IV Activity Kit (Abcam, ab109906). Relative complex IV activity was compared to vehicle (H_2O) controls. Potassium cyanide (Sigma, 60178) was used as a positive control for the assay. Complex V activity was assayed using the MitoTox Complex V OXPHOS Activity Microplate Assay (Abcam, ab109907). **c**, *atp-2* RNAi worms have lower oxygen consumption compared to control (*gfp* in RNAi vector), $P < 0.0001$ (*t*-test, two-tailed, two-sample unequal variance) for the entire time series (two independent experiments); similar to α-KG-treated worms shown in Fig. 2g. **d**, α-KG does not affect the electron flow through the ETC. Oxygen consumption rate (OCR) from isolated mouse liver mitochondria at basal (pyruvate and malate as complex I substrate and complex II inhibitor, respectively, in the presence of FCCP) and in response to sequential injection of rotenone (Rote; complex I inhibitor), succinate (Succ; complex II substrate), antimycin A (AA; complex III inhibitor), ascorbate/tetramethylphenylenediamine (Asc/TMPD; cytochrome *c* (complex IV) substrate). No difference in complex I (C I), complex II (C II) or complex IV (C IV) respiration was observed after 30 min treatment with 800 μM octyl α-KG, whereas complex V was inhibited (see Fig. 2h) by the same treatment (two independent experiments). **e**, **f**, No significant difference in coupling (**e**) or electron flow (**f**) was observed with either octanol or DMSO vehicle control. **g**, **h**, Treatment with 1-octyl α-KG or 5-octyl α-KG gave identical results in coupling (**g**) or electron flow (**h**) assays. Mean ± s.d. is plotted in all cases.

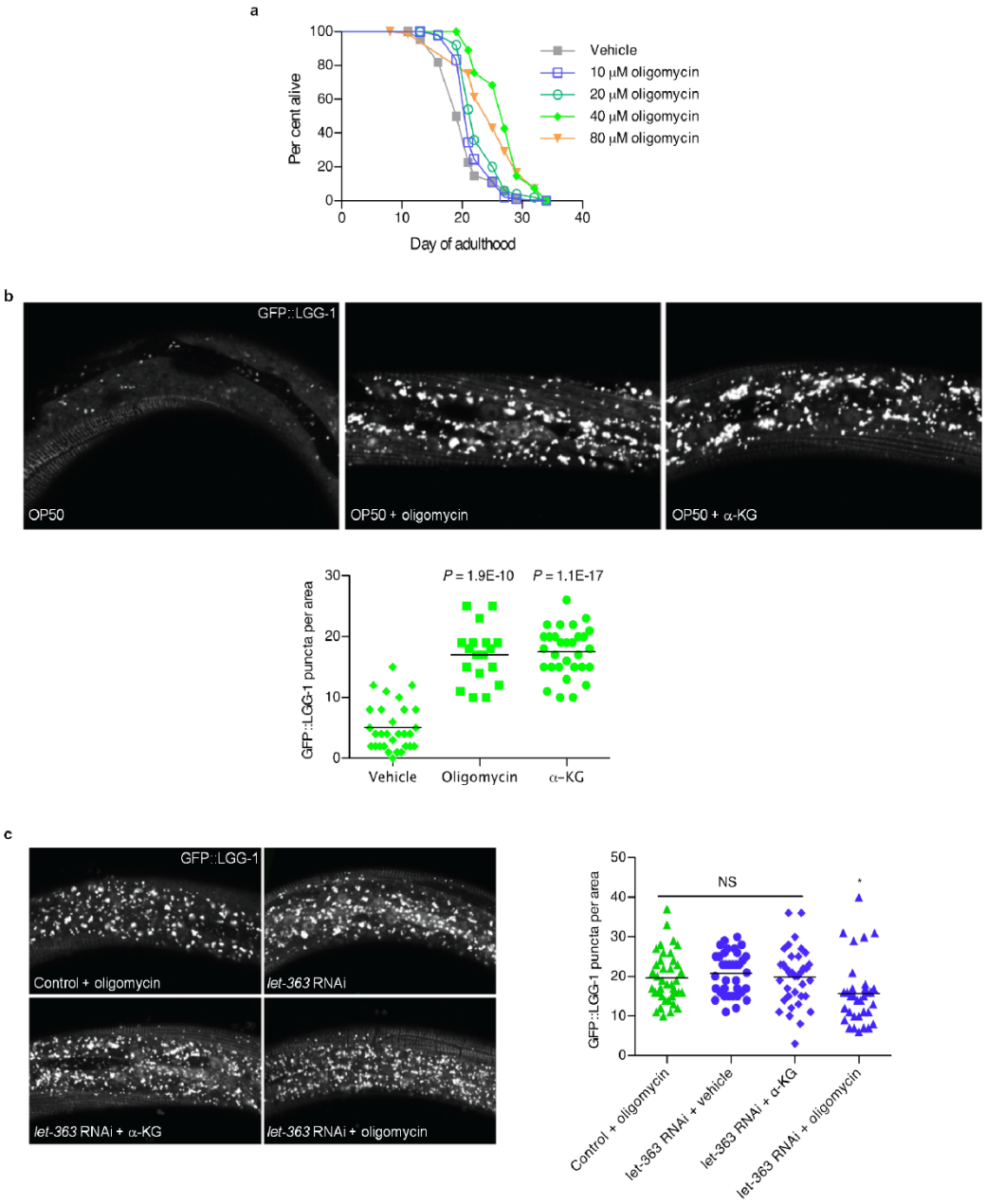

Extended Data Figure 3 | Treatment with oligomycin extends *C. elegans* lifespan and enhances autophagy in a manner dependent on *let-363*. **a**, Oligomycin extends the lifespan of adult *C. elegans* in a concentration-dependent manner. Treatment with oligomycin began at the young adult stage. 40 μM oligomycin increased the mean lifespan of N2 worms by 32.3% ($P < 0.0001$, by log-rank test); see Extended Data Table 2 for details. **b**, Confocal images of GFP::LGG-1 puncta in L3 epidermis of *C. elegans* with vehicle, oligomycin (40 μM) or α-KG (8 mM), and number of GFP::LGG-1-containing puncta quantified using ImageJ. Bars indicate the mean. Autophagy in *C. elegans* treated with oligomycin or α-KG is significantly higher than in vehicle-treated control animals (*t*-test, two-tailed, two-sample unequal variance). **c**, There is no significant difference (NS) between control worms treated with oligomycin and *let-363* RNAi worms treated with vehicle, nor between vehicle- and α-KG-treated *let-363* RNAi worms, consistent with independent experiments in Fig. 4b, c; also, oligomycin does not augment autophagy in *let-363* RNAi worms (if anything, there may be a small decrease, as indicated by an asterisk); by *t*-test, two-tailed, two-sample unequal variance. Bars indicate the mean. Photographs were taken at ×100 magnification.

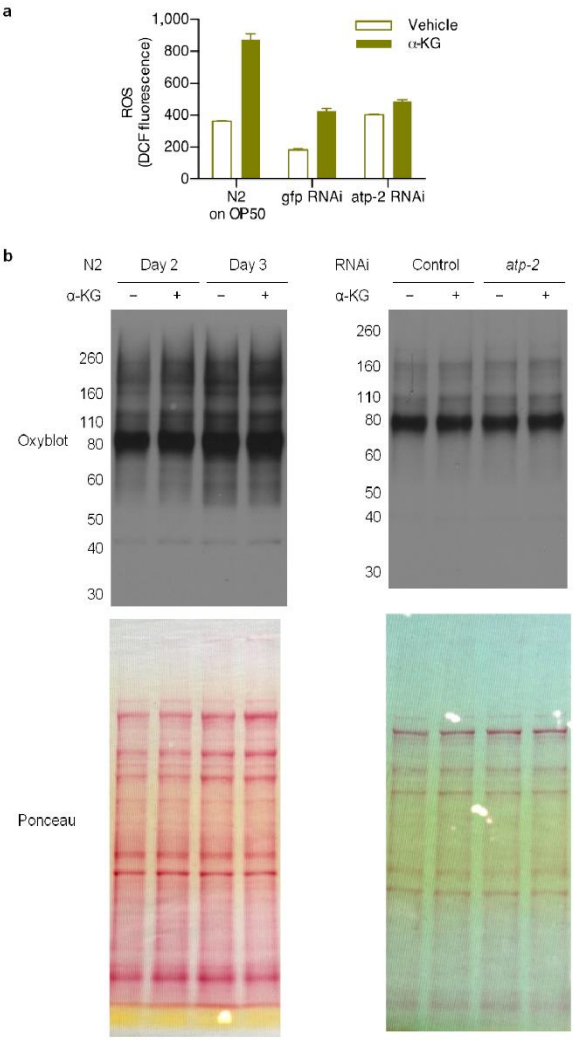

Extended Data Figure 4 | Analyses of oxidative stress in worms treated with α-KG or *atp-2* RNAi. **a**, The *atp*-2 RNAi worms have higher levels of 2′,7′-dichlorofluorescein (DCF) fluorescence than *gfp* control worms ($P < 0.0001$, by *t*-test, two-tailed, two-sample unequal variance). Supplementation with α-KG also leads to higher DCF fluorescence, in both HT115- (for RNAi) and OP50-fed worms ($P = 0.0007$ and $P = 0.0012$, respectively). Reactive oxygen species (ROS) levels were measured using 2′, 7′-dichlorodihydrofluorescein diacetate (H_2DCF-DA). As whole worm lysates were used, total cellular oxidative stress was measured here. H_2DCF-DA (Molecular Probes, D399) was dissolved in ethanol to a stock concentration of 1.5 mg ml^{-1}. Fresh stock was prepared every time before use. For measuring ROS in worm lysates, a working concentration of H_2DCF-DA at 30 ng ml^{-1} was hydrolysed by 0.1 M NaOH at room temperature for 30 min to generate 2′,7′-dichlorodihydrofluorescein (DCFH) before mixing with whole worm lysates in a black 96-well plate (Greiner Bio-One). Oxidation of DCFH by ROS yields the highly fluorescent DCF. DCF fluorescence was read at excitation/emission of 485/530 nm using SpectraMax MS (Molecular Devices). H_2O_2 was used as positive control (data not shown). To prepare the worm lysates, synchronized young adult animals were cultivated on plates containing vehicle or 8 mM α-KG and OP50 or HT115 *E. coli* for 1 day, and then collected and lysed as described in Methods. Mean ± s.d. is plotted. **b**, There was no significant change in protein oxidation upon α-KG treatment or *atp-2* RNAi. Oxidized protein levels were determined by OxyBlot. Synchronized young adult N2 animals were placed onto plates containing vehicle or 8 mM α-KG, and seeded with OP50 or HT115 bacteria that expressed control or *atp-2* dsRNA. Adult day 2 and day 3 worms were collected and washed four times with M9 buffer, and then stored at −80 °C for at least 24 h. Laemmli buffer (Biorad, 161-0737) was added to every sample and animals were lysed by alternate boil/freeze cycles. Lysed animals were centrifuged at 14,000 r.p.m. for 10 min at 4 °C to pellet worm debris, and supernatant was collected for OxyBlot analysis. Protein concentration of samples was determined by the 660 nm Protein Assay (Thermo Scientific, 1861426) and normalized for all samples. Carbonylation of proteins in each sample was detected using the OxyBlot Protein Oxidation Detection Kit (Millipore, S7150).

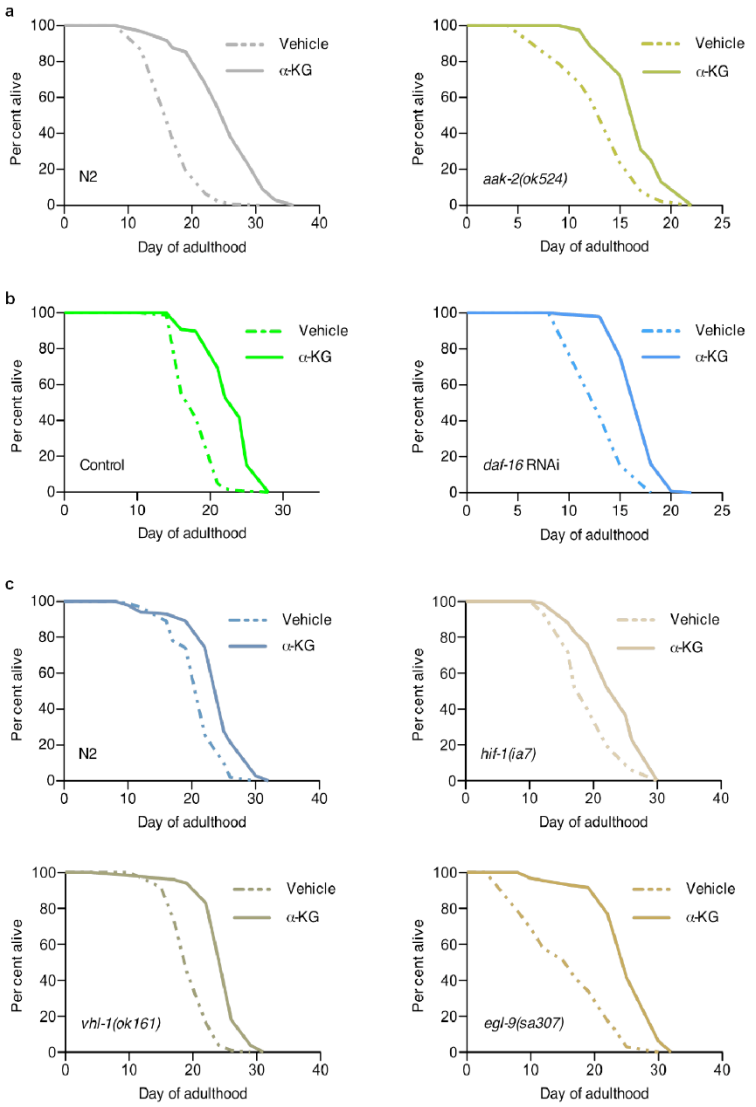

Extended Data Figure 5 | Lifespan extension by α-KG in the absence of *aak-2, daf-16, hif-1, vhl-1* or *egl-9*. **a**, Lifespans of α-KG-supplemented N2 worms, $m_{veh} = 17.5$ ($n = 119$), $m_{\alpha\text{-KG}} = 25.4$ ($n = 97$), $P < 0.0001$; or *aak-2(ok524)* mutants, $m_{veh} = 13.7$ ($n = 85$), $m_{\alpha\text{-KG}} = 17.1$ ($n = 83$), $P < 0.0001$. **b**, N2 worms fed *gfp* RNAi control, $m_{veh} = 18.5$ ($n = 101$), $m_{\alpha\text{-KG}} = 23.1$ ($n = 98$), $P < 0.0001$; or *daf-16* RNAi, $m_{veh} = 14.3$ ($n = 99$), $m_{\alpha\text{-KG}} = 17.6$ ($n = 99$), $P < 0.0001$. **c**, N2 worms, $m_{veh} = 21.5$ ($n = 101$), $m_{\alpha\text{-KG}} = 24.6$ ($n = 102$), $P < 0.0001$; *hif-1(ia7)* mutants, $m_{veh} = 19.6$ ($n = 102$), $m_{\alpha\text{-KG}} = 23.6$ ($n = 101$), $P < 0.0001$; *vhl-1(ok161)* mutants, $m_{veh} = 20.0$ ($n = 98$), $m_{\alpha\text{-KG}} = 24.9$ ($n = 100$), $P < 0.0001$; or *egl-9(sa307)* mutants, $m_{veh} = 16.2$ ($n = 97$), $m_{\alpha\text{-KG}} = 25.6$ ($n = 96$), $P < 0.0001$. *P* values were determined by the log-rank test. Number of independent experiments: N2 (8), *hif-1* (5), *vhl-1* (1) and *egl-9* (2); see Extended Data Table 2 for details. Two different *hif-1* mutant alleles[27] have been used: *ia4* (shown in Fig. 3g) is a deletion over several introns and exons; *ia7* (shown here) is an early stop codon, causing a truncated protein. Both alleles have the same effect on lifespan[27]. We tested both alleles for α-KG longevity and obtained the same results.

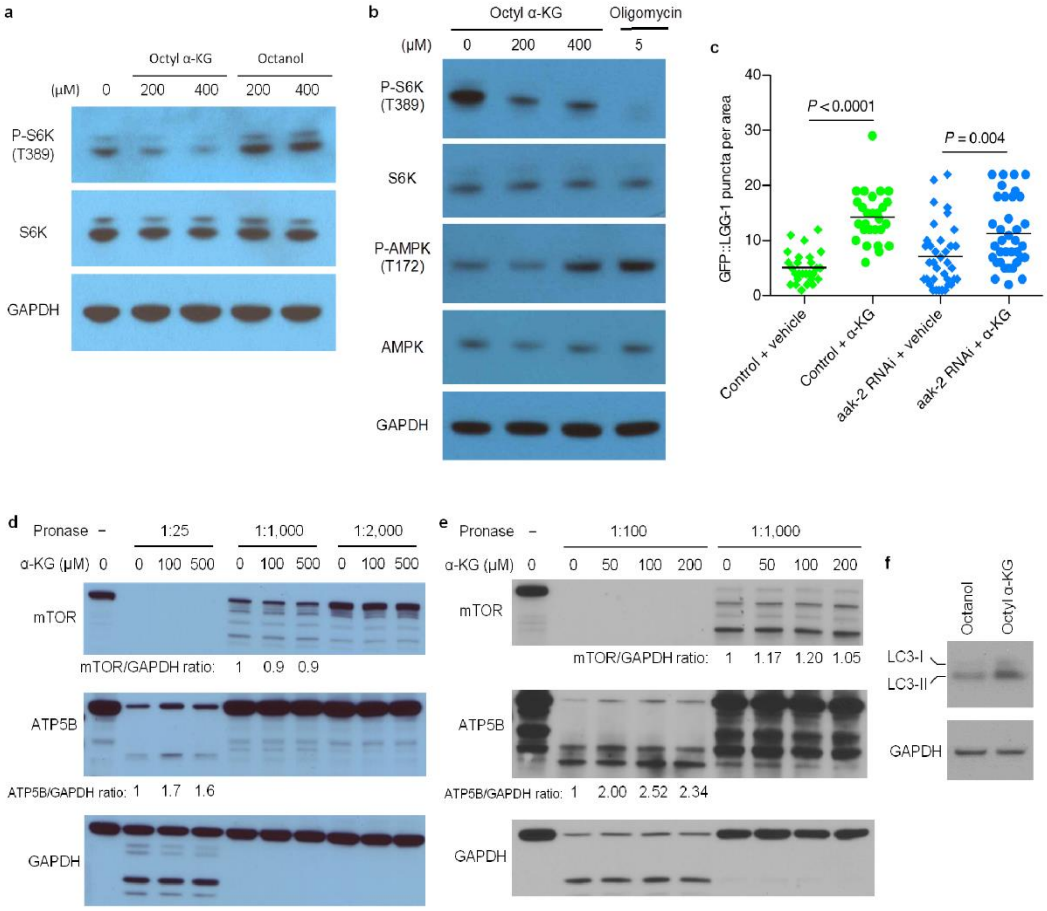

Extended Data Figure 6 | α-KG decreases TOR pathway activity but does not directly interact with TOR. **a**, Phosphorylation of S6K (T389) was decreased in U87 cells treated with octyl α-KG, but not in cells treated with octanol control. The same results were obtained using HEK-293 and MEF cells. **b**, Phosphorylation of AMPK(T172) is upregulated in WI-38 cells upon complex V inhibition by α-KG, consistent with decreased ATP content in α-KG-treated cells and animals. However, this activation of AMPK appears to require more severe complex V inhibition than the inactivation of mammalian TOR, as either oligomycin or a higher concentration of octyl α-KG was required for increasing phospho (P)-AMPK whereas concentrations of octyl α-KG comparable to those that decreased cellular ATP content (Fig. 2d) or oxygen consumption (Fig. 2f) were also sufficient for decreasing P-S6K. The same results were obtained using U87 cells. Samples were subjected to SDS–PAGE on 4–12% Bis-Tris gradient gel (Invitrogen, NP0322BOX) and western blotted with specific antibodies against P-AMPK T172 (Cell Signaling, 2535S) and AMPK (Cell Signaling, 2603S). **c**, α-KG still induces autophagy in *aak-2* RNAi worms; $^{**}P < 0.01$ (*t*-test, two-tailed, two-sample unequal variance). The number of GFP::LGG-1 containing puncta was quantified using ImageJ. Bars indicate the mean. **d**, **e**, α-KG does not bind to TOR directly as determined by DARTS. HEK-293 (**d**) or HeLa (**e**) cells were lysed in M-PER buffer (Thermo Scientific, 78501) with the addition of protease inhibitors (Roche, 11836153001) and phosphatase inhibitors (50 mM NaF, 10 mM β-glycerophosphate, 5 mM sodium pyrophosphate, 2 mM Na_3VO_4). Protein concentration of the lysate was measured by BCA Protein Assay kit (Pierce, 23227). Chilled TNC buffer (50 mM Tris-HCl pH 8.0, 50 mM NaCl, 10 mM $CaCl_2$) was added to the protein lysate, and the protein lysate was then incubated with vehicle control (DMSO) or varying concentrations of α-KG for 1 h (**d**) or 3 h (**e**) at room temperature. Pronase (Roche, 10165921001) digestions were performed for 20 min at room temperature, and stopped by adding SDS loading buffer and immediately heating at 95 °C for 5 min (**d**) or 70 °C for 10 min (**e**). Samples were subjected to SDS–PAGE on 4–12% Bis-Tris gradient gel (Invitrogen, NP0322BOX) and western blotted with specific antibodies against ATP5B (Santa Cruz, sc58618), mammalian TOR (Cell Signaling, 2972) or GAPDH (Ambion, AM4300). ImageJ was used to quantify the mammalian TOR/GAPDH and ATP5B/GAPDH ratios. Susceptibility of the mammalian TOR protein to Pronase digestion is unchanged in the presence of α-KG, whereas, as expected, Pronase resistance in the presence of α-KG is increased for ATP5B, which we identified as a new binding target of α-KG. **f**, Increased autophagy in HEK-293 cells treated with octyl α-KG was confirmed by western blot analysis of MAP1 LC3 (Novus, NB100-2220), consistent with decreased phosphorylation of the autophagy-initiating kinase ULK1 (Fig. 4a).

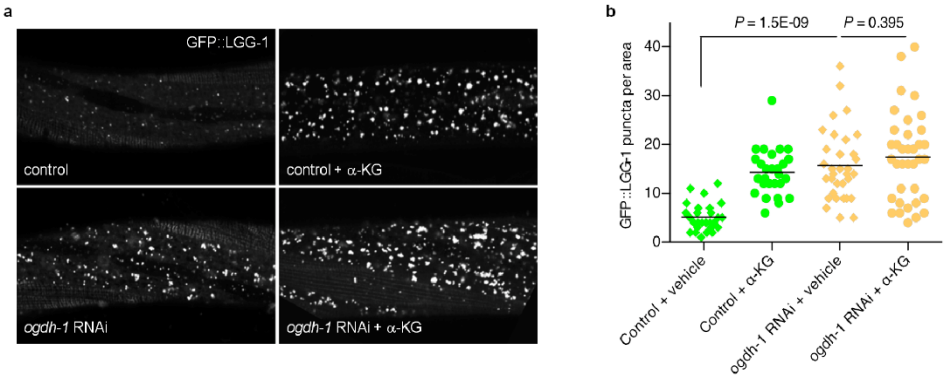

Extended Data Figure 7 | Autophagy is enhanced in *C. elegans* treated with *ogdh-1* RNAi. **a**, Confocal images of GFP::LGG-1 puncta in the epidermis of mid-L3 stage, control or *ogdh-1* knockdown *C. elegans* treated with vehicle or α-KG (8 mM). **b**, Number of GFP::LGG-1 puncta quantified using ImageJ. Bars indicate the mean. *ogdh-1* RNAi worms have significantly higher autophagy levels, and α-KG does not significantly augment autophagy in *ogdh-1* RNAi worms (*t*-test, two-tailed, two-sample unequal variance). Photographs were taken at ×100 magnification.

Extended Data Table 1 | Enriched proteins in the α-KG DARTS sample

Protein Symbol	Protein Name	Score	Control sample		α-KG sample		Enrichment
			Spectra	Peptides	Spectra	Peptides	
ATP5B	ATP synthase subunit beta	4088	23	9	121	15	5.3
HSPD1	60 kDa heat shock protein	2352	31	11	138	29	4.5
PKM2	Pyruvate kinase isozymes M1/M2	2203			56	7	
LCP1	Plastin-2	1865	14	8	76	13	5.4
ATP5A1	ATP synthase subunit alpha	1616	41	9	61	12	1.5
SHMT2	Serine hydroxymethyltransferase	1060	7	5	33	10	4.7
HSP90AA1	Heat shock protein HSP 90-alpha	952	29	8	44	8	1.5
EEF2	Elongation factor 2	943	4	2	37	9	9.3
DDX5	Probable ATP-dependent RNA helicase DDX5	652	7	3	33	10	4.7
HSPA8	Heat shock cognate 71 kDa protein	615	4	2	35	10	8.8

Only showing those proteins with at least 15 spectra in α-KG sample and enriched at least 1.5 fold.

Extended Data Table 2 | Summary of lifespan data

Strain	*m* (mean lifespan, days)		% difference	*P*-value	*n* (number of animals)	
	Vehicle	α-KG			Vehicle	α-KG
N2	18.9	25.8	36.3	< 0.0001	87	96
N2	17.5	25.4	45.6	< 0.0001	119	97
N2	16.3	26.1	60.2	< 0.0001	100	104
eat-2(ad1116)	22.8	22.9	0.5	0.79	59	40
daf-16(mu86)	16.3	18.8	15.1	< 0.0001	106	105
eat-2(ad1116)	21.1	24.0	13.4	0.23	39	59
daf-2(e1370)	38.0	47.6	25.1	< 0.0001	72	69
N2	13.2	22.3	69.8	< 0.0001	100	104
daf-16(mu86)	13.4	17.4	29.5	< 0.0001	71	72
daf-16 RNAi	14.3	17.6	22.9	< 0.0001	99	99
N2	16.1	19.1	19.3	0.0003	97	96
daf-2(e1370)	38.3	43.9	14.6	< 0.0001	109	101
aak-2(ok524)	13.7	17.1	24.3	< 0.0001	85	83
aak-2(ok524)	16.4	17.5	6.7	< 0.0001	97	97
aak-2 RNAi	16.2	19.9	23.3	< 0.0001	93	92
N2	15.6	26.3	68.8	< 0.0001	95	102
N2	15.6	26.3	68.5	< 0.0001	95	102
egl-9(sa307)	16.2	25.6	58.6	< 0.0001	97	96
egl-9(sa307)	19.5	27.3	40.3	< 0.0001	95	101
N2	14.7	21.6	46.9	< 0.0001	100	88
N2	14.0	20.7	47.9	< 0.0001	112	114
N2	21.5	24.6	14.6	< 0.0001	101	102
hif-1(ia4)	20.5	26.0	26.5	< 0.0001	85	71
hif-1(ia7)	19.6	23.6	20.4	< 0.0001	102	101
hif-1(ia4)	21.5	24.7	14.7	< 0.0001	88	87
N2	16.7	23.4	39.7	< 0.0001	104	103
N2	15.8	22.2	40.5	< 0.0001	104	94
N2	18.4	24.6	33.4	< 0.0001	99	89
vhl-1(ok161)	20.0	25.0	24.9	< 0.0001	98	100
hif-1(ia7)	12.4	17.3	38.9	< 0.0001	97	90
hif-1(ia7)	17.9	23.7	32.0	< 0.0001	58	55
N2	16.8	22.4	32.7	< 0.0001	104	101
N2	15.7	21.6	37.6	< 0.0001	85	99
smg-1(cc546ts)	18.4	23.8	29.5	< 0.0001	110	87
smg-1(cc546ts);pha-4(zu225)	14.2	13.5	-4.9	0.5482	94	109
smg-1(cc546ts);pha-4(zu225)	17.6	15.2	-14.0	0.0877	28	34
N2	13.6	20.7	51.8	< 0.0001	103	104
smg-1(cc546ts)	16.2	23.0	42.2	< 0.0001	114	121
smg-1(cc546ts);pha-4(zu225)	13.8	15.2	10.2	0.254	45	45
EV RNAi control	18.6	23.4	26.1	< 0.0001	94	91
atp-2 RNAi	22.8	22.5	-1.3	0.3471	97	94
EV RNAi control	18.8	22.7	20.6	< 0.0001	97	94
gfp RNAi control	18.5	23.1	25.3	< 0.0001	101	98
ogdh-1 RNAi	21.2	21.1	-0.7	0.65	98	100
let-363 RNAi	22.1	23.6	6.8	0.02	94	95
gfp RNAi control	20.2	27.7	37.4	< 0.0001	99	81
let-363 RNAi	25.1	25.7	2.1	0.9511	96	74
EV RNAi control	22.8	27.2	21.6	<0.0001	70	72
let-363 RNAi	27.4	27.2	-0.8	0.7239	64	80
EV RNAi control	19.7	24.3	23.8	< 0.0001	93	84
atp-2 RNAi	25.3	23.4	-7.4	< 0.0001	87	63

Strain	*m*		% difference	*P*-value	*n*		[Oligomycin]
	Vehicle	Oligomycin			Vehicle	Oligomycin	
N2	20.4	25.5	25.2	< 0.0001	88	72	80 μM
N2		27.0	32.3	< 0.0001		82	40 μM
N2		23.1	13.2	0.0005		50	20 μM
N2		22.0	7.9	0.0106		90	10 μM

Strain	*m*		% difference	*P*-value	*n*		Treatment
	Vehicle	Treatment			Vehicle	Treatment	
N2	14.5	16.9	16.8	0.0005	73	71	Octyl α-KG (500 μM)
N2	14.5	17.0	16.8	< 0.0001	73	60	α-KG
N2	14.0	18.8	33.9	< 0.0001	112	114	Dimethyl α-KG
N2	14.0	20.7	47.8	< 0.0001	112	114	α-KG
N2	15.7	21.6	37.6	< 0.0001	85	99	Disodium α-KG

Strain	*m*		% difference	*P*-value	*n*		Food source
	Vehicle	α-KG			Vehicle	α-KG	
N2	17.4	21.2	21.6	0.0001	108	55	Live OP50
N2	19.0	23.0	21.0	0.0003	88	46	Dead OP50 (γ-irradiated)

SUPPLEMENTARY NOTES

α-KG dehydrogenase knockdown. Similar to α-KG supplemented animals, animals with RNAi knockdown of α-KGDH (encoded by *ogdh-1*) also have increased endogenous levels of α-KG (Extended Data Fig. 1b). These animals are also long-lived (Fig. 1f). While it is possible that *ogdh-1* knockdown extends lifespan by affecting other unknown pathways, the simplest interpretation is that the increase in endogenous α-KG levels in these animals is sufficient for long life. Consistent with this model, lifespan of *ogdh-1(RNAi)* animals is not increased by α-KG supplementation. The *ogdh-1(RNAi)* worms also have higher level of autophagy with larger number of GFP::LGG-1 puncta compared to empty vector control, which cannot be augmented by addition of α-KG (Extended Data Fig. 7). While the results together strongly support the idea that the effect of α-KG in longevity is largely direct and worm autonomous, an important caveat is that *ogdh-1* knockdown may not necessarily give all the same effects as exogenous α-KG supplementation. For example, we found that whereas α-KG supplemented worms have normal brood size (Extended Data Fig. 1h) *ogdh-1* knockdown animals are sterile.

$$\alpha\text{-KG} + NAD^+ + CoA \rightarrow \text{Succinyl CoA} + CO_2 + NADH$$

Since α-KGDH catalyzes the above reaction in the TCA cycle, loss of α-KGDH activity would not only lead to α-KG accumulation but also diminish succinyl CoA and perturb NAD^+/NADH, as well as halt the TCA cycle. Defective α-KGDH function has been associated with severe neurological dysfunction [1].

Physiological regulation of α-KG levels. Although the concentration of α-KG was considered to be constant in the TCA cycle, we have found that one can in fact increase α-KG concentration in *C. elegans* either by supplementation or by knocking down the α-KGDH enzyme (Extended Data Fig. 1b). An increase in α-KG levels has also been observed in human HEK293 cells treated with α-keto-β-methyl-n-valeric acid, an inhibitor of α-KGDH [2]. Moreover, it has been documented that α-KG levels are subject to change under physiological conditions. For example, α-KG accumulates in starved bacteria and yeast cells [3]; in *E. coli* α-KG accumulates rapidly by up to 10-fold in response to nitrogen starvation [4-6] and in cyanobacteria α-KG is a signal of nitrogen status [7,8]. In metazoans the issue is harder to address, due to the enormous complexity involving multitudes of cell types, organs, and tissues. But there also appear to be regulations of α-KG levels in response to feeding and starvation. For instance, starved pigeons have ~50% higher α-KG in the liver [9]. Recently, it has emerged that physical exercise can also increase α-KG levels. For example, after acute exercise urine α-KG concentrations increased by 27% [10] and serum α-KG concentrations increased by over 50% [11]. We found that α-KG levels are elevated in starved *C. elegans* (Fig. 4d).

The biochemical basis for this increase in α-KG upon starvation may be explained; in gluconeogenesis, an increased rate of deamination of amino acids (to provide carbon) by the glutamate-linked transaminases in the liver will lead to an increased formation of α-KG. Consistently, caloric restriction has been shown to increase gluconeogenic and transaminase enzyme activities in mouse liver [12]. Dynamic regulations of α-KG occur in physiological scenarios and represent an exciting avenue for future studies.

Evolutionary conservation of the ATP synthase. ATP synthase (Complex V) is highly conserved throughout evolution, although the *C. elegans* mitochondrial genome lacks the ATP8 gene [13]. The sequence of ATP8 differs among animals, plants, and fungi. Functionally, the ATP8 subunit is not well studied and does not appear to be important for Complex V biology. α-KG binds to the highly conserved ATP-2 subunit, and elicits its effects (both biochemically and phenotypically) through ATP-2.

Comparison of ATP-2 inhibition by α-KG and by genetic means. Overall, α-KG appears to inhibit ATP-2 more mildly than either the knockdown of *atp-2* by RNAi or null alleles. For example, *atp-2(RNAi)* animals arrest development as larvae, as do *atp-2* null mutants [14,15]. In contrast, larvae treated with α-KG do not arrest. Further, null mutations in *atp-2* are associated with very slow pharyngeal pumping [15], whereas α-KG treatment is not (Extended Data Fig. 1g). On the other hand, α-KG treatment resembles RNAi of *atp-2* on most levels, including a decrease in ATP content (Fig. 2e, and data not shown), reduction of oxygen consumption (Fig. 2g and Extended Data Fig. 2c), induction of autophagy (Fig. 4b-c), increase in ROS (Extended Data Fig. 4), and extension of lifespan (Fig. 3a). Although α-KG supplementation and *atp-2* RNAi are associated with many similar phenotypes, the differences noted above likely reflect variable thresholds for responses to decreased ATP synthase activity in specific cells, biological processes, or developmental events. In fact, work by Tsang and Lemire postulated that low ATP-2 levels are sufficient to support many basic cellular and organismal processes, whereas higher levels of ATP-2 are required for energy-intensive processes such as development and reproduction [15]. The longevity benefit derived from mild inhibition of ATP-2 by α-KG offers hope for the future development of anti-aging therapies that are safe and effective.

Mode of inhibition of ATP synthase by α-KG. α-KG acts as an uncompetitive inhibitor of ATP synthase, decreasing both the effective V_{max} and K_m of the enzyme (Fig. 2i). As expected of an uncompetitive mechanism, inhibition of ATP synthase by α-KG works better at higher substrate concentrations. This mechanism may serve to safeguard that ATP production would not be inhibited inappropriately. An uncompetitive inhibitory mechanism means that the inhibitor binds to the enzyme-substrate complex, but not to the free enzyme, resulting in an inactive enzyme-substrate-inhibitor complex. Thus, α-KG binds only after ATP synthase has formed a complex with its substrate; that is, the binding site of α-KG is created after, but away from, substrate

binding. Consistently, using DARTS, we have mapped the binding site of α-KG in ATP synthase by mass spectrometry identification of protected peptides. The single most highly protected peptide, indicative of the putative α-KG binding site, is a 24-amino acid sequence corresponding to residues 433-456 of ATP5B. The peptide count for this region was 33 in α-KG treated samples, but undetectable in vehicle treated samples. This site is distinct from the Walker A motif for substrate (nucleotide) binding [16], or the Walker B motif important for Mg^{2+} binding and catalysis [16,17]. However, the site is exceptionally well conserved. For example, a comparison of human, bovine, and *C. elegans* orthologues shows that this region is 100% identical among the mitochondrial enzymes, and nearly identical to the sequences in Arabidopsis chloroplasts and *E. coli* (the latter having 4 non-identical, but similar, residues). Therefore, α-KG binding could be an important property of ATP5B that has evolved to regulate energy homeostasis by this endogenous metabolite. A precise understanding of the detailed mechanism of α-KG inhibition of ATP synthase will only be obtained when structural information is available.

Would known chemical inhibitors of the ETC have the similar lifespan extending effect as α-KG? Among the known chemical inhibitors of the ETC, only antimycin A [18], an inhibitor of Complex III, and oxaloacetate [19], which is a potent inhibitor of Complex II, have been reported in the context of lifespan studies; both were shown to extend *C. elegans* lifespan. A well-known, potent inhibitor of Complex V (ATP synthase) is oligomycin, which binds to the F_O subunit and blocks proton transport. Like α-KG, oligomycin also extends the lifespan of adult *C. elegans* (Extended Data Fig. 3a).

Involvement of *daf-16*/FOXO and *aak-2*/AMPK in α-KG longevity. Genetically, *daf-16*/FOXO (Fig. 3e, and Extended Data Fig. 5b) and *aak-2*/AMPK (Extended Data Fig. 5a) are not essential for lifespan extension by α-KG. However, in *aak-2* and *daf-1*6 mutant worms the longevity effect of α-KG appears to be smaller than in N2 (Extended Data Fig. 5a, and Fig. 3e), suggesting that AMPK and FOXO partially contribute to the longevity conferred by α-KG.

This is in contrast to OAA, which was found to require *aak-2*/AMPK and *daf-16*/FOXO for its longevity effect [19], suggesting that the mechanisms behind the lifespan extension by the two TCA cycle intermediates are distinct. Our finding is consistent with the fact that the loss of function of *aak-2* suppresses the lifespan of the long-lived *daf-2* mutant [20], since α-KG also increases longevity of *daf-2* worms (Fig. 3b).

aak-2 encodes the catalytic (α) subunit of AMP-activated protein kinase (AMPK), the cellular sensor of low energy levels [21]. AMPK and TOR are two major regulators of cellular energy homeostasis. AMPK is activated by increased AMP:ATP ratios, e.g., in glucose deprivation and other metabolic stresses [21], whereas TOR is inactivated upon amino acid limitation and other nutrient stresses [22,23] and by decreased ATP [24]. There is also emerging evidence for complex crosstalk between the two pathways [25-28] and with FOXO and SIRT1 [29,30].

Activation of AMPK leads to enhanced energy production, decreased energy expenditure, and redirection of cellular proper (e.g., through the induction of autophagy). However, the requirements for AMPK vary under different starvation stresses. For example, in mammalian cells AMPK is required for autophagy induction under glucose starvation but not amino acid starvation [31]. In *C. elegans*, AMPK/*aak-2* has been shown to mediate dietary restriction (DR) in *C. elegans* fed diluted bacteria but not DR in the *eat-2* model [20,29,32,33].

Consistent with decreased ATP content in α-KG treated cells and animals, P-AMPK is upregulated upon Complex V inhibition by α-KG (Extended Data Fig. 6b). However, this activation of AMPK appears to require more severe Complex V inhibition than the inactivation of mTORC1, as either oligomycin or 400 μM of octyl α-KG was required for increased P-AMPK whereas 200 μM of octyl α-KG was sufficient for decreased P-S6K (Extended Data Fig. 6b). Interestingly, P-Akt was also only mildly decreased by octyl α-KG treatment but was strongly diminished by oligomycin treatment (Fig. 4a). These differential effects by α-KG may explain why *aak-2*/AMPK is not essential for α-KG to extend lifespan even though the extent of life extension by α-KG may be smaller in the mutants. Consistent with the lifespan effects, we also found that α-KG treatment induced the formation of additional GFP::LGG-1 puncta in *aak-2(RNAi)* worms (**$P < 0.01$) (Extended Data Fig. 6c).

What is the role of reactive oxygen species (ROS) in lifespan extension by α-KG? The relationship between ROS and lifespan regulation is not well understood. Increased levels of ROS are thought to activate stress responses that protect the organism and ultimately enhance longevity. However, ROS *per se* does not correlate with lifespan. For example, increased ROS is found in both short-lived (e.g., *mev-1*, *gas-1*, and *sdhb-1*) [34] and long-lived (e.g., *sod-2*) mutants. The ROS levels in ATP synthase mutants or knockdowns are not well characterized. However, It has been reported that *atp-3(RNAi)* animals show a very slight, if any, increase in the level of protein oxidization levels (which occurs as a result of damage from ROS) as assessed by Oxyblot [35]. We also observed a slight increase in the abundance of oxidized proteins in animals treated with α-KG by Oxyblot (Extended Data Fig. 4b). Likewise, when ROS levels were measured by DCF fluorescence, both α-KG treated and *atp-2(RNAi)* adults exhibited increased ROS levels (Extended Data Fig. 4a). Together, our data suggest that ROS levels are increased in both α-KG treated and *atp-2(RNAi)* animals, further substantiating the model that α-KG inhibits ATP-2 *in vivo*. However, we consider this increase in ROS levels unlikely to play a major role in the lifespan extension conferred by α-KG for the following reasons.

First, as described above, increased ROS does not necessarily dictate a longer lifespan. Second, it has previously been shown that supplementation of long-lived *eat-2* mutant animals with the prooxidant paraquat further extends their lifespan [36], whereas α-KG does not further

extend the lifespan of *eat-2* mutants (Fig. 3c). Third, ROS has been shown to activate the TOR pathway [37,38], whereas α-KG has the opposite effect—inhibiting TOR and activating autophagy (Fig. 4b-c). Lastly, it has been postulated that the increased ROS in mitochondrial ETC mutants promotes longevity by increasing the activity of hypoxia-inducible factor 1 (HIF-1) [39], whereas α-KG longevity does not require HIF-1 (Fig. 3g, and Extended Data Fig. 5c).

References

1 Tretter, L. & Adam-Vizi, V. Alpha-ketoglutarate dehydrogenase: a target and generator of oxidative stress. *Philos Trans R Soc Lond B Biol Sci* 360, 2335-2345 (2005).

2 MacKenzie, E. D. *et al.* Cell-permeating alpha-ketoglutarate derivatives alleviate pseudohypoxia in succinate dehydrogenase-deficient cells. *Mol Cell Biol* 27, 3282-3289 (2007).

3 Brauer, M. J. *et al.* Conservation of the metabolomic response to starvation across two divergent microbes. *Proc Natl Acad Sci U S A* 103, 19302-19307 (2006).

4 Yuan, J. *et al.* Metabolomics-driven quantitative analysis of ammonia assimilation in E. coli. *Mol Syst Biol* 5, 302 (2009).

5 Radchenko, M. V., Thornton, J. & Merrick, M. Control of AmtB-GlnK complex formation by intracellular levels of ATP, ADP, and 2-oxoglutarate. *J Biol Chem* 285, 31037-31045 (2010).

6 Boogerd, F. C. *et al.* AmtB-mediated NH3 transport in prokaryotes must be active and as a consequence regulation of transport by GlnK is mandatory to limit futile cycling of NH4(+)/NH3. *FEBS Lett* 585, 23-28 (2011).

7 Muro-Pastor, M. I., Reyes, J. C. & Florencio, F. J. Cyanobacteria perceive nitrogen status by sensing intracellular 2-oxoglutarate levels. *J Biol Chem* 276, 38320-38328 (2001).

8 Forchhammer, K. Global carbon/nitrogen control by PII signal transduction in cyanobacteria: from signals to targets. *FEMS Microbiol Rev* 28, 319-333 (2004).

9 Kaminsky, Y. G., Kosenko, E. A. & Kondrashova, M. N. Metabolites of citric acid cycle, carbohydrate and phosphorus metabolism, and related reactions, redox and phosphorylating states of hepatic tissue, liver mitochondria and cytosol of the pigeon, under normal feeding and natural nocturnal fasting conditions. *Comp Biochem Physiol B* 73, 957-963 (1982).

10 Pechlivanis, A. *et al.* (1)H NMR-based metabonomic investigation of the effect of two different exercise sessions on the metabolic fingerprint of human urine. *J Proteome Res* 9, 6405-6416 (2010).

11 Brugnara, L. *et al.* Metabolomics approach for analyzing the effects of exercise in subjects with type 1 diabetes mellitus. *PLoS One* 7, e40600 (2012).

12 Hagopian, K., Ramsey, J. J. & Weindruch, R. Caloric restriction increases gluconeogenic and transaminase enzyme activities in mouse liver. *Exp Gerontol* 38, 267-278 (2003).

13 Okimoto, R., Macfarlane, J. L., Clary, D. O. & Wolstenholme, D. R. The mitochondrial genomes of two nematodes, Caenorhabditis elegans and Ascaris suum. *Genetics* 130, 471-498 (1992).

14 Curran, S. P. & Ruvkun, G. Lifespan regulation by evolutionarily conserved genes essential for viability. *PLoS Genet* 3, e56 (2007).

15 Tsang, W. Y., Sayles, L. C., Grad, L. I., Pilgrim, D. B. & Lemire, B. D. Mitochondrial respiratory chain deficiency in Caenorhabditis elegans results in developmental arrest and increased life span. *J Biol Chem* 276, 32240-32246 (2001).

16 Walker, J. E., Saraste, M., Runswick, M. J. & Gay, N. J. Distantly related sequences in the alpha- and beta-subunits of ATP synthase, myosin, kinases and other ATP-requiring enzymes and a common nucleotide binding fold. *EMBO J* 1, 945-951 (1982).

17 Abrahams, J. P., Leslie, A. G., Lutter, R. & Walker, J. E. Structure at 2.8 A resolution of F1-ATPase from bovine heart mitochondria. *Nature* 370, 621-628 (1994).

18 Dillin, A. *et al.* Rates of behavior and aging specified by mitochondrial function during development. *Science* 298, 2398-2401 (2002).

19 Williams, D. S., Cash, A., Hamadani, L. & Diemer, T. Oxaloacetate supplementation increases lifespan in Caenorhabditis elegans through an AMPK/FOXO-dependent pathway. *Aging Cell* 8, 765-768 (2009).

20 Apfeld, J., O'Connor, G., McDonagh, T., DiStefano, P. S. & Curtis, R. The AMP-activated protein kinase AAK-2 links energy levels and insulin-like signals to lifespan in C. elegans. *Genes Dev* 18, 3004-3009 (2004).

21 Hardie, D. G. AMP-activated/SNF1 protein kinases: conserved guardians of cellular energy. *Nat Rev Mol Cell Biol* 8, 774-785 (2007).

22 Wullschleger, S., Loewith, R. & Hall, M. N. TOR signaling in growth and metabolism. *Cell* 124, 471-484 (2006).

23 Laplante, M. & Sabatini, D. M. mTOR signaling in growth control and disease. *Cell* 149, 274-293 (2012).

24 Dennis, P. B. *et al.* Mammalian TOR: a homeostatic ATP sensor. *Science* 294, 1102-1105 (2001).

25 Kimura, N. *et al.* A possible linkage between AMP-activated protein kinase (AMPK) and mammalian target of rapamycin (mTOR) signalling pathway. *Genes Cells* 8, 65-79 (2003).

26 Gwinn, D. M. *et al.* AMPK phosphorylation of raptor mediates a metabolic checkpoint. *Mol Cell* 30, 214-226 (2008).

27 Shaw, R. J. LKB1 and AMP-activated protein kinase control of mTOR signalling and growth. *Acta Physiol (Oxf)* 196, 65-80 (2009).

28 Inoki, K., Kim, J. & Guan, K. L. AMPK and mTOR in cellular energy homeostasis and drug targets. *Annu Rev Pharmacol Toxicol* 52, 381-400 (2012).

29 Greer, E. L. *et al.* An AMPK-FOXO pathway mediates longevity induced by a novel method of dietary restriction in C. elegans. *Curr Biol* 17, 1646-1656 (2007).

30 Canto, C. *et al.* AMPK regulates energy expenditure by modulating NAD+ metabolism and SIRT1 activity. *Nature* 458, 1056-1060 (2009).

31 Kim, J., Kundu, M., Viollet, B. & Guan, K. L. AMPK and mTOR regulate autophagy through direct phosphorylation of Ulk1. *Nat Cell Biol* 13, 132-141 (2011).

32 Curtis, R., O'Connor, G. & DiStefano, P. S. Aging networks in Caenorhabditis elegans: AMP-activated protein kinase (aak-2) links multiple aging and metabolism pathways. *Aging Cell* 5, 119-126 (2006).

33 Greer, E. L. & Brunet, A. Different dietary restriction regimens extend lifespan by both independent and overlapping genetic pathways in C. elegans. *Aging Cell* 8, 113-127 (2009).

34 Van Raamsdonk, J. M. & Hekimi, S. Reactive Oxygen Species and Aging in Caenorhabditis elegans: Causal or Casual Relationship? *Antioxid Redox Signal* 13, 1911-1953 (2010).

35 Rea, S. L., Ventura, N. & Johnson, T. E. Relationship between mitochondrial electron transport chain dysfunction, development, and life extension in Caenorhabditis elegans. *PLoS Biol* 5, e259 (2007).

36 Yang, W. & Hekimi, S. A mitochondrial superoxide signal triggers increased longevity in Caenorhabditis elegans. *PLoS Biol* 8, e1000556 (2010).

37 Bae, G. U. *et al.* Hydrogen peroxide activates p70(S6k) signaling pathway. *J Biol Chem* 274, 32596-32602 (1999).

38 Radisavljevic, Z. M. & Gonzalez-Flecha, B. TOR kinase and Ran are downstream from PI3K/Akt in H2O2-induced mitosis. *J Cell Biochem* 91, 1293-1300 (2004).

39 Hwang, A. B. & Lee, S. J. Regulation of life span by mitochondrial respiration: the HIF-1 and ROS connection. *Aging (Albany NY)* 3, 304-310 (2011).

CHAPTER 3

2-Hydroxyglutarate Inhibits ATP Synthase and mTOR Signaling

(A reprint of “2-Hydroxyglutarate Inhibits ATP Synthase and mTOR Signaling,” which was previously published in Cell Metabolism (2015; 22: 508-515), is provided here as Chapter 3)

Short Article

Cell Metabolism

2-Hydroxyglutarate Inhibits ATP Synthase and mTOR Signaling

Graphical Abstract

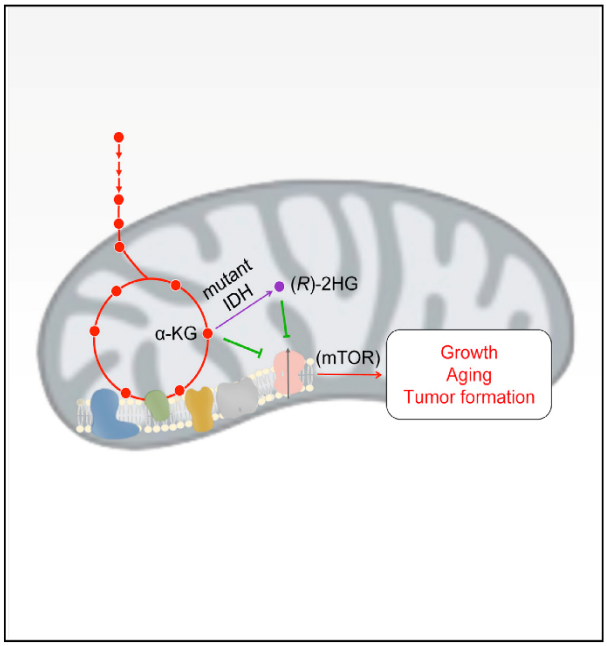

Authors

Xudong Fu, Randall M. Chin, Laurent Vergnes, ..., Michael E. Jung, Karen Reue, Jing Huang

Correspondence

jinghuang.ucla@gmail.com

In Brief

Aberrant isocitrate dehydrogenase enzymes encoded by cancer-associated IDH1 and IDH2 gene mutations produce an oncometabolite, (*R*)-2HG. Fu et al. discover a growth-suppressive function of (*R*)-2-HG mediated by its binding and inhibition of ATP synthase. The resulting OXPHOS perturbation imparts extra vulnerability to glucose limitation in IDH mutant glioblastoma cells.

Highlights

- 2-HG, like α-KG, inhibits ATP synthase and extends the lifespan of *C. elegans*
- IDH1(R132H) mutant cells have reduced ATP content, respiration, and mTOR signaling
- IDH1(R132H) mutant cells exhibit an intrinsic vulnerability to glucose limitation
- ATP synthase is a target of 2-HG's growth-suppressive activity in IDH mutant cells

Fu et al., 2015, Cell Metabolism 22, 508–515
September 1, 2015
http://dx.doi.org/10.1016/j.cmet.2015.06.009

CellPress

CellPress

Cell Metabolism
Short Article

2-Hydroxyglutarate Inhibits ATP Synthase and mTOR Signaling

Xudong Fu,[1] Randall M. Chin,[2] Laurent Vergnes,[3] Heejun Hwang,[1] Gang Deng,[4] Yanpeng Xing,[4] Melody Y. Pai,[2] Sichen Li,[5] Lisa Ta,[1] Farbod Fazlollahi,[6] Chuo Chen,[7] Robert M. Prins,[8] Michael A. Teitell,[2,9,10] David A. Nathanson,[1] Albert Lai,[5] Kym F. Faull,[6] Meisheng Jiang,[1] Steven G. Clarke,[2,4] Timothy F. Cloughesy,[5,10] Thomas G. Graeber,[1,10,11,12] Daniel Braas,[1,11] Heather R. Christofk,[1,10,11] Michael E. Jung,[1,2,4,10] Karen Reue,[2,3] and Jing Huang[1,2,10,*]

[1]Department of Molecular and Medical Pharmacology, David Geffen School of Medicine, University of California Los Angeles, Los Angeles, CA 90095, USA
[2]Molecular Biology Institute, University of California Los Angeles, Los Angeles, CA 90095, USA
[3]Department of Human Genetics, David Geffen School of Medicine, University of California Los Angeles, Los Angeles, CA 90095, USA
[4]Department of Chemistry and Biochemistry, University of California Los Angeles, Los Angeles, CA 90095, USA
[5]Department of Neurology, David Geffen School of Medicine, University of California Los Angeles, Los Angeles, CA 90095, USA
[6]Pasarow Mass Spectrometry Laboratory, Department of Psychiatry and Biobehavioral Sciences, and Semel Institute for Neuroscience and Human Behavior, University of California Los Angeles, Los Angeles, CA 90095, USA
[7]Department of Biochemistry, University of Texas Southwestern Medical Center, Dallas, TX 75390, USA
[8]Department of Neurosurgery, David Geffen School of Medicine, University of California Los Angeles, Los Angeles, CA 90095, USA
[9]Department of Pathology and Laboratory Medicine, David Geffen School of Medicine, University of California Los Angeles, Los Angeles, CA 90095, USA
[10]Jonsson Comprehensive Cancer Center, David Geffen School of Medicine, University of California Los Angeles, Los Angeles, CA 90095, USA
[11]UCLA Metabolomics Center, University of California Los Angeles, Los Angeles, CA 90095, USA
[12]Crump Institute for Molecular Imaging, University of California Los Angeles, Los Angeles, CA 90095, USA
*Correspondence: jinghuang.ucla@gmail.com
http://dx.doi.org/10.1016/j.cmet.2015.06.009

SUMMARY

We discovered recently that the central metabolite α-ketoglutarate (α-KG) extends the lifespan of *C. elegans* through inhibition of ATP synthase and TOR signaling. Here we find, unexpectedly, that (*R*)-2-hydroxyglutarate ((*R*)-2HG), an oncometabolite that interferes with various α-KG-mediated processes, similarly extends worm lifespan. (*R*)-2HG accumulates in human cancers carrying neomorphic mutations in the isocitrate dehydrogenase (IDH) 1 and 2 genes. We show that, like α-KG, both (*R*)-2HG and (*S*)-2HG bind and inhibit ATP synthase and inhibit mTOR signaling. These effects are mirrored in IDH1 mutant cells, suggesting a growth-suppressive function of (*R*)-2HG. Consistently, inhibition of ATP synthase by 2-HG or α-KG in glioblastoma cells is sufficient for growth arrest and tumor cell killing under conditions of glucose limitation, e.g., when ketone bodies (instead of glucose) are supplied for energy. These findings inform therapeutic strategies and open avenues for investigating the roles of 2-HG and metabolites in biology and disease.

INTRODUCTION

Aberrant metabolism, long symbolic of inherited metabolic diseases, is now recognized as a hallmark of many other pathogenic conditions, including cancer (Warburg, 1956; Vander Heiden et al., 2009). Recently, we discovered that the common metabolite α-ketoglutarate (α-KG) increases the lifespan of adult *C. elegans* by inhibiting the highly conserved ATP synthase and the TOR pathway, mimicking dietary restriction in longevity (Chin et al., 2014). Furthermore, the observation that α-KG inhibits mTOR function in normal human cells implies a role for α-KG as an endogenous tumor suppressor metabolite (Chin et al., 2014). Known for its role in central carbon metabolism as a tricarboxylic acid (TCA) cycle intermediate, α-KG is universal to all cellular life. α-KG also serves as a co-substrate for a large family of dioxygenases with functions in cellular processes such as hypoxic response and epigenetic regulation. The identification of α-KG as a regulator of ATP synthase reveals a new mechanism for longevity regulation through metabolite signaling and suggests that there likely exist other metabolites that play signaling roles in aging. Particularly, metabolites that are similar in structure to α-KG may also modify lifespan through interactions with ATP synthase, and the lifespan effects of metabolites may correlate with their involvement in human disease.

In the TCA cycle, α-KG is produced from isocitrate by isocitrate dehydrogenase (IDH). Catalytic arginine mutations in the *IDH1* and *IDH2* genes found in gliomas and acute myeloid leukemia (AML) result in neomorphic enzymes that, instead, convert α-KG to the structurally similar (*R*)-2-hydroxyglutarate ((*R*)-2HG), which accumulates to exceedingly high levels in these patients (Dang et al., 2009; Gross et al., 2010; Ward et al., 2010; Xu et al., 2011). (*R*)-2HG is now considered an oncometabolite, impairing epigenetic and hypoxic regulation through its binding to α-KG-dependent dioxygenases (Lu

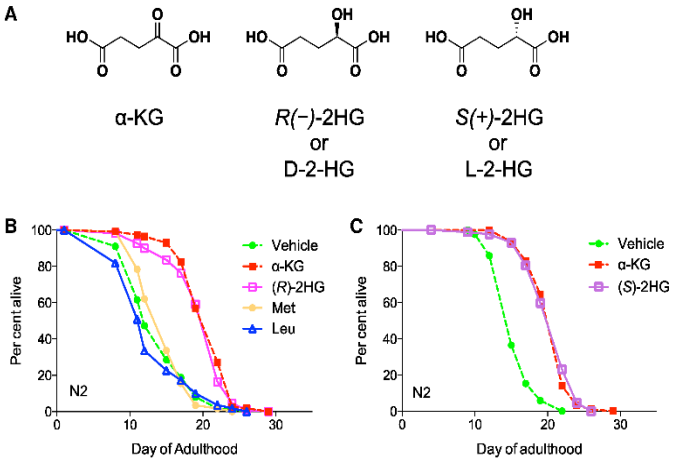

Figure 1. 2-HG Extends the Lifespan of Adult *C. elegans*

(A) Chemical structures of 2-hydroxyglutaric acid and α-ketoglutaric acid.

(B) (*R*)-2HG-supplemented worms. The mean lifespan (days of adulthood) with vehicle treatment (m_{veh}) = 14.0 (n = 112 animals tested). $m_{\alpha\text{-KG}}$ = 20.7 (n = 114), p < 0.0001 (log-rank test); $m_{(R)\text{-2HG}}$ = 20.0 (n = 110), p < 0.0001 (log-rank test); m_{Met} = 14.7 (n = 116), p = 0.4305 (log-rank test); mL_{eu} = 13.2 (n = 110), p = 0.3307 (log-rank test).

(C) (*S*)-2HG-supplemented worms. m_{veh} = 15.7 (n = 85); $m_{\alpha\text{-KG}}$ = 21.5 (n = 99), p < 0.0001 (log-rank test); $m_{(S)\text{-2HG}}$ = 20.7 (n = 87), p < 0.0001 (log-rank test).

All metabolites were given at a concentration of 8 mM. Two independent experiments were performed.

et al., 2012; Koivunen et al., 2012). The development of inhibitors of mutant IDH that normalize (*R*)-2HG levels is an attractive cancer therapeutic strategy (Wang et al., 2013; Rohle et al., 2013). Paradoxically, however, brain cancer patients with IDH mutations have a longer median overall survival than patients without mutations (Parsons et al., 2008; Yan et al., 2009; van den Bent et al., 2010), hinting at additional complexity in the biology of these cancers. (*R*)-2HG and (*S*)-2-hydroxyglutarate ((*S*)-2HG) have also been found to accumulate in tissues of individuals with germline mutations in genes encoding the corresponding 2-HG dehydrogenases (Kranendijk et al., 2012; Steenweg et al., 2010). The resulting 2-HG aciduria is associated with neurological manifestations whose molecular mechanisms are unknown (Kranendijk et al., 2010). We set out to identify additional targets of 2-HG to elucidate the mechanisms underlying the seemingly disparate 2-HG-related phenotypes.

RESULTS AND DISCUSSION

2-HG Extends the Lifespan of Adult *C. elegans*

We have demonstrated that α-KG promotes longevity through inhibition of ATP synthase (Chin et al., 2014). Given the structural similarity between α-KG and 2-HG (Figure 1A) and the association of 2-HG with cancer and neurological dysfunction, we asked whether 2-HG influences longevity. Surprisingly, both (*R*)-2HG and (*S*)-2HG increase the lifespan of *C. elegans* (Figures 1B and 1C). Notably, (*R*)-2HG, (*S*)-2HG, and α-KG interact distinctly with the α-KG-dependent dioxygenases (Koivunen et al., 2012; Tarhonskaya et al., 2014). Therefore, the similar effect of α-KG and (*R*)- and (*S*)-2-HG on lifespan points to a common mechanism that is independent of dioxygenases or any enantiomer-specific 2-HG effects (da Silva et al., 2002; Latini et al., 2005; Wajne et al., 2002; Chan et al., 2015). Because we identified the ATP synthase β subunit (ATP5B) as a target of α-KG (Chin et al., 2014), we asked whether 2-HG acts by a similar mechanism.

ATP Synthase Is a Molecular Target of 2-HG

To determine whether 2-HG targets ATP5B, we first performed a drug affinity-responsive target stability (DARTS) analysis (Lomenick et al., 2009) using U87 human glioblastoma cells. We found that both (*R*)-2HG and (*S*)-2HG bind to ATP5B (Figure 2A; data not shown). Like α-KG, both 2-HG enantiomers inhibit ATP synthase (complex V) (Figures 2B and 2C; Figures S1A–S1C). This inhibition is specific because there is no inhibition by either enantiomer on other electron transport chain (ETC) complexes (Figures S1D–S1F) or ADP import into the mitochondria (Figure S1G). The inhibition of ATP synthase by 2-HG is also readily detected in live cells. Treatment of U87 cells (wild-type IDH1/2) with membrane-permeable octyl esters of 2-HG or α-KG results in decreased cellular ATP content (Figure S2A) and a decreased ATP/ADP ratio (Figure 2D; Figure S2B) under mitochondrially oxidative phosphorylation (OXPHOS) conditions, as with the ATP synthase inhibitor oligomycin (Figures S2A and S2B). As expected, both basal and ATP synthase-linked oxygen consumption rates (OCRs) are decreased in 2-HG-treated cells (Figure 2E; Figures S2C and S2D), and lifespan increase by 2-HG is dependent on ATP synthase (Figure S2E).

IDH1(R132H) Mutant Cells Have Decreased ATP Content and Mitochondrial Respiration

At normal cellular concentrations of ~200 μM (Gross et al., 2010), (*R*)-2HG is unlikely to cause significant inhibition of ATP synthase. However, in glioma patients with IDH mutations where (*R*)-2HG accumulates to 10–100 times of natural levels (Dang et al., 2009; Gross et al., 2010), inhibition of ATP synthase would be possible. To test this idea, we used U87 cells stably expressing IDH1(R132H), the most common IDH mutation in glioma (Yan et al., 2009). Similar to octyl (*R*)-2HG-treated cells, U87/IDH1(R132H) cells exhibit decreased ATP content and ATP/ADP ratio (Figure 3A) and OCR (Figure 3B) compared with isogenic IDH1(WT)-expressing U87 cells. Importantly, the decrease in respiration in IDH1(R132H) cells is attributable to ATP synthase (complex V) inhibition. Although there is a clear difference in basal respiration rates in U87/IDH1(WT)

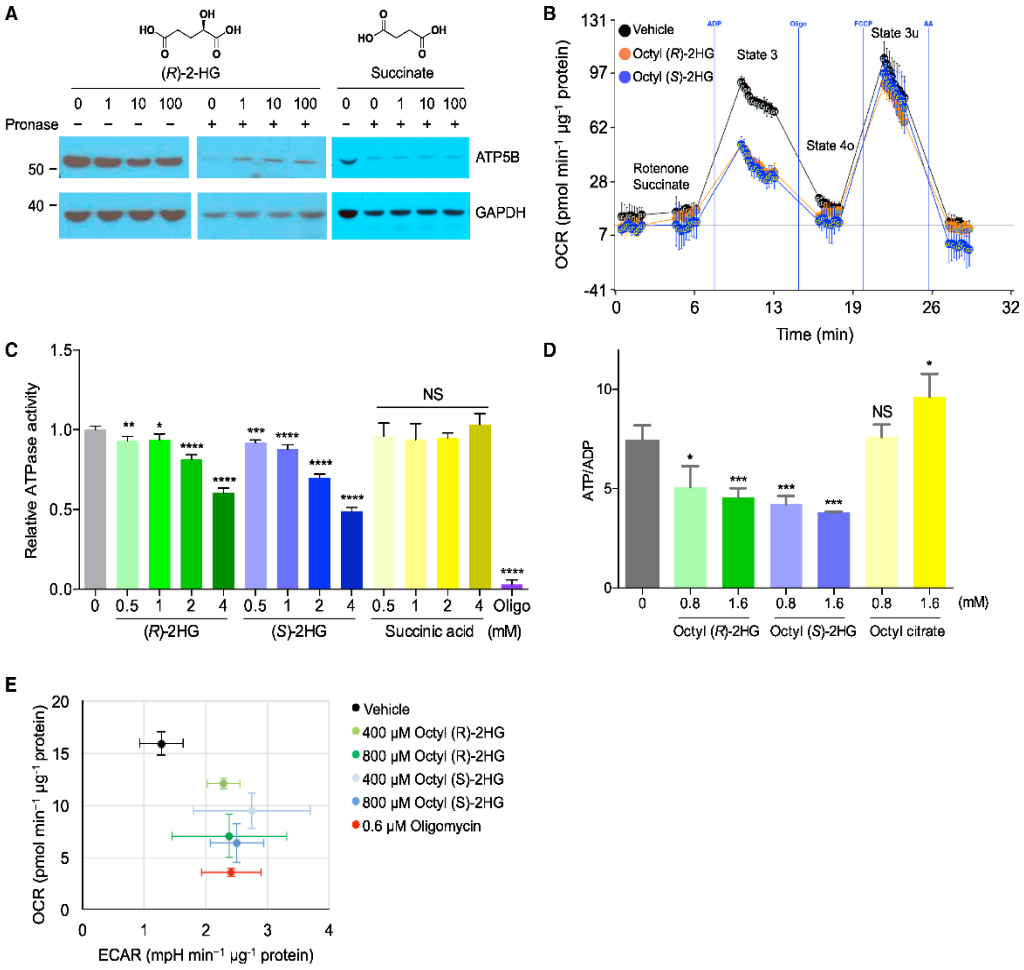

Figure 2. 2-HG Binds and Inhibits ATP Synthase

(A) DARTS identifies ATP5B as a 2-HG binding protein. U87 cell extracts were used. Succinate served as a negative control.

(B) Inhibition of ATP synthase by 2-HG. 2-HG, released from octyl 2-HG (600 µM), decreases ($p < 0.001$) state 3, but not state 4o or 3u, respiration in mitochondria isolated from mouse liver. Octanol was used as vehicle. Oligo, oligomycin; FCCP, carbonyl cyanide-*4*-(trifluoromethoxy)phenylhydrazone; AA, antimycin A.

(C) Inhibition of submitochondrial particle ATPase by 2-HG acid but not by succinic acid. *$p < 0.05$, **$p < 0.01$, ***$p < 0.001$, ****$p < 0.0001$; NS, $p > 0.05$. Oligo, oligomycin (32 µM).

(D) Decreased ATP/ADP ratio in U87 cells treated with octyl 2-HG but not octyl citrate, indicating specificity and excluding any effect involving octanol. *$p < 0.05$, ***$p < 0.001$; NS, $p > 0.05$.

(E) Decreased respiration as indicated by OCR (**$p < 0.01$) in octyl 2-HG-treated U87 cells in glucose medium. Octanol shows no effect on OCR compared with DMSO.

For (A)–(E), results were replicated in at least two independent experiments. Unpaired t test, two-tailed, two-sample unequal variance was used for (B)–(E). Mean ± SD is plotted.

versus U87/IDH1(R132H) cells, oligomycin-insensitive respiration, which is independent of complex V, is not significantly different between IDH1(WT) and IDH1(R132H) cells (Figure 3C). Furthermore, complex V knockdown using ATP5B RNAi normalizes the respiration difference between IDH1(R132H) and IDH1(WT) cells (Figure 3D). Consistently, the difference in ATP content of U87/IDH1(WT) and U87/IDH1(R132H) cells is diminished upon treatment with octyl (*R*)-2HG (Figure 3E). Similar results were obtained in HCT 116 IDH1(R132H/+) cells (Figures S3A and S3B). In addition, the mitochondrial membrane potential in IDH1 mutant cells is higher than in IDH1 wild-type cells (Figure 3F; Figure S3C), consistent with the inhibition of complex V

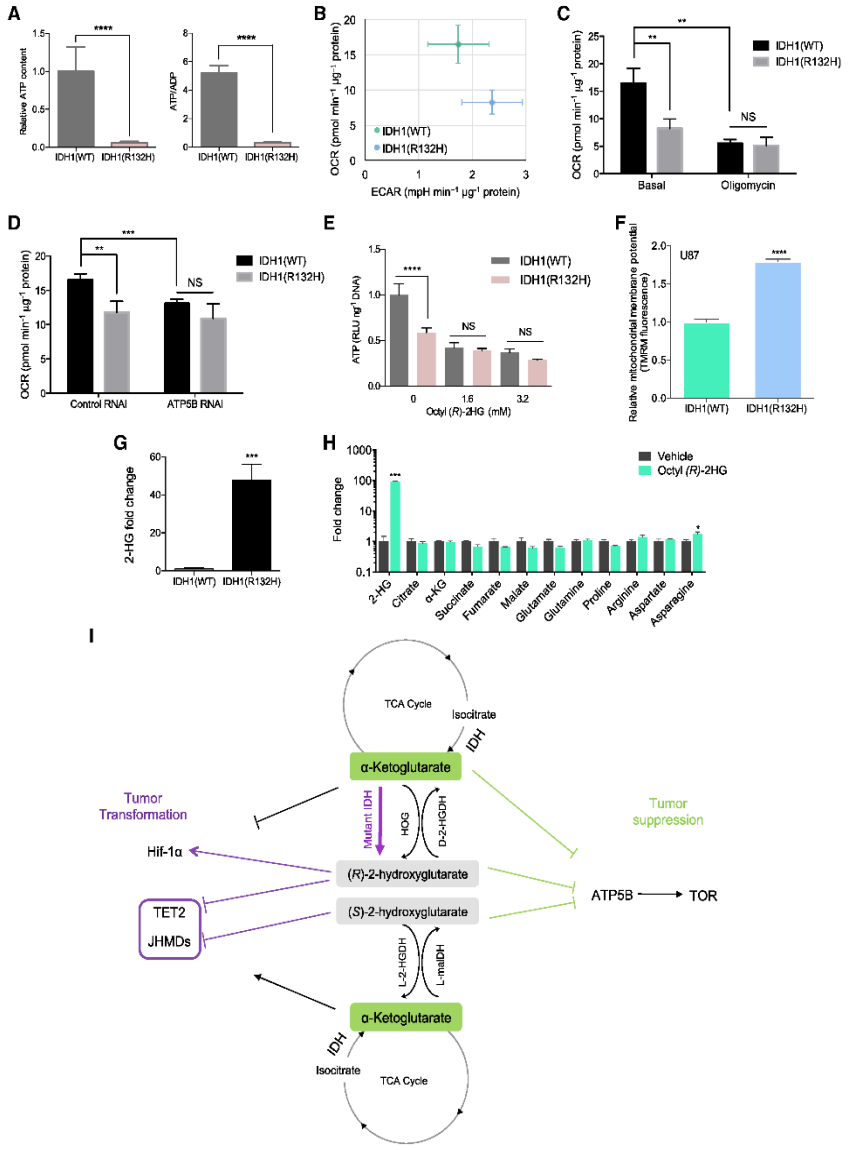

Figure 3. Inhibition of ATP Synthase in IDH1(R132H) Cells

(A) Decreased ATP levels and ATP/ADP ratio in U87/IDH1(R132H) cells (****$p < 0.0001$).

(B) Decreased respiration in U87/IDH1(R132H) cells (**$p = 0.0037$).

(C and D) Decreased respiration in U87/IDH1(R132H) cells is complex V-dependent (**$p < 0.01$, ***$p < 0.001$; NS, $p > 0.05$).

(E) Decreased ATP content in U87/IDH1(R132H) cells is attributable to *(R)*-2HG (****$p < 0.0001$; NS, $p > 0.05$).

(F) Increased mitochondrial membrane potential in U87/IDH1(R132H) cells normalized to cell number (****$p < 0.0001$).

(G) 2-HG accumulation in U87/IDH1(R132H) cells (***$p = 0.0003$).

(H) Metabolic profile of octyl *(R)*-2HG-treated U87 cells (***$p < 0.001$, *$p = 0.0435$). It is possible that the flux rate changed without affecting the absolute abundance of the intermediates.

(I) Model of metabolite signaling through ATP synthase inhibition.

Unpaired t test, two-tailed, two-sample unequal variance was used for (A)–(H). Mean ± SD is plotted. Results were replicated in at least two independent experiments.

(Johnson et al., 1981). In contrast, inhibition of ETC complex I, III, or IV causes dissipation of the mitochondrial membrane potential (Johnson et al., 1981).

The intracellular (*R*)-2HG levels are ~20- to 100-fold higher in U87 and HCT 116 cells expressing IDH1(R132H) than in control cells (Figure 3G; Figure S3D). The elevated (*R*)-2HG levels are comparable with those found in cells treated with octyl (*R*)-2HG (Figure 3H), and levels reported for IDH1 mutant tumor samples (Dang et al., 2009; Gross et al., 2010; Reitman et al., 2011). The detection of similar (*R*)-2HG levels in tumors as in octyl (*R*)-2HG-treated cells suggests that the tumor cells likely experience reduced ATP synthase and mitochondrial respiration, raising potential prognostic or therapeutic implications (see below).

2-HG Accumulation Does Not Alter the Levels of Common Metabolites

The metabolite 2-HG is linked to the TCA cycle and related amino acid metabolic pathways (Figure 3I). To explore potential metabolic changes upon octyl 2-HG treatment, we measured metabolite levels in octyl 2-HG-treated cells cultured in 1,2-^{13}C-glucose-containing medium by liquid chromatography/mass spectrometry (LC/MS). As expected, 2-HG accumulates 20- to 100-fold more after octyl 2-HG treatment (Figure 3H; Figure S3E). There is no dramatic change (<2-fold) in TCA cycle metabolites or related amino acids (Figure 3H; Figure S3E). As expected, the bulk of the increased 2-HG came from the hydrolysis of exogenously provided octyl 2-HG, as indicated by the unlabeled M+0 isotopomer (Figure S3F; data not shown for octyl (*S*)-2HG treatment). There is also no major change (<2-fold) in labeled TCA cycle intermediates and related amino acids (Figure S3G). Similarly, treatment with octyl α-KG causes an increase in α-KG levels without other substantial changes in the metabolic profile (Figure S3H). The steady-state metabolic profiles observed in 2-HG-treated (or α-KG-treated) cells support the notion that the bioenergetic shift results from the direct inhibition of ATP synthase by 2-HG (or α-KG) rather than secondary effects (Figure 3I).

IDH1(R132H) Mutant Cells Exhibit Intrinsic Vulnerability to Glucose Limitation

As the end component of the mitochondrial ETC, ATP synthase is a major source of cellular energy and the sole site for OXPHOS (Walker, 2013). When glycolysis is inhibited, for example, under conditions of glucose insufficiency, cells are forced to rely on mitochondrial respiration as a source of ATP. The inherent inhibition of ATP synthase and mitochondrial respiration in mutant IDH1 cancer cells therefore suggests a potential Achilles heel for these cancers. Supporting this idea, when cultured in glucose-free, galactose-containing medium to ensure that respiration is the primary source of energy, IDH1(R132H) cells exhibit drastically decreased cell viability (Figure 4A; Figure S4A). These results indicate a particular sensitivity of IDH1(R132H) mutant cells to the deprivation of glucose. The mutant cell line is not sensitive to fetal bovine serum (FBS) deprivation (data not shown), indicating that its increased vulnerability to glucose starvation is specific. This vulnerability to glucose starvation is also evident in U87 cells treated with octyl α-KG or octyl 2-HG (Figures 4B–4D; Figure S4B) and in ATP5B knockdown cells (Figure 4E). These findings raise the possibility that cancer cells with the IDH1(R132H) mutation (and the concomitant ATP synthase/mitochondrial respiration defect) may also be particularly sensitive to nutrient conditions analogous to glucose limitation.

In complex organisms, glucose limitation can occur as a consequence of ketosis, wherein cells use ketone bodies (instead of glucose) for energy. Ketosis is naturally induced upon prolonged starvation (or fasting), during which cells derive energy from fat reservoirs while sparing protein in muscle and other tissues from catabolism. Ketosis can also be induced by feeding a low-carbohydrate, high-fat "ketogenic diet," which has shown benefits against cancer (Stafford et al., 2010). One reason for this may be that tumor cells largely depend on glucose for growth and survival. Because the metabolism of ketone bodies depends entirely on OXPHOS, one prediction is that inhibiting ATP synthase (or other ETC components) in cancer cells would confer a survival disadvantage if ketone bodies were the only source of energy. Because U87 cells are unable to utilize ketone bodies for energy, we determined the effect of ketogenic conditions using HCT 116 cells expressing mutant IDH1. When cultured in glucose-free medium containing the ketone body *(R)*-3-hydroxybutyrate, IDH1 mutant HCT 116 cells showed a profound decrease in viability compared with the parental cells (Figure 4F), confirming the suspected metabolic weakness of IDH mutant cells. These results further support our discovery that (*R*)-2HG accumulation in mutant IDH cancer cells results in ATP synthase inhibition and also suggest novel metabolic therapeutic strategies in cancer treatment.

Decreased mTOR Signaling and Cell Growth by 2-HG

Inhibition of ATP synthase leads to decreased TOR signaling in mammalian cells, worms, and flies (Chin et al., 2014; Sun et al., 2014). We found that ATP5B knockdown (Figure 4G), treatment with octyl esters of 2-HG (Figure 4H), and IDH1(R132H) mutation (Figure 4I) all decrease the phosphorylation of mTOR complex 1 substrates. This effect occurs initially (4 h) in an AMPK-independent manner, with 2-HG decreasing mTOR signaling without significantly altering AMPK activity. However, prolonged exposure to 2-HG (24 h) also activates AMPK (Figure S4C), consistent with the idea that mTOR itself may directly sense ATP (Dennis et al., 2001) in addition to responding to AMP levels through crosstalk with AMPK (Shaw, 2009; Inoki et al., 2012).

TOR is a major regulator of cell growth (Blagosklonny and Hall, 2009). Consistent with the decreased TOR signaling, we observed growth inhibition in ATP5B knockdown cells (Figure S4D), in cells treated with octyl α-KG or octyl 2-HG (Figures S4E–S4G), and in IDH1(R132H)-expressing cells (Figures S4H and S4I). ATP5B RNAi normalizes the growth difference between IDH1(R132H) and IDH1(WT) cells (Figure S4J). Growth inhibition by 2-HG (and by α-KG) is also observed in WI-38 normal human diploid fibroblasts, in immortalized non-malignant HEK293 cells, and in other cancer cell lines tested (Figures S4K–S4N). These results suggest that, when present in excess, 2-HG acts as a growth-inhibitory metabolite across cell types. Further work is warranted to test whether the growth-inhibitory effect of (*R*)-2HG underlies the longer median overall survival of glioma patients with IDH mutations.

SUMMARY

We demonstrate that, similar to α-KG, both enantiomers of 2-HG bind and inhibit ATP synthase and extend the lifespan of

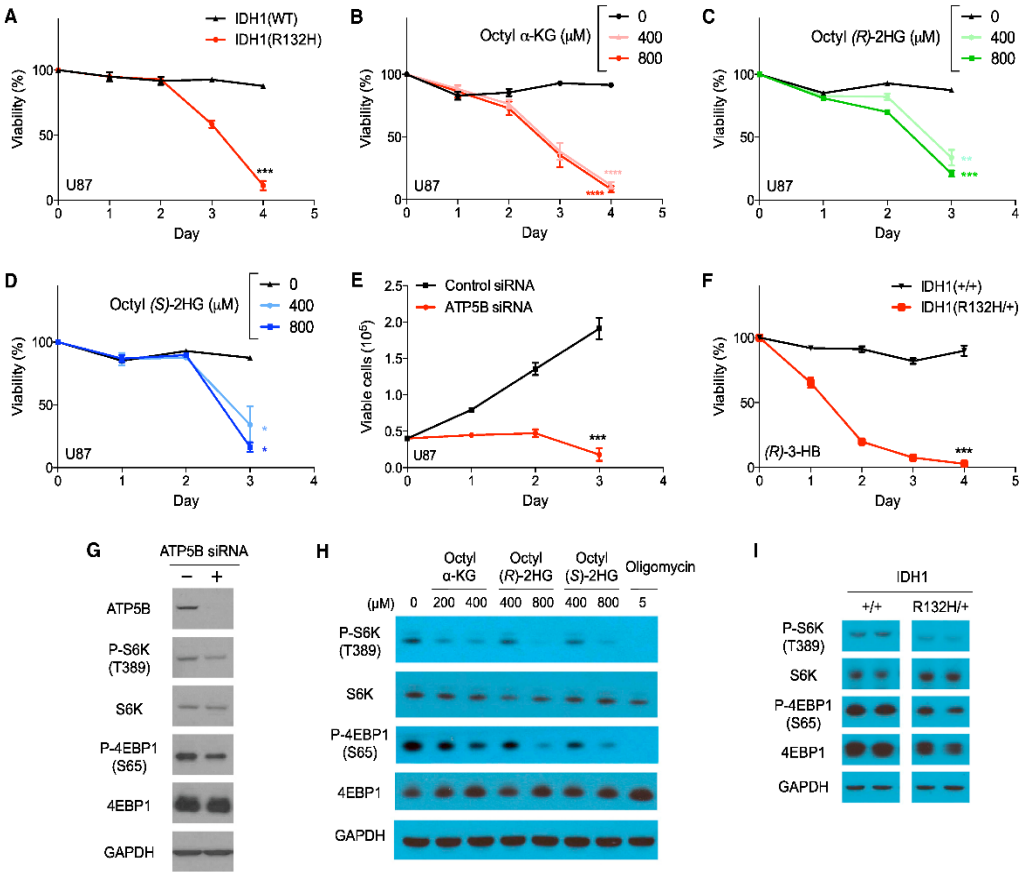

Figure 4. Inherent Vulnerability, or the Loss of Cell Viability, Characteristic of Cells with ATP5B Knockdown, 2-HG Accumulation, or IDH Mutations

(A) U87/IDH1(R132H) cells have increased vulnerability to glucose starvation (***$p < 0.001$).

(B–D) Octyl α-KG- or octyl 2-HG-treated U87 cells exhibit decreased viability upon glucose starvation (****$p < 0.0001$, ***$p < 0.001$, **$p < 0.01$, *$p < 0.05$).

(E) ATP5B knockdown inhibits U87 cell growth (***$p = 0.0004$).

(F) HCT 116 IDH1(R132H/+) cells exhibit increased vulnerability to glucose-free medium supplemented with *(R)*-3-hydroxybutyrate (***$p < 0.001$).

(G–I) U87 cells with ATP5B knockdown or octyl esters of α-KG or 2-HG treatment and HCT 116 IDH1(R132H/+) cells exhibit decreased mTOR complex 1 activity in glucose-free, galactose-containing medium.

For (A)–(E), cells were cultured in galactose medium. All lanes in (I) are on the same blot. Spaces indicate the positions of unnecessary lanes that were removed digitally. Octanol has no effect on mTOR activity. Unpaired t test, two-tailed, two-sample unequal variance was used for (A)–(F). Mean ± SD is plotted. Results in (A)–(I) were replicated in at least two independent experiments.

C. elegans. Inhibition of ATP synthase by these related metabolites decreases mitochondrial respiration and mTOR signaling. Both 2-HG and α-KG exhibit broad growth-inhibitory effects and reduce cancer cell viability under glucose-restricted conditions. It is now recognized that *(R)*-2HG, which accumulates in IDH mutant cancers, facilitates oncogenic transformation. Little is known, however, about how *(R)*-2HG modifies the phenotype of IDH mutant gliomas when the tumors are formed. Our findings suggest that, in addition to interfering with various α-KG binding factors with importance in cancer, *(R)*-2HG also acts, through inhibition of ATP synthase and mTOR signaling downstream, to decrease tumor cell growth and viability. The latter property may contribute to the improved prognosis of IDH mutant glioma patients. This idea is consistent with emerging findings that the inhibition of ETC complex I in cancer could be an effective therapeutic strategy (Wheaton et al., 2014; Birsoy et al., 2014). Together, these findings highlight a hopeful approach to cancer prevention and treatment by targeting certain aging pathways through metabolic modulation.

The effects of excess 2-HG are likely to be context-dependent. Although its growth-inhibitory effects may be beneficial in cancer, in 2-HG aciduria, the inhibition of ATP synthase and

the resulting impaired mitochondrial function could contribute to neurological dysfunction (da Silva et al., 2002; Wajne et al., 2002; Kölker et al., 2002; Latini et al., 2005). Therefore, the identification of ATP synthase as a target of both 2-HG enantiomers provides a congruent molecular basis for 2-HG-associated cancer and neurological disorders. We postulate that altered mitochondrial energy metabolism may contribute to the inverse susceptibility to cancer and neurodegenerative diseases (*e.g.*, Parkinson's disease). Finally, our findings raise the possibility that nutrient and/or metabolic intervention per se, such as diets that lower the reliance on glucose, and/or approaches that perturb cellular energy metabolism (e.g., by targeting OXPHOS), may benefit glioma patients. Such approaches may be particularly valuable for improving the survival of glioma patients without IDH mutations, who otherwise have no means to inherently curb mitochondrial respiration, and for cancer prevention and treatment in general.

EXPERIMENTAL PROCEDURES

Lifespan Analysis

Lifespan experiments were performed as described previously (Chin et al., 2014). Lifespan assays were conducted at 20°C on solid nematode growth medium (NGM). L4 or young adult animals were placed onto NGM assay plates containing D-2-HG (Sigma, catalog no. H8378), L-2-HG (Sigma, catalog no. 90790), α-KG (Sigma, catalog no. K1128), or vehicle control (H_2O). Assay plates were seeded with OP50. For RNAi experiments, NGM assay plates also contained 1 mM isopropyl-β-D-thiogalactoside (IPTG) and 50 μg/ml ampicillin and were seeded with the appropriate RNAi feeding clone (Thermo Scientific/OpenBiosystems). The *C. elegans* TOR (*let-363*) RNAi clone was obtained from Joseph Avruch (Massachusetts General Hospital/Harvard). To assess the survival of the worms, the animals were prodded with a platinum wire every 2–3 days, and those that failed to respond were scored as dead. Worms that ruptured, bagged, or crawled off the plates were censored. Lifespan data were analyzed using GraphPad Prism. *p* Values were calculated using the log-rank (Mantel-Cox) test unless stated otherwise.

Target Identification Using DARTS

DARTS was performed as described previously (Lomenick et al., 2009).

Measurement of Mitochondrial Respiration

Mitochondrial respiration was analyzed using isolated mitochondria (Brand and Nicholls, 2011). Animal studies were performed under approved University of California Los Angeles (UCLA) animal research protocols.

Cell Growth and Viability Assays

Cells were seeded in 12-well plates and, after overnight incubation, treated with the indicated concentrations of each compound. After harvesting, cells were stained with acridine orange (AO) and 4′,6-diamidino-2-phenylindole (DAPI). Cell number and viability were measured based on AO and DAPI fluorescence as measured by NC3000 (ChemoMetec) following the manufacturer's instructions.

Metabolic Profile Analysis

Cells were cultured for 24 hr and rinsed with PBS, and medium containing 1,2-^{13}C-glucose (1 g/l) was added. After 24-hr culture, cells were rinsed with ice-cold 150 mM NH_4AcO (pH 7.3), followed by addition of 400 μl cold methanol and 400 μl cold water. Cells were scraped off and transferred to an Eppendorf tube, and 10 nmol norvaline as well as 400 μl chloroform were added to each sample. For the metabolite extraction, samples were vortexed for 5 min on ice and spun down, and the aqueous layer was transferred into a glass vial and dried. Metabolites were resuspended in 70% ACN, and a 5-μl sample was loaded onto a Phenomenex Luna 3u NH2 100A (150 × 2.0 mm) column. The chromatographic separation was performed on an UltiMate 3000RSLC (Thermo Scientific) with mobile phases A (5 mM NH_4AcO [pH 9.9]) and B (ACN) and a flow rate of 300 μl/ min. The gradient ran from 15% A to 95% A over 18 min, 9 min isocratic at 95% A, and re-equilibration for 7 min. Metabolite detection was achieved with a Thermo Scientific Q Exactive mass spectrometer run in polarity switching mode (+3.0 kV / −2.25 kV). TraceFinder 3.1 (Thermo Scientific) was used to quantify metabolites as the area under the curve using retention time and accurate mass measurements (≤3 ppm). Relative amounts of metabolites were calculated by summing up all isotopomers of a given metabolite and normalized to the internal standard and cell number. Natural occurring ^{13}C was accounted for as described by Yuan et al. (2008).

Statistical Analyses

All experiments were repeated at least two times with identical or similar results. Data represent biological replicates. Appropriate statistical tests were used for every figure. Mean ± SD is plotted in all figures. See the Supplemental Experimental Procedures for details.

SUPPLEMENTAL INFORMATION

Supplemental Information includes Supplemental Experimental Procedures and four figures and can be found with this article online at http://dx.doi.org/10.1016/j.cmet.2015.06.009.

AUTHOR CONTRIBUTIONS

The majority of experiments were designed and performed by X.F.; lifespan assays by R.M.C.; DARTS by H.H.; mitochondrial respiration study design and analyses by L.V. and K.R.; enzyme inhibition assays by R.M.C.; compound syntheses by G.D., Y.X., and M.E.J.; and metabolomic profiling and analysis by X.F. and D.B. S.L., L.T., D.A.N., M.Y.P., F.F., C.C., R.M.P., M.A.T., A.L., K.F.F., M.J., S.G.C., T.F.C., T.G.G., D.B., H.R.C., M.E.J., L.V., and K.R. provided guidance, specialized reagents, and expertise. X.F., K.R., and J.H. wrote the paper. X.F., R.M.C., and J.H. analyzed data. All authors discussed the results and contributed to aspects of preparing the manuscript.

ACKNOWLEDGMENTS

We thank Chris Walsh for insightful suggestions and advice. This work was supported by the Oppenheimer Program, NIH grants R01 AT006889 and P01 HL028481, and UCLA Jonsson Cancer Center Foundation and National Center for Advancing Translational Sciences UCLA Clinical and Translational Science Institute (CTSI) Grant UL1TR000124. X.F. is a recipient of a China Scholarship Council scholarship. R.M.C. is a postdoctoral fellow supported by the UCLA Tumor Immunology Training Program (NIH T32 CA009120). M.Y.P. was a trainee of the UCLA C&MB training grant (NIH T32 GM007185). Support for L.V. and K.R. was from the Leducq Foundation. This paper is dedicated to Dr. Judith Gasson in honor of her 20 years as Director of the Jonsson Comprehensive Cancer Center.

Received: October 16, 2014
Revised: February 27, 2015
Accepted: June 10, 2015
Published: July 16, 2015

REFERENCES

Birsoy, K., Possemato, R., Lorbeer, F.K., Bayraktar, E.C., Thiru, P., Yucel, B., Wang, T., Chen, W.W., Clish, C.B., and Sabatini, D.M. (2014). Metabolic determinants of cancer cell sensitivity to glucose limitation and biguanides. Nature *508*, 108–112.

Blagosklonny, M.V., and Hall, M.N. (2009). Growth and aging: a common molecular mechanism. Aging (Albany, N.Y. Online) *1*, 357–362.

Brand, M.D., and Nicholls, D.G. (2011). Assessing mitochondrial dysfunction in cells. Biochem. J. *435*, 297–312.

Chan, S.M., Thomas, D., Corces-Zimmerman, M.R., Xavy, S., Rastogi, S., Hong, W.J., Zhao, F., Medeiros, B.C., Tyvoll, D.A., and Majeti, R. (2015). Isocitrate dehydrogenase 1 and 2 mutations induce BCL-2 dependence in acute myeloid leukemia. Nat. Med. *21*, 178–184.

Chin, R.M., Fu, X., Pai, M.Y., Vergnes, L., Hwang, H., Deng, G., Diep, S., Lomenick, B., Meli, V.S., Monsalve, G.C., et al. (2014). The metabolite α-ketoglutarate extends lifespan by inhibiting ATP synthase and TOR. Nature *510*, 397–401.

da Silva, C.G., Ribeiro, C.A., Leipnitz, G., Dutra-Filho, C.S., Wyse AT, A.T., Wannmacher, C.M., Sarkis, J.J., Jakobs, C., and Wajner, M. (2002). Inhibition of cytochrome c oxidase activity in rat cerebral cortex and human skeletal muscle by D-2-hydroxyglutaric acid in vitro. Biochim. Biophys. Acta *1586*, 81–91.

Dang, L., White, D.W., Gross, S., Bennett, B.D., Bittinger, M.A., Driggers, E.M., Fantin, V.R., Jang, H.G., Jin, S., Keenan, M.C., et al. (2009). Cancer-associated IDH1 mutations produce 2-hydroxyglutarate. Nature *462*, 739–744.

Dennis, P.B., Jaeschke, A., Saitoh, M., Fowler, B., Kozma, S.C., and Thomas, G. (2001). Mammalian TOR: a homeostatic ATP sensor. Science *294*, 1102–1105.

Gross, S., Cairns, R.A., Minden, M.D., Driggers, E.M., Bittinger, M.A., Jang, H.G., Sasaki, M., Jin, S., Schenkein, D.P., Su, S.M., et al. (2010). Cancer-associated metabolite 2-hydroxyglutarate accumulates in acute myelogenous leukemia with isocitrate dehydrogenase 1 and 2 mutations. J. Exp. Med. *207*, 339–344.

Inoki, K., Kim, J., and Guan, K.L. (2012). AMPK and mTOR in cellular energy homeostasis and drug targets. Annu. Rev. Pharmacol. Toxicol. *52*, 381–400.

Johnson, L.V., Walsh, M.L., Bockus, B.J., and Chen, L.B. (1981). Monitoring of relative mitochondrial membrane potential in living cells by fluorescence microscopy. J. Cell Biol. *88*, 526–535.

Koivunen, P., Lee, S., Duncan, C.G., Lopez, G., Lu, G., Ramkissoon, S., Losman, J.A., Joensuu, P., Bergmann, U., Gross, S., et al. (2012). Transformation by the (R)-enantiomer of 2-hydroxyglutarate linked to EGLN activation. Nature *483*, 484–488.

Kölker, S., Pawlak, V., Ahlemeyer, B., Okun, J.G., Hörster, F., Mayatepek, E., Krieglstein, J., Hoffmann, G.F., and Köhr, G. (2002). NMDA receptor activation and respiratory chain complex V inhibition contribute to neurodegeneration in d-2-hydroxyglutaric aciduria. Eur. J. Neurosci. *16*, 21–28.

Kranendijk, M., Struys, E.A., van Schaftingen, E., Gibson, K.M., Kanhai, W.A., van der Knaap, M.S., Amiel, J., Buist, N.R., Das, A.M., de Klerk, J.B., et al. (2010). IDH2 mutations in patients with D-2-hydroxyglutaric aciduria. Science *330*, 336.

Kranendijk, M., Struys, E.A., Salomons, G.S., Van der Knaap, M.S., and Jakobs, C. (2012). Progress in understanding 2-hydroxyglutaric acidurias. J. Inherit. Metab. Dis. *35*, 571–587.

Latini, A., da Silva, C.G., Ferreira, G.C., Schuck, P.F., Scussiato, K., Sarkis, J.J., Dutra Filho, C.S., Wyse, A.T., Wannmacher, C.M., and Wajner, M. (2005). Mitochondrial energy metabolism is markedly impaired by D-2-hydroxyglutaric acid in rat tissues. Mol. Genet. Metab. *86*, 188–199.

Lomenick, B., Hao, R., Jonai, N., Chin, R.M., Aghajan, M., Warburton, S., Wang, J., Wu, R.P., Gomez, F., Loo, J.A., et al. (2009). Target identification using drug affinity responsive target stability (DARTS). Proc. Natl. Acad. Sci. USA *106*, 21984–21989.

Lu, C., Ward, P.S., Kapoor, G.S., Rohle, D., Turcan, S., Abdel-Wahab, O., Edwards, C.R., Khanin, R., Figueroa, M.E., Melnick, A., et al. (2012). IDH mutation impairs histone demethylation and results in a block to cell differentiation. Nature *483*, 474–478.

Parsons, D.W., Jones, S., Zhang, X., Lin, J.C., Leary, R.J., Angenendt, P., Mankoo, P., Carter, H., Siu, I.M., Gallia, G.L., et al. (2008). An integrated genomic analysis of human glioblastoma multiforme. Science *321*, 1807–1812.

Reitman, Z.J., Jin, G., Karoly, E.D., Spasojevic, I., Yang, J., Kinzler, K.W., He, Y., Bigner, D.D., Vogelstein, B., and Yan, H. (2011). Profiling the effects of isocitrate dehydrogenase 1 and 2 mutations on the cellular metabolome. Proc. Natl. Acad. Sci. USA *108*, 3270–3275.

Rohle, D., Popovici-Muller, J., Palaskas, N., Turcan, S., Grommes, C., Campos, C., Tsoi, J., Clark, O., Oldrini, B., Komisopoulou, E., et al. (2013). An inhibitor of mutant IDH1 delays growth and promotes differentiation of glioma cells. Science *340*, 626–630.

Shaw, R.J. (2009). LKB1 and AMP-activated protein kinase control of mTOR signalling and growth. Acta Physiol. (Oxf.) *196*, 65–80.

Stafford, P., Abdelwahab, M.G., Kim, Y., Preul, M.C., Rho, J.M., and Scheck, A.C. (2010). The ketogenic diet reverses gene expression patterns and reduces reactive oxygen species levels when used as an adjuvant therapy for glioma. Nutr. Metab. (Lond) *7*, 74.

Steenweg, M.E., Jakobs, C., Errami, A., van Dooren, S.J., Adeva Bartolomé, M.T., Aerssens, P., Augoustides-Savvapoulou, P., Baric, I., Baumann, M., Bonafé, L., et al. (2010). An overview of L-2-hydroxyglutarate dehydrogenase gene (L2HGDH) variants: a genotype-phenotype study. Hum. Mutat. *31*, 380–390.

Sun, X., Wheeler, C.T., Yolitz, J., Laslo, M., Alberico, T., Sun, Y., Song, Q., and Zou, S. (2014). A mitochondrial ATP synthase subunit interacts with TOR signaling to modulate protein homeostasis and lifespan in Drosophila. Cell Rep. *8*, 1781–1792.

Tarhonskaya, H., Rydzik, A.M., Leung, I.K., Loik, N.D., Chan, M.C., Kawamura, A., McCullagh, J.S., Claridge, T.D., Flashman, E., and Schofield, C.J. (2014). Non-enzymatic chemistry enables 2-hydroxyglutarate-mediated activation of 2-oxoglutarate oxygenases. Nat. Commun. *5*, 3423.

van den Bent, M.J., Dubbink, H.J., Marie, Y., Brandes, A.A., Taphoorn, M.J., Wesseling, P., Frenay, M., Tijssen, C.C., Lacombe, D., Idbaih, A., et al. (2010). IDH1 and IDH2 mutations are prognostic but not predictive for outcome in anaplastic oligodendroglial tumors: a report of the European Organization for Research and Treatment of Cancer Brain Tumor Group. Clin. Cancer Res. *16*, 1597–1604.

Vander Heiden, M.G., Cantley, L.C., and Thompson, C.B. (2009). Understanding the Warburg effect: the metabolic requirements of cell proliferation. Science *324*, 1029–1033.

Wajner, M., Vargas, C.R., Funayama, C., Fernandez, A., Elias, M.L., Goodman, S.I., Jakobs, C., and van der Knaap, M.S. (2002). D-2-Hydroxyglutaric aciduria in a patient with a severe clinical phenotype and unusual MRI findings. J. Inherit. Metab. Dis. *25*, 28–34.

Walker, J.E. (2013). The ATP synthase: the understood, the uncertain and the unknown. Biochem. Soc. Trans. *41*, 1–16.

Wang, F., Travins, J., DeLaBarre, B., Penard-Lacronique, V., Schalm, S., Hansen, E., Straley, K., Kernytsky, A., Liu, W., Gliser, C., et al. (2013). Targeted inhibition of mutant IDH2 in leukemia cells induces cellular differentiation. Science *340*, 622–626.

Warburg, O. (1956). On the origin of cancer cells. Science *123*, 309–314.

Ward, P.S., Patel, J., Wise, D.R., Abdel-Wahab, O., Bennett, B.D., Coller, H.A., Cross, J.R., Fantin, V.R., Hedvat, C.V., Perl, A.E., et al. (2010). The common feature of leukemia-associated IDH1 and IDH2 mutations is a neomorphic enzyme activity converting alpha-ketoglutarate to 2-hydroxyglutarate. Cancer Cell *17*, 225–234.

Wheaton, W.W., Weinberg, S.E., Hamanaka, R.B., Soberanes, S., Sullivan, L.B., Anso, E., Glasauer, A., Dufour, E., Mutlu, G.M., Budigner, G.S., and Chandel, N.S. (2014). Metformin inhibits mitochondrial complex I of cancer cells to reduce tumorigenesis. eLife *3*, e02242.

Xu, W., Yang, H., Liu, Y., Yang, Y., Wang, P., Kim, S.H., Ito, S., Yang, C., Wang, P., Xiao, M.T., et al. (2011). Oncometabolite 2-hydroxyglutarate is a competitive inhibitor of α-ketoglutarate-dependent dioxygenases. Cancer Cell *19*, 17–30.

Yan, H., Parsons, D.W., Jin, G., McLendon, R., Rasheed, B.A., Yuan, W., Kos, I., Batinic-Haberle, I., Jones, S., Riggins, G.J., et al. (2009). IDH1 and IDH2 mutations in gliomas. N. Engl. J. Med. *360*, 765–773.

Yuan, J., Bennett, B.D., and Rabinowitz, J.D. (2008). Kinetic flux profiling for quantitation of cellular metabolic fluxes. Nat. Protoc. *3*, 1328–1340.

Cell Metabolism, Volume *22*

Supplemental Information

2-Hydroxyglutarate Inhibits ATP Synthase and mTOR Signaling

Xudong Fu, Randall M. Chin, Laurent Vergnes, Heejun Hwang, Gang Deng, Yanpeng Xing, Melody Y. Pai, Sichen Li, Lisa Ta, Farbod Fazlollahi, Chuo Chen, Robert M. Prins, Michael A. Teitell, David A. Nathanson, Albert Lai, Kym F. Faull, Meisheng Jiang, Steven G. Clarke, Timothy F. Cloughesy, Thomas G. Graeber, Daniel Braas, Heather R. Christofk, Michael E. Jung, Karen Reue, and Jing Huang

Supplemental Figures

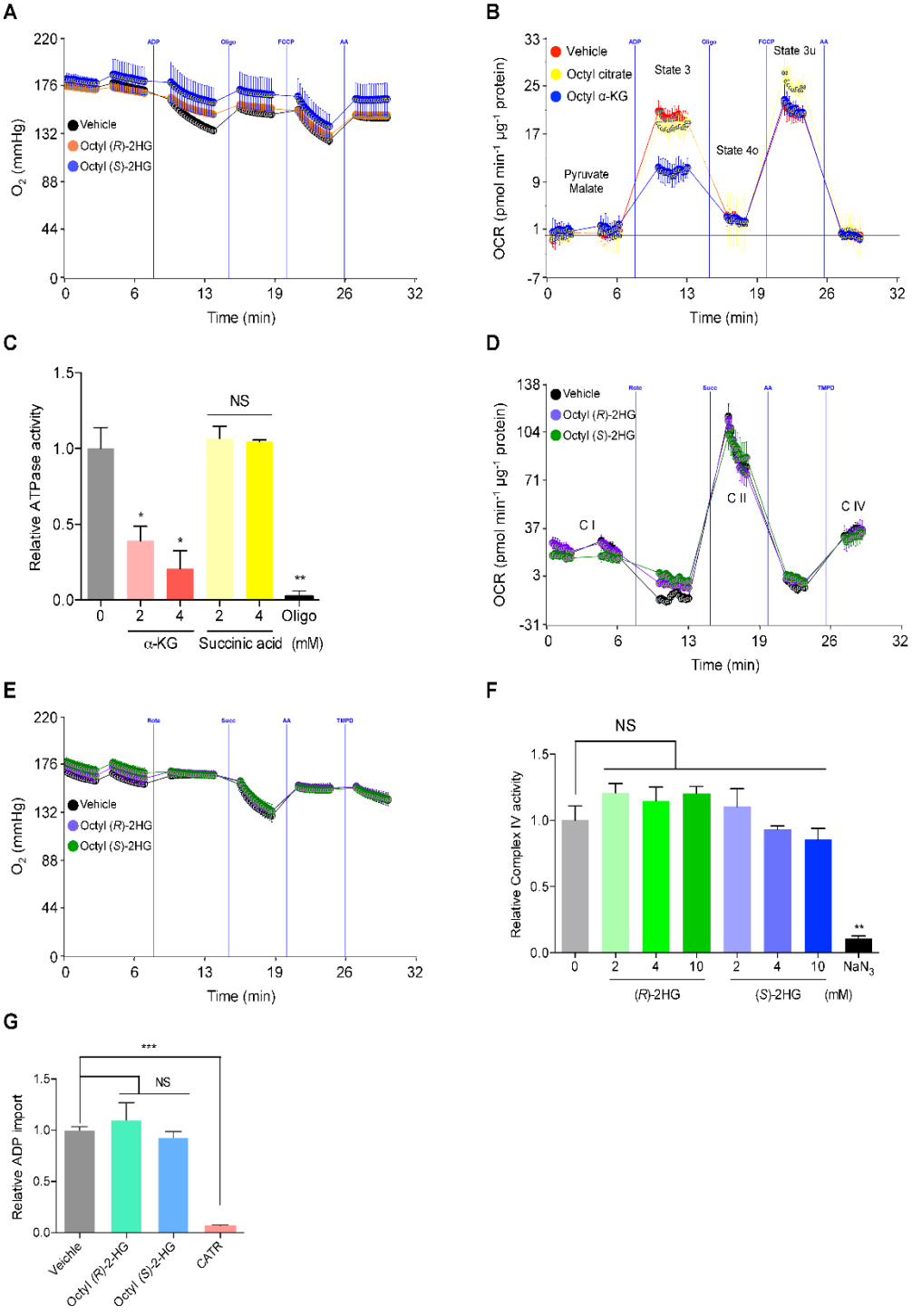

Figure S1, related to Figure 2. 2-HG does not affect the electron flow through the electron transport chain and does not affect ADP import

(A) Kinetic graphs of oxygen tension for Complex II coupling assay shown in Figure 2B, indicating that oxygen is not limiting in the assay.

(B) Octyl citrate (600 μM) has no effect on mitochondrial respiration and serves as a negative control for octyl 2-HG in Figure 2B; octyl α-KG (Chin et al., 2014) serves as a positive control.

(C) Inhibition of submitochondrial particle ATPase activity by α-KG acid and not by succinic acid (*P < 0.05, **P < 0.01; NS, P > 0.05; unpaired t-test, two-tailed, two-sample unequal variance). Oligo, oligomycin (32 μM). Mean ± s.d. is plotted.

(D) OCR from isolated mouse liver mitochondria at basal (pyruvate and malate as Complex I substrates, in presence of FCCP) and in response to sequential injection of rotenone (Rote; Complex I inhibitor), succinate (Complex II substrate), antimycin A (AA; complex III inhibitor), tetramethylphenylenediamine (TMPD; cytochrome c (Complex IV) substrate). No difference in Complex I (C I), Complex II (C II), or Complex IV (C IV) respiration is observed after 30 min treatment with 600 μM of octyl 2-HG, whereas Complex V is inhibited (Figure 2B) by the same treatment (2 independent experiments). Octanol is used as vehicle.

(E) Kinetic graphs of oxygen tension for the electron flow assay shown in (D), indicating that oxygen is not limiting in the assay.

(F) 2-HG does not inhibit Complex IV (NS, P > 0.05). NaN_3 (5 mM), a known Complex IV inhibitor, is used as positive control (**P = 0.0037; unpaired t-test, two-tailed, two-sample unequal variance). Mean ± s.d. is plotted.

(G) ADP import was measured in the presence of octanol (vehicle control) or octyl 2-HG (600 μM). Octyl *(R)*-2HG, P = 0.4237; octyl *(S)*-2HG, P = 0.1623. CATR (carboxyatractyloside, 10 μM), a known inhibitor for ADP import, was used as a positive control for the assay (***P = 0.0003). By unpaired t-test, two-tailed, two-sample unequal variance. Mean ± s.d. is plotted in all cases.

(A-G) Results were replicated in at least two independent assays.

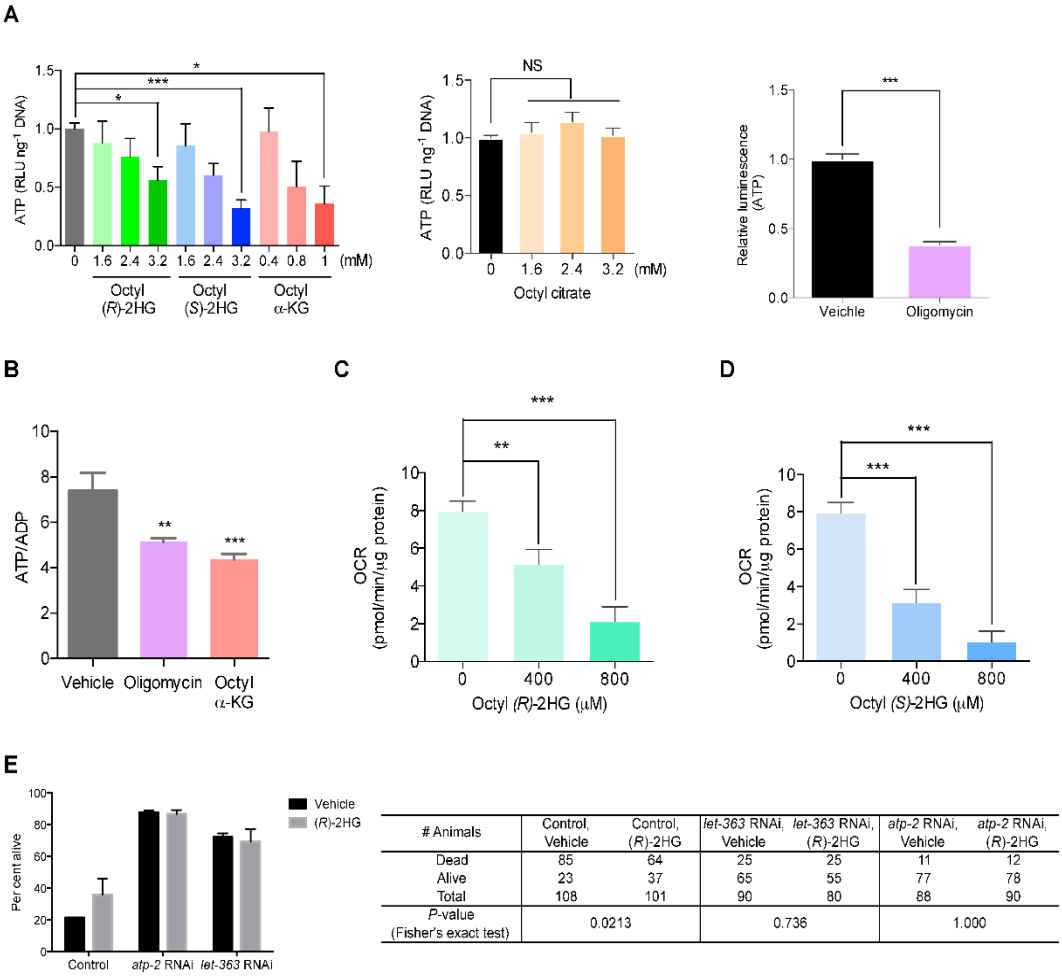

# Animals	Control, Vehicle	Control, (*R*)-2HG	*let-363* RNAi, Vehicle	*let-363* RNAi, (*R*)-2HG	*atp-2* RNAi, Vehicle	*atp-2* RNAi, (*R*)-2HG
Dead	85	64	25	25	11	12
Alive	23	37	65	55	77	78
Total	108	101	90	80	88	90
P-value (Fisher's exact test)	0.0213		0.736		1.000	

Figure S2, related to Figure 2. 2-HG inhibits cellular respiration and decreases ATP levels
(A) Decreased ATP content in U87 cells treated with octyl 2-HG or octyl α-KG (**P* < 0.05, ****P* < 0.001), but not with octyl citrate (NS, *P* > 0.05). Oligomycin (5 μM), a known inhibitor of ATP synthase, is used as a positive control. Octanol has no effect on ATP content.
(B) Octyl α-KG (800 μM) decreases ATP/ADP ratio. Oligomycin (5 μM) is a positive control. ***P* < 0.01, ****P* < 0.001.
(C-D) U87 cells treated with octyl 2-HG have decreased ATP synthase dependent (oligomycin sensitive) oxygen consumption rate (OCR) (***P* < 0.01, ****P* < 0.001).
By unpaired *t*-test, two-tailed, two-sample unequal variance.
(E) 2-HG longevity is mediated through ATP synthase and TOR. *atp-2* and *let-363* are the *C. elegans* homologs of ATP5B and TOR, respectively. Percent alive at day 19 of adulthood is plotted. **P* < 0.05, by Fisher's exact test, two-tailed.
(A-E) Results were replicated in at least two independent assays. Mean ± s.d. is plotted in all cases.

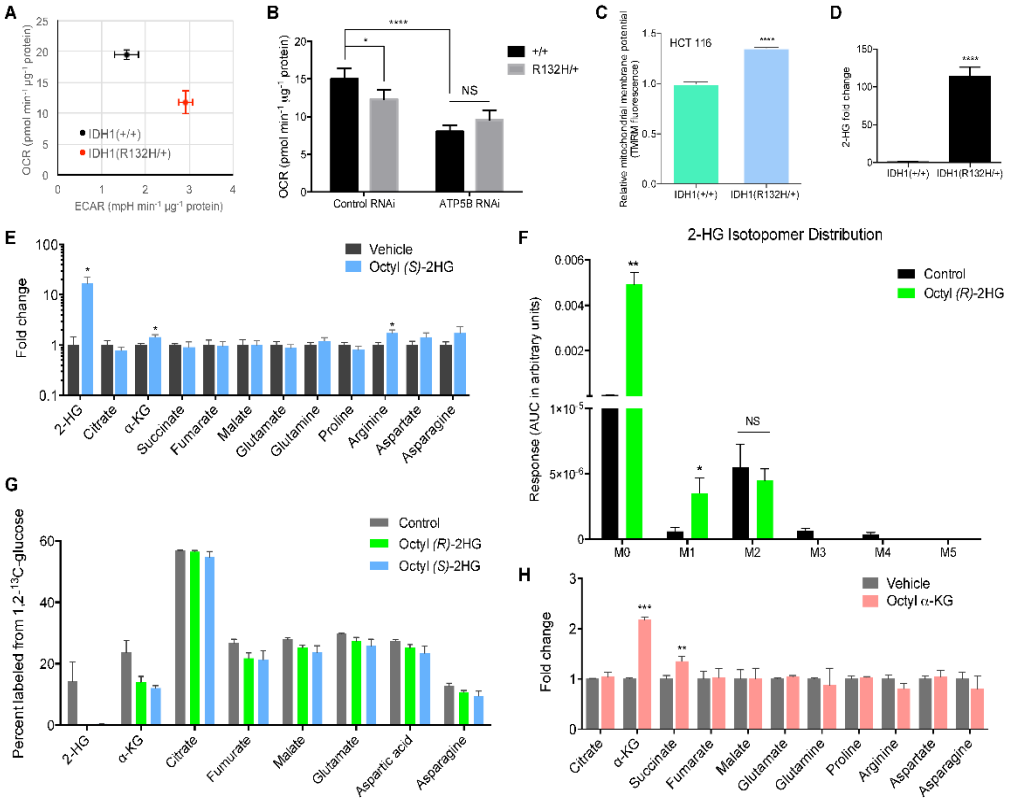

Figure S3, related to Figure 3. Cellular energetics and metabolic profiles of 2-HG accumulated cells

(A) HCT 116 IDH1(R132H/+) cells exhibit decreased respiration (***P* = 0.0015).

(B) Decreased respiration in HCT 116 IDH1(R132H/+) cells is ATP synthase dependent (**P* = 0.01; *****P* < 0.0001; NS, *P* = 0.0868).

(C) HCT 116 IDH1(R132H/+) cells exhibit increased mitochondrial membrane potential (*****P* < 0.0001); data were normalized to cell number.

(D) 2-HG levels are ~100 folder higher in HCT 116/IDH1(R132H/+) cells than in parental control cells (*****P* < 0.0001).

(E) Metabolic profile of TCA cycle intermediates and related amino acids in octyl *(S)*-2HG treated U87 cells (**P* < 0.05).

(F) 2-HG isotopomer distribution in cells cultured in medium containing 1,2-^{13}C-glucose. ***P* = 0.0039, **P* = 0.0407; NS, *P* = 0.4399.

(G) Percentage of labeled metabolites in cells cultured in medium containing 1,2-^{13}C-glucose. By unpaired *t*-test, two-tailed, two-sample unequal variance. Mean ± s.d. is plotted in all cases. Oligomycin has been reported to affect the total glucose contribution to citrate (Fendt et al., 2013). Since oligomycin inhibits the F_O subunit whereas 2-HG (and α-KG) targets the F_1 subunit, it is not likely that they will confer completely the same effects. Different levels of ATP synthase inhibition by α-KG, oligomycin, and genetic alterations are also known to elicit similar but non-identical phenotypes (Chin *et al.*, 2014).

(H) Metabolic profile of TCA cycle intermediates and related amino acids in octyl α-KG treated HEK 293 cells (***$P < 0.001$, **$P < 0.01$).
(A-G) Results were replicated in two independent experiments; (H) results were obtained from three biological replicates in one experiment.

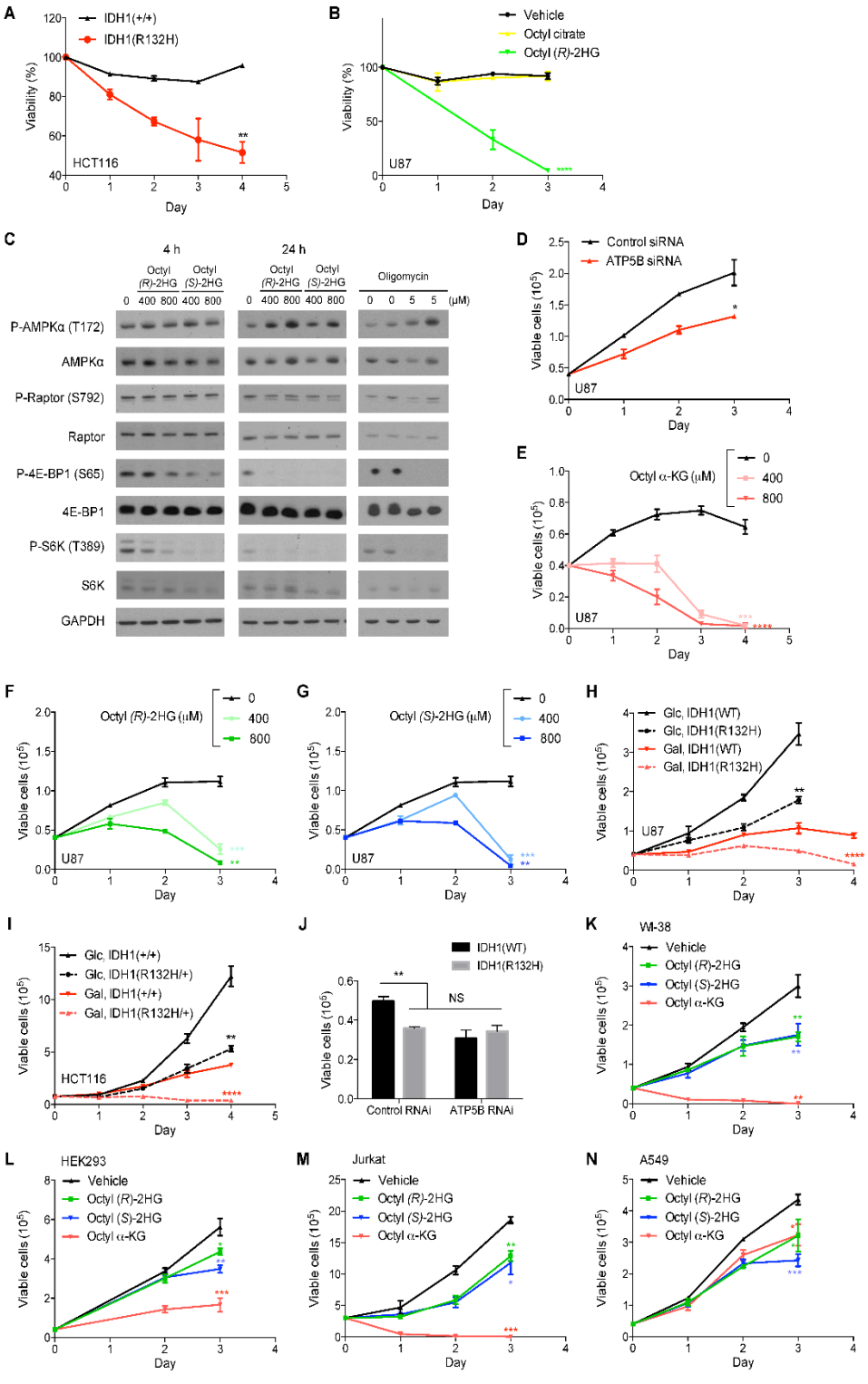
A
IDH1(+/+)
IDH1(R132H)
Viability (%)
HCT116
Day
B
Vehicle
Octyl citrate
Octyl (R)-2HG
Viability (%)
U87
Day
C
4 h
24 h
Octyl (R)-2HG
Octyl (S)-2HG
Oligomycin
0 400 800 400 800 0 400 800 400 800 0 0 5 5 (μM)
P-AMPKα (T172)
AMPKα
P-Raptor (S792)
Raptor
P-4E-BP1 (S65)
4E-BP1
P-S6K (T389)
S6K
GAPDH
D
Control siRNA
ATP5B siRNA
Viable cells (10^5)
U87
Day
E
Octyl α-KG (μM)
0
400
800
Viable cells (10^5)
U87
Day
F
Octyl (R)-2HG (μM)
0
400
800
Viable cells (10^5)
U87
Day
G
Octyl (S)-2HG (μM)
0
400
800
Viable cells (10^5)
U87
Day
H
Glc, IDH1(WT)
Glc, IDH1(R132H)
Gal, IDH1(WT)
Gal, IDH1(R132H)
Viable cells (10^5)
U87
Day
I
Glc, IDH1(+/+)
Glc, IDH1(R132H/+)
Gal, IDH1(+/+)
Gal, IDH1(R132H/+)
Viable cells (10^5)
HCT116
Day
J
IDH1(WT)
IDH1(R132H)
NS
Viable cells (10^5)
Control RNAi
ATP5B RNAi
K
WI-38
Vehicle
Octyl (R)-2HG
Octyl (S)-2HG
Octyl α-KG
Viable cells (10^5)
Day
L
HEK293
Vehicle
Octyl (R)-2HG
Octyl (S)-2HG
Octyl α-KG
Viable cells (10^5)
Day
M
Jurkat
Vehicle
Octyl (R)-2HG
Octyl (S)-2HG
Octyl α-KG
Viable cells (10^5)
Day
N
A549
Vehicle
Octyl (R)-2HG
Octyl (S)-2HG
Octyl α-KG
Viable cells (10^5)
Day

Figure S4, related to Figure 4. Cells with ATP5B knockdown, octyl α-KG or octyl 2-HG treatment, or IDH mutations exhibit decreased viability and proliferation rate.
(A) HCT 116 IDH1(R132H/+) cells exhibit decreased viability upon glucose starvation. Cells were cultured in glucose-free, galactose-containing medium.
(B) Octyl citrate treated U87 cells do not exhibit altered viability upon glucose starvation. Cells were cultured in galactose medium. Octyl citrate and octyl (*R*)-2HG were each at 800 μM.
(C) mTOR complex I activity is decreased in U87 cells treated with octyl 2-HG through both an AMPK-independent and AMPK-depenent manner. Cells were cultured in glucose-free, galactose-containing medium. Phospho-raptor (S792) is not clearly modulated upon octyl 2-HG treatment, suggesting that raptor phosphorylation may not play a major role in 2-HG mediated mTOR signaling in U87 cells, consistent with results using oligomycin treatment.
(D) ATP5B knockdown decreases the growth rate of U87 cells even in glucose-containing medium.
(E-G) U87cells exhibit decreased growth rate upon treatment with octyl α-KG (E), octyl *(R)*-2HG (F), or octyl *(S)*-2HG (G) in glucose-free medium (galactose medium). In glucose-containing medium growth rate was also reduced albeit to a lesser extent (not shown).
(H) Compared to U87/IDH(WT) cells, U87/IDH1(R132H) cells exhibit decreased growth rate both in glucose-containing (Glc) and in glucose-free, galactose-contaning (Gal) media.
(I) HCT 116 IDH1(R132H/+) cells present decreased proliferation both in glucose-containing (Glc) and in glucose-free, galactose-containing (Gal) media.
(J) Reduced growth in U87/IDH1(R132H) cells is ATP synthase dependent.
(K-N) WI-38, HEK293,Jurkat, A549 cells also exhibit decreased growth rate upon treatment with octyl 2-HG or octyl α-KG in glucose-containing medium.
$^{****}P < 0.0001$, $^{***}P < 0.001$, $^{**}P < 0.01$, $^{*}P < 0.05$; NS, $P > 0.05$; unpaired *t*-test, two-tailed, two-sample unequal variance. Mean ± s.d. is plotted in all cases. All growth curve results were replicated in at least two independent experimens.

Supplemental Experimental Procedures

Lifespan analysis

Lifespan experiments were performed as previously described (Chin et al., 2014). Lifespan assays were conducted at 20 °C on solid nematode growth media (NGM) using standard protocols and were replicated in at least two independent experiments. *C. elegans* were synchronized by performing either a timed egg lay (Sutphin and Kaeberlein, 2009) or an egg preparation (lysing ~100 gravid worms in 70 µl M9 buffer (Brenner, 1974), 25 µl bleach (10% sodium hypochlorite solution) and 5 µl 10 N NaOH). L4 or young adult animals were picked onto NGM assay plates containing 1.5% dimethyl sulfoxide (DMSO; Sigma, D8418), 49.5 µM 5-fluoro-2′-deoxyuridine (Sutphin and Kaeberlein, 2009)(FUDR; Sigma, F0503), and D-2-HG (Sigma, H8378), L-2-HG (Sigma, 90790), α-KG (Sigma, K1128), or vehicle control (H_2O). FUDR was included to prevent progeny production. All compounds were mixed into the NGM media after autoclaving and before solidification of the media. Assay plates were seeded with OP50. For RNAi experiments, NGM assay plates also contained 1 mM isopropyl-b-D-thiogalactoside (IPTG) and 50 µg/mL ampicillin, and were seeded with the appropriate RNAi feeding clone (Thermo Scientific / OpenBiosystems). The *C. elegans* TOR (*let-363*) RNAi clone was obtained from Joseph Avruch (MGH/Harvard). Worms were moved to new assay plates every 4 days (to ensure sufficient food was present at all times and to reduce the risk of mould contamination). To assess the survival of the worms, the animals were prodded with a platinum wire every 2–3 days, and those that failed to respond were scored as dead. Animals were assigned randomly to the experimental groups. Worms that ruptured, bagged (that is, exhibited internal progeny hatching), or crawled off the plates were censored. Lifespan data were analysed using GraphPad Prism; *P* values were calculated using the log-rank (Mantel–Cox) test unless stated otherwise.

Target identification using drug affinity responsive target stability (DARTS)

DARTS was performed as described (Lomenick et al., 2009; Lomenick et al., 2011). Briefly, U87 cells were lysed in M-PER buffer (Thermo Scientific, 78501) with the addition of protease (Roche, 11836153001) and phosphatase (50 mM NaF, 2 mM Na_3VO_4) inhibitors. Chilled TNC buffer (50 mM Tris-HCl pH 8.0, 50 mM NaCl, 10 mM $CaCl_2$) was added to the lysate, and protein concentration of the solution was measured on an aliquot by the BCA Protein Assay kit (Pierce, 23227). The remaining lysate was then incubated with vehicle control (H_2O) or varying concentrations of 2-HG or α-KG for 0.5 h at room temperature. The samples were then subjected to Pronase (Roche, 10165921001) digestions (5 min at room temperature) that were stopped by addition of SDS loading buffer and immediate heating (95 °C, 5 min). Samples were subjected to SDS-PAGE on 4-12% Bis-Tris gradient gel (Invitrogen, NP0322BOX), and Western blotting was carried out with antibodies against ATP5B (Sigma, AV48185) or GAPDH (Santa Cruz, SC25778).

Cell Culture

U87 cells were cultured in glucose-free DMEM (Life technologies, 11966-025) supplemented with 10% fetal bovine serum (FBS) and 10 mM glucose or 10 mM galactose when indicated. IDH1(R132H) and IDH1(WT) expressing U87 cells were as reported (Li et al., 2013). U87 cells are unable to utilize ketone bodies for energy (Maurer et al., 2011; Seyfried et al., 2011). HCT 116 IDH1(R132H/+) and parental control cells (Horizon Discovery, HD 104-013) were cultured in RPMI (Life technologies, 11875-093) supplemented with 10% FBS or DMEM (Life technologies, 11966-025) supplemented with 10% FBS and

10 mM glucose or 10 mM galactose. Normal human diploid fibroblasts WI-38 (ATCC, CCL-75) were cultured with EMEM (ATCC, 30-2003) supplemented with 10% FBS. HEK 293, A549, and HeLa cells were cultured with DMEM (Life technologies, 11966-065) supplemented with 10% FBS. Jurkat cells were cultured in RPMI supplemented with 10% FBS. All cells were cultured at 37°C and 5% CO2. Cells were transfected with indicated siRNA using DharmaFECT 1 Transfection Reagent by following the manufacturer's instructions. Knockdown efficiency was confirmed by Western blotting.

Assay for cellular ATP levels

For Figure S2A, U87 cells were seeded in 96-well plates at 2 x 10^4 cells per well and treated with indicated compound for 2 h in triplicate. ATP levels were measured using the CellTiter-Glo luminescent ATP assay (Promega, G7572); luminescence was read using Analyst HT (Molecular Devices). To confirm that the number of cells was consistent between treatments, cell lysates were further subjected to dsDNA staining using QuantiFluor dsDNA system (Promega). Statistical analysis was performed using GraphPad Prism (unpaired *t*-test).

Determination of ATP/ADP ratio

For Figure 2D and Figure S2B, U87 cells were seeded in 96-well plates at 10^4 cells/well and treated with indicated compound for 24 h. ATP/ADP ratios were measured by using EnzyLight ADP/ATP Ratio Assay Kit (BioAssay Systems); luminescence was read using Synergy H1m (BioTek). For Figure 3A, ATP and ADP levels were measured by LC-MS.

Measurement of oxygen consumption rates (OCR) and extracellular acidification rates (ECAR)

OCR and ECAR measurements were made using a Seahorse XF-24 analyzer (Seahorse Bioscience)(Wu et al., 2007). U87 cells were seeded in Seahorse XF-24 cell culture microplates at 50,000 cells per well in DMEM supplemented with 10% FBS and either 10 mM glucose or 10 mM galactose, and incubated O/N at 37 °C in 5% CO_2. Treatment with octyl α-KG, octyl (*R*)-2HG, octyl (*S*)-2HG, or DMSO (vehicle control) was for 1 h. Cells were washed in unbuffered DMEM (pH 7.4, 10 mM glucose) immediately prior to measurement, and maintained in this buffer with indicated concentrations of compound. OCR or ECAR were measured 3 times under basal conditions and normalized to protein concentration per well. Statistical analysis was performed using GraphPad Prism (unpaired *t*-test, two-tailed, two-sample unequal variance).

Isolation of mitochondria from mouse liver

Animal studies were performed under approved UCLA animal research protocols. Mitochondria from 3-month-old C57BL/6 mice were isolated as described (Rogers et al., 2011). Briefly, livers were extracted, minced at 4 °C in MSHE+BSA (70 mM sucrose, 210 mM mannitol, 5 mM HEPES, 1 mM EGTA, and 0.5% fatty acid free BSA, pH 7.2), and rinsed several times to remove blood. All subsequent steps were performed on ice or at 4 °C. The tissue was disrupted in 10 volumes of MSHE+BSA with a glass Dounce homogenizer (5-6 strokes) and the homogenate was centrifuged at 800 x *g* for 10 min to remove tissue debris and nuclei. The supernatant was decanted through a cell strainer and centrifuged at 8,000 x *g* for 10 min. The dark mitochondrial pellet was resuspended in MSHE+BSA and re-centrifuged at 8,000 x *g* for 10 min. The final mitochondrial pellets were used for various assays as described below.

Measurement of mitochondrial respiration

Mitochondrial respiration was analyzed using isolated mouse liver mitochondria (see (Brand and Nicholls, 2011) and refs therein). Mitochondria were isolated from mouse liver as described above. The final mitochondrial pellet was resuspended in 30 µL of MAS buffer (70 mM sucrose, 220 mM mannitol, 10 mM KH2PO4, 5 mM MgCl2, 2 mM HEPES, 1 mM EGTA, and 0.2% fatty acid free BSA, pH 7.2).
Isolated mitochondrial respiration was measured by running coupling and electron flow assays as described (Rogers et al., 2011). For the coupling assay, 5 µg of mitochondria in complete MAS buffer (MAS buffer supplemented with 10 mM succinate and 2 µM rotenone) were seeded into a XF24 Seahorse plate by centrifugation at 2,000 x *g* for 20 min at 4 °C. Just before the assay, the mitochondria were supplemented with complete MAS buffer for a total of 500 µL (with octanol or octyl 2-HG), and warmed at 37 °C for 30 min before starting the oxygen consumption rate measurements. Mitochondrial respiration begins in a coupled State 2; State 3 is initiated by 2 mM ADP; State 4o (oligomycin-insensitive, that is, complex V independent) is induced by 2.5 µM oligomycin and State 3u (FCCP-uncoupled maximal respiratory capacity) by 4 µM FCCP. Finally, 1.5 µg/mL antimycin A was injected at the end of the assay. For the electron flow assay, the MAS buffer was supplemented with 10 mM sodium pyruvate, 2 mM malate and 4 µM FCCP, and the mitochondria are seeded the same way as described for the coupling assay. After basal readings, the sequential injections were as follows: 2 µM rotenone (complex I inhibitor), 10 mM succinate (complex II substrate), 4 µM antimycin A (complex III inhibitor), and 10 mM/100 µM ascorbate/tetramethylphenylenediamine (complex IV substrate).
There is no known transporter for 2-HG in the mitochondria; transport of α-KG by the α-KG/malate shuttle is rate limiting. If unmodified 2-HG or α-KG were to be used to inhibit ATP synthase, an excessively longer incubation time – which jeopardizes mitochondrial integrity – would be required to allow intra-mitochondrial 2-HG and α-KG to accumulate. Octyl esters of 2-HG and α-KG allow rapid uptake across the intact inner mitochondrial membrane, upon which 2-HG or α-KG is produced through in situ hydrolysis by intramitochondrial esterases.

Submitochondrial particle (SMP) ATPase assay

ATP hydrolysis by ATP synthase was measured using submitochondrial particles (see (Alberts, 1994) and refs therein). Mitochondria were isolated from mouse liver as described above. The final mitochondrial pellet was resuspended in buffer A (250 mM sucrose, 10 mM Tris-HCl, 1 mM ATP, 5 mM $MgCl_2$, and 0.1 mM EGTA, pH 7.4) at 10 µg/µL, subjected to sonication on ice (Fisher Scientific Model 550 Sonic Dismembrator; medium power, alternating between 10 s intervals of sonication and resting on ice for a total of 60 s of sonication), and then centrifuged at 18,000 x *g* for 10 min at 4 °C. The supernatant was collected and centrifuged at 100,000 x *g* for 45 min at 4 °C. The final pellet (submitochondrial particles) was resuspended in buffer B (250 mM sucrose, 10 mM Tris-HCl, and 0.02 mM EGTA, pH 7.4).
Submitochondrial particles were diluted to 2.75 ng/µl in reaction buffer (40 mM Tris pH 7.5, 0.1 mg/mL BSA, 3 mM $MgCl_2$), and then incubated with either vehicle or drug for 45 min at room temperature. To start the ATPase reaction, ATP was added to a final concentration of 125 µM. The amount of phosphate produced after 6 min was determined by the Malachite Green Phosphate Assay Kit (BioAssay POMG-25H) and was used to calculate ATPase activity. Oligomycin (Cell signaling, 9996) was used as a positive control for the assay. Unmodified 2-HG and α-KG were used in the SMP assay since submitochondrial particles are essentially inside-out mitochondria that allow the otherwise inner mitochondrial membrane components access to non-membrane permeable molecules (Alberts, 1994).

Complex IV activity assay

Complex IV activity was assayed using the MitoTox OXPHOS Complex IV Activity Kit (Abcam, ab109906), according to the manufacturer's instructions.

Assay for ADP import

Freshly prepared mice liver mitochondria were suspended at 1 μg/μL in medium consisting of 220 mM mannitol, 70 mM sucrose, 2 mM HEPES, 2.74 μM antimycin A, 5 μM rotenone, 1 mM EGTA, and 10 mM potassium phosphate buffer, pH 7.4. The mitochondria suspension was incubated with designated drug for 30 min in 37 °C. After incubation, the suspension was transferred to ice for 10 min incubation. Afterwards, 100 μM [^{3}H]ADP (specific radioactivity, 185 kBq/pmol) was added, and the mixture was immediately vortexed and incubated for 20 s on ice. The reaction was terminated by addition of 10 μM carboxyatractyloside, and the mixture was centrifuged at 10,000 g for 10 min at 4 °C. After centrifuge, the supernatant was collected for reading and the pellet was washed twice with the same medium supplemented with 10 μM carboxyatractyloside. After washing, the pellet was lysed by the addition of 0.2 ml of 1% SDS. The radioactivity of the lysate and supernatant was determined by TRI-CARB 2300 TR liquid scintillation analyzer. The ADP-ATP translocation rate was determined by the ratio of the pellet versus the sum reading of the pellet and supernatant.

Assay for mitochondria membrane potential

Mitochondrial membrane potential was determined using the MitoPT TMRM kit (ImmunoChemistry, #9105). Readings were normalized to cell number.

Assay for mammalian TOR (mTOR) pathway activity

mTOR pathway activity in cells treated with octyl 2-HG or oligomycin was determined by the levels of phosphorylation of known mTOR substrates, including S6K (T389), 4E-BP1 (S65), AKT (S473), and ULK1 (S757) (Pullen and Thomas, 1997; Burnett et al., 1998; Brunn et al., 1997; Choo et al., 2008; Sengupta et al., 2010; Gingras et al., 2001; Sarbassov et al., 2005; Kim et al., 2011). Specific antibodies used: phospho (P)-S6K T389 (Cell Signaling, 9234), S6K (Cell Signaling, 9202S), P-4E-BP1 S65 (Cell Signaling, 9451S), 4E-BP1 (Cell Signaling, 9452S), P-AKT S473 (Cell Signaling, 4060S), AKT (Cell Signaling, 4691S), P-ULK1 S757 (Cell Signaling, 6888), ULK1 (Cell Signaling, 4773S), P-AMPKα T172 (Cell Signaling, 2535S), AMPKα (Cell Signaling, 2532S), P-Raptor S792 (Cell Signaling, 2083S), Raptor (Cell Signaling, 2280S), and GAPDH (Santa Cruz Biotechnology, 25778).

Synthesis of octyl esters of α-KG, 2-HG, and citrate

Synthesis of 1-octyl α-KG has recently been published by GD and MEJ (Jung and Deng, 2012). Syntheses of octyl (*S*)-2HG and octyl (*R*)-2HG were carried out as reported (Albert et al., 1987; Xu et al., 2011) with modifications below.

Synthesis of 1-Octyl (*S*) 2-hydroxypentanedioate (Octyl (*S*)-2HG)

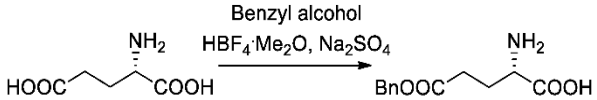

L-Glutamic acid

(*S*)-2-Amino-5-(benzyloxy)-5-oxopentanoic acid: L-Glutamic acid (2.0 g, 13.6 mmol) and anhydrous sodium sulfate (2.0 g) was dissolved in benzyl alcohol (25 mL), and then tetrafluoroboric acid diethyl ether

complex (3.7 mL, 27.2 mmol) was added. The suspended mixture was stirred at 21 °C overnight. Anhydrous THF (75 mL) was added to the mixture and it was filtered through a thick pad of activated charcoal. Anhydrous triethylamine (4.1 mL) was added to the clear filtrate to obtain a milky white slurry. Upon trituration with ethyl acetate (100 mL), the monoester monoacid precipitated. It was collected, washed with additional ethyl acetate (2 X 10 mL), and dried in vacuo to give the desired product (*S*)-2-amino-5-(benzyloxy)-5-oxopentanoic acid (3.07 g, 95%) as a white solid. ^{1}H NMR (500 MHz, Acetic acid-d_4): δ 7.41 – 7.25 (m, 5H), 5.14 (s, 2H), 4.12 (m, 1H), 2.75 – 2.60 (m, 2H), 2.27 (m, 2H). ^{13}C NMR (125 MHz, Acetic acid-d_4): δ 174.6, 174.4, 136.9, 129.5, 129.2, 129.1, 67.7, 55.0, 30.9, 26.3.

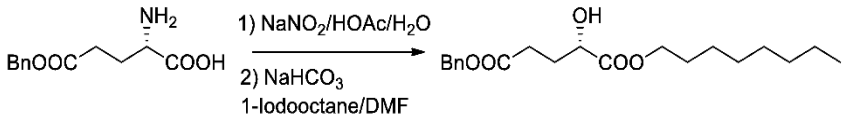

(*S*)-5-Benzyl 1-octyl 2-hydroxypentanedioate: To a solution of (*S*)-2-amino-5-(benzyloxy)-5-oxopentanoic acid (1.187 g, 5.0 mmol) in H_2O (25 mL) and acetic acid (10 mL) cooled to 0 °C was added slowly a solution of aqueous sodium nitrite (1.07 g in 15 mL H_2O). The reaction mixture was allowed to warm slowly to room temperature and was stirred overnight. The mixture was concentrated. The resulting residue was dissolved in DMF (15 mL) and $NaHCO_3$ (1.26 g, 15 mmol) and 1-iodooctane (1.84 mL, 10 mmol) were added to the mixture. The mixture was stirred at 21 °C overnight and then extracted with ethyl acetate (3 × 50 mL). The combined organic phase was washed with water and brine and dried over anhydrous $MgSO_4$. Flash column chromatography on silica gel eluting with 7/1 hexanes/ethyl acetate gave the desired mixed diester (*S*)-5-benzyl 1-octyl 2-hydroxypentanedioate (0.785 g, 45%) as a colorless oil. ^{1}H NMR (500 MHz, $CDCl_3$): δ 7.37 – 7.28 (m, 5H), 5.12 (s, 2H), 4.26 – 4.19 (m, 1H), 4.16 (t, *J* = 6.8 Hz, 2H), 3.11 (m, 1H), 2.61 – 2.46 (m, 2H), 2.26 – 2.14 (m, 1H), 1.95 (m, 1H), 1.71 – 1.57 (m, 2H), 1.39 – 1.20 (m, 10H), 0.88 (t, *J* = 6.9 Hz, 3H). ^{13}C NMR (125 MHz, $CDCl_3$): δ 174.6, 172.8, 135.8, 128.4, 128.1, 128.0, 69.3, 66.2, 65.8, 31.6, 29.6, 29.2, 29.0 (2C's), 28.4, 25.6, 22.5, 13.9.

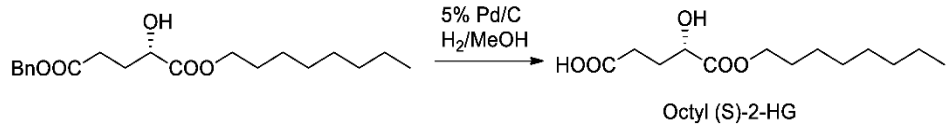

Octyl (S)-2-HG

1-Octyl (*S*) 2-hydroxypentanedioate (octyl (*S*)-2-hydroxyglutarate; octyl (*S*)-2HG): To a solution of (*S*)-5-benzyl 1-octyl 2-hydroxypentanedioate (0.71 g, 2.0 mmol) in MeOH (50 mL) was added 5% Pd/C (80 mg). Over the mixture was passed argon and then the argon was replaced with hydrogen and the mixture was stirred vigorously for 1 h. The mixture was filtered through a thick pad of Celite and the organic phase was evaporated. The residue was purified via flash column chromatography on silica gel eluting with 25/1 CH_2Cl_2/MeOH to give octyl (*S*)-2HG (0.495 g, 48%) as a white solid. ^{1}H NMR (500 MHz, $CDCl_3$): δ 4.23 (dd, *J* = 8.0, 4.2 Hz, 1H), 4.16 (t, *J* = 6.8 Hz, 2H), 2.60 – 2.42 (m, 2H), 2.15 (m, 1H), 1.92 (m, 1H), 1.69 – 1.59 (m, 2H), 1.38 – 1.16 (m, 10H), 0.86 (t, *J* = 7.0 Hz, 3H). ^{13}C NMR (125 MHz, $CDCl_3$): δ 178.8, 174.8, 69.3, 66.1, 31.7, 29.4, 29.1 (2C's), 28.9, 28.4, 25.7, 22.5, 14.0.

Synthesis of 1-Octyl (*R*) 2-hydroxypentanedioate (Octyl (*R*)-2HG)

The synthesis of the opposite enantiomer, i.e., Octyl (*R*)-2HG, was carried out by the exact same procedure starting with D-glutamic acid. The spectroscopic data was identical to that of the enantiomeric compounds.

Synthesis of 1-octyl citrate ester (Kotick, 1991; Weaver and Gilbert, 1997; Takeuchi et al., 1999)

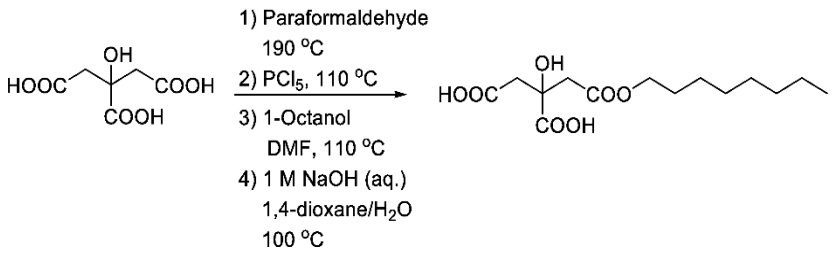

The mixture of citric acid (3.862 g, 0.02 mol) and paraformaldehyde (1.276 g, 0.04 mol) was stirred at 190 °C for 2 h. After cooling down to room temperature, the mixture was purified by flash column chromatography on silica gel eluting with 10/1 dichloromethane/methanol gave the desired methylene acetal of citric acid. The diacetic acid product (0.816 g, 4.0 mmol) and phosphorus (V) chloride (0.850 g, 4.0 mmol) were stirred with heating from room temperature to 110 °C in 1 h and kept at 110 °C until there was no further emission of hydrogen chloride. After cooling the mixture to room temperature, the phosphorus oxychloride was evaporated under vacuum. The residue was dissolved in ethyl acetate, the mixture was filtered, and the organic phase was evaporated. The resulting residue was dissolved in DMF (3.0 mL) and 1-octanol (1.89 mL, 0.012 mol) was added. The mixture was heated to 110 °C for 3 h and then extracted with ethyl acetate (3 × 50 mL). The combined organic phase was washed with water and brine and dried over anhydrous $MgSO_4$. Flash column chromatography on silica gel eluting with 15/1 dichloromethane/methanol gave the mono-octyl methylene acetal of citric acid ester (0.652 g, 52%) as a colorless oil. This mono-octyl ester (0.2576 g, 0.814 mmol) was dissolved in 1,4-dioxane (3.0 mL) and H_2O (3.0 mL). An aqueous solution of NaOH (1.0 M, 0.82 mL) was added to the mixture and the temperature was raised to 100 °C for 2 h. After cooling down the mixture to room temperature, an aqueous solution of NaOH (0.2 M, 10 mL) was added. The mixture was extracted with ethyl acetate (3 X 10mL) and the aqueous phase was acidified with 1.0 M aqueous HCl to pH 1. The acidified aqueous layer was extracted with ethyl acetate (3 X 30 mL), and the combined organic phases were washed with water and brine and dried over anhydrous $MgSO_4$. Flash column chromatography on silica gel, eluting with 10/1 dichloromethane/methanol, gave the 1-octyl citrate ester as an oil (0.183 g, 74%). ^{1}H NMR (500 MHz, $CDCl_3$) δ 10.55 (s, 2H), 4.05 (t, J = 6.5 Hz, 2H), 2.88 (m, 4H), 1.57 (m, 2H), 1.23 (m, 10H), 0.84 (t, J = 6.2 Hz, 3H). ^{13}C NMR (125 MHz, $CDCl_3$) δ 177.63, 174.68, 170.08, 72.82, 65.45, 42.81, 42.69, 31.63, 29.03, 29.01, 28.25, 25.66, 22.48, 13.92.

Supplemental References

Albert, R., Danklmaier, J., Honig, H., and Kandolf, H. (1987). A Simple and Convenient Synthesis of Beta-Aspartates and Gamma-Glutamates. Synthesis-Stuttgart, 635-637.

Alberts, B. (1994). Molecular biology of the cell. (New York: Garland Pub.).

Brand, M.D., and Nicholls, D.G. (2011). Assessing mitochondrial dysfunction in cells. Biochem J *435*, 297-312.

Brenner, S. (1974). The genetics of Caenorhabditis elegans. Genetics *77*, 71-94.

Brunn, G.J., Hudson, C.C., Sekulic, A., Williams, J.M., Hosoi, H., Houghton, P.J., Lawrence, J.C., Jr., and Abraham, R.T. (1997). Phosphorylation of the translational repressor PHAS-I by the mammalian target of rapamycin. Science *277*, 99-101.

Burnett, P.E., Barrow, R.K., Cohen, N.A., Snyder, S.H., and Sabatini, D.M. (1998). RAFT1 phosphorylation of the translational regulators p70 S6 kinase and 4E-BP1. Proc Natl Acad Sci U S A *95*, 1432-1437.

Choo, A.Y., Yoon, S.O., Kim, S.G., Roux, P.P., and Blenis, J. (2008). Rapamycin differentially inhibits S6Ks and 4E-BP1 to mediate cell-type-specific repression of mRNA translation. Proc Natl Acad Sci U S A *105*, 17414-17419.

Fendt, S.M., Bell, E.L., Keibler, M.A., Olenchock, B.A., Mayers, J.R., Wasylenko, T.M., Vokes, N.I., Guarente, L., Vander Heiden, M.G., and Stephanopoulos, G. (2013). Reductive glutamine metabolism is a function of the alpha-ketoglutarate to citrate ratio in cells. Nat Commun *4*, 2236.

Gingras, A.C., Raught, B., Gygi, S.P., Niedzwiecka, A., Miron, M., Burley, S.K., Polakiewicz, R.D., Wyslouch-Cieszynska, A., Aebersold, R., and Sonenberg, N. (2001). Hierarchical phosphorylation of the translation inhibitor 4E-BP1. Genes Dev *15*, 2852-2864.

Jung, M.E., and Deng, G. (2012). Synthesis of the 1-monoester of 2-ketoalkanedioic acids, for example, octyl alpha-ketoglutarate. J Org Chem *77*, 11002-11005.

Kim, J., Kundu, M., Viollet, B., and Guan, K.L. (2011). AMPK and mTOR regulate autophagy through direct phosphorylation of Ulk1. Nat Cell Biol *13*, 132-141.

Kotick, M.P. (1991). Method for regioselective preparation of 1- or 2-monoalkyl citrates as surfactants. U.S. Patent *US5049699*, A19910917.

Li, S., Chou, A.P., Chen, W., Chen, R., Deng, Y., Phillips, H.S., Selfridge, J., Zurayk, M., Lou, J.J., Everson, R.G., et al. (2013). Overexpression of isocitrate dehydrogenase mutant proteins renders glioma cells more sensitive to radiation. Neuro Oncol *15*, 57-68.

Lomenick, B., Jung, G., Wohlschlegel, J.A., and Huang, J. (2011). Target identification using drug affinity responsive target stability (DARTS). Curr Protoc Chem Biol *3*, 163-180.

Maurer, G.D., Brucker, D.P., Bahr, O., Harter, P.N., Hattingen, E., Walenta, S., Mueller-Klieser, W., Steinbach, J.P., and Rieger, J. (2011). Differential utilization of ketone bodies by neurons and glioma cell lines: a rationale for ketogenic diet as experimental glioma therapy. BMC Cancer *11*, 315.

Pullen, N., and Thomas, G. (1997). The modular phosphorylation and activation of p70s6k. FEBS Lett *410*, 78-82.

Rogers, G.W., Brand, M.D., Petrosyan, S., Ashok, D., Elorza, A.A., Ferrick, D.A., and Murphy, A.N. (2011). High throughput microplate respiratory measurements using minimal quantities of isolated mitochondria. PLoS One *6*, e21746.

Sarbassov, D.D., Guertin, D.A., Ali, S.M., and Sabatini, D.M. (2005). Phosphorylation and regulation of Akt/PKB by the rictor-mTOR complex. Science *307*, 1098-1101.

Sengupta, S., Peterson, T.R., and Sabatini, D.M. (2010). Regulation of the mTOR complex 1 pathway by nutrients, growth factors, and stress. Mol Cell *40*, 310-322.

Seyfried, T.N., Kiebish, M.A., Marsh, J., Shelton, L.M., Huysentruyt, L.C., and Mukherjee, P. (2011). Metabolic management of brain cancer. Biochim Biophys Acta *1807*, 577-594.

Sutphin, G.L., and Kaeberlein, M. (2009). Measuring Caenorhabditis elegans life span on solid media. J Vis Exp.

Takeuchi, Y., Nagao, Y., Toma, K., Yoshikawa, Y., Akiyama, T., Nishioka, H., Abe, H., Harayama, T., and Yamamoto, S. (1999). Synthesis and siderophore activity of vibrioferrin and one of its diastereomeric isomers. Chemical & Pharmaceutical Bulletin *47*, 1284-1287.

Weaver, R., and Gilbert, I.H. (1997). The design and synthesis of nucleoside triphosphate isosteres as potential inhibitors of HIV reverse transcriptase. Tetrahedron *53*, 5537-5562.

Wu, M., Neilson, A., Swift, A.L., Moran, R., Tamagnine, J., Parslow, D., Armistead, S., Lemire, K., Orrell, J., Teich, J., et al. (2007). Multiparameter metabolic analysis reveals a close link between attenuated mitochondrial bioenergetic function and enhanced glycolysis dependency in human tumor cells. Am J Physiol Cell Physiol *292*, C125-136.

CHAPTER 4

The metabolite α-ketobutyrate promotes longevity by perturbing pyruvate oxidation and activating AMPK

Abstract

Aging is a complex process that is directly related to human health and disease. The extraordinary finding that aging is malleable, as shown in model organisms whose life and health spans are extended by specific gene mutations, dietary restriction, or pharmacological perturbations, has offered enormous hope for transforming our understanding and treatment of aging and age-related diseases [1,2]. Here we show that an unfamiliar endogenous metabolite, α-ketobutyrate (α-KB), increases the lifespan of adult *Caenorhabditis elegans*, and that α-KB supplementation confers robust protection against an Alzheimer's disease model in *C. elegans*. We find that α-KB perturbs pyruvate oxidation by acting as a competitive alternative substrate of pyruvate dehydrogenase (PDH), rewiring mitochondrial metabolism and activating AMP-activated protein kinase (AMPK). Furthermore, the lifespan increase by α-KB requires PDH and AMPK, which are highly conserved throughout evolution. Our findings suggest that human aging and related degeneration may be remedied by α-KB or α-KB like drugs.

Introduction

Metabolism plays an important role in aging and disease. Increasing evidence has shown that endogenous metabolites, as basic as α-ketoglutarate (α-KG) and nicotinamide adenine dinucleotide (NAD^+), can delay the aging process and increase healthy lifespan[3-5]. Identifying such longevity metabolites and understanding their mechanisms not only can illuminate the biological regulation of aging, but also provide new interventions for aging-related diseases.

Alpha-keto acids are important intermediates in metabolic pathways. Familiar examples include α-KG in the tricarboxylic acid (TCA) cycle, pyruvate as the end product of glycolysis, and branch chain α-keto acids (including α-ketoisovalerate (KIV), α-ketoisocaproate (KIC) and α-keto-β-methylvalerate (KMV) – which are α-keto acid analogues of the branch chain amino acids valine, leucine and isoleucine, respectively) associated with the metabolic disorder maple syrup urine disease. We previously discovered that α-KG extends the lifespan of adult *C. elegans* and identified the highly conserved ATP synthase as a novel target of α-KG in longevity[3]. The unexpected findings suggest that the regulatory networks acted on by metabolites are more complex than currently appreciated. Here we identify a new longevity-promoting α-keto acid, α-ketobutyrate (α-KB), and seek to understand the basis of its mechanism in lifespan regulation.

Results and Discussion

α-KB increases the lifespan of adult *C. elegans*

α-KB (Figure 1A) is a short-chain α-keto acid found in all cells. It is a metabolite in the catabolism of methionine, threonine, and homocysteine. α-KB is formed by cystathionine gamma-lyase from cystathionine, which is generated from homocysteine and serine by cystathionine beta synthase. Transamination of α-KB produces α-aminobutyric acid, a component of the nonribosomal tripeptide ophthalmic acid first found in calf lens. Unlike

pyruvate, α-KG, or branched-chain α-keto acids, there is no specific enzyme for α-KB oxidation. Instead, α-KB can be consumed by the branched-chain α-keto acid dehydrogenase complex (BCKDC) or the pyruvate dehydrogenase complex (PDC) [6]. Additionally, when respiration is inhibited, α-KB can serve as an electron acceptor and be converted to (*R*)-2-hydroxybutyrate (2-HB) by lactate dehydrogenase (LDH) [7]. Although the metabolism of α-KB has been well characterized, its biological function remains poorly understood.

We discovered that α-KB increases the lifespan of adult *C. elegans* by up to ~60% (Figure 1B). α-KB extended the lifespan of wild-type N2 worms in a concentration-dependent manner, with 4 mM α-KB yielding the largest lifespan extension (Figure 1C); 4 mM was the concentration used in all subsequent *C. elegans* experiments unless otherwise stated. α-KB not only extends lifespan, but also delays age-related phenotypes, such as the decline in rapid, coordinated body movement (video not shown). The dilution of the *C. elegans* bacterial food source has been shown to extend worm lifespan [8]. However, α-KB does not inhibit bacterial proliferation (Figure S1), and there is no significant change in food intake, foraging behavior, or body size in α-KB treated animals (data not shown).

α-KB inhibits pyruvate-driven mitochondrial complex I respiration

We previously found that α-KG increases longevity by inhibiting mitochondrial complex V [3]. Given the similarities in structure and lifespan effects of α-KB and α-KG, we first asked whether α-KB may also affect the electron transport chain (ETC) by measuring mitochondrial respiration [9]. Interestingly, we found that when respiration is driven by the complex I substrates pyruvate and malate, there is a significant decrease in ADP-induced (state 3) and FCCP-induced (state 3u) respiration in isolated mitochondria upon α-KB treatment (Figure 2A-B). However, when glutamate and malate are used as complex I substrates or when the complex II substrate

succinate is provided, respiration is unaffected by α-KB (Figure 2A-B). These results show the specificity of α-KB in inhibiting pyruvate-driven complex I respiration, rather than directly interfering with complex I or other ETC complex activity.

α-KB reduces pyruvate oxidation by acting as a competitive alternative substrate of the PDC

The rate of pyruvate oxidation in isolated mitochondria is controlled by the mitochondrial pyruvate carrier (MPC) and PDC [10]. It has been shown that unlike pyruvate, α-KB is able to cross the mitochondrial inner membrane rapidly as a free acid [11]. Given that in our experimental conditions with the concentration of α-KB (500 μM) being 20-fold lower compared to pyruvate (10 mM), any effect of α-KB on pyruvate import by MPC should be negligible, and therefore any inhibitory effect on pyruvate oxidation by α-KB should be attributable to PDC inhibition by α-KB. To test this idea, we utilized methyl pyruvate, which freely diffuses into the mitochondrion without requiring transportation by MPC. As shown in Figure 2A-B, α-KB still inhibits pyruvate oxidation using methyl pyruvate as a respiratory substrate, indicating a direct inhibition of PDC by α-KB and ruling out any potential inhibitory effect on mitochondrial substrate import as rate limiting in the respiration inhibition by α-KB. Consistently, α-KB also inhibits respiration when methyl pyruvate is provided together with glutamate and malate as complex I substrates (Figure 2A-B). These findings further support the model in which α-KB indirectly inhibits complex I respiration via disruption of pyruvate oxidation. Indeed, using the DARTS (drug affinity responsive target stability) assay [12], we showed that α-KB directly binds to PDC but not to mitochondrial complex I (Figures 2C). In concordance, α-KB decreases pyruvate oxidation by PDC using purified enzyme (Figure 2D), but does not directly inhibit the activity of complex I in vitro (Figure S2A).

PDC is a large nuclear-encoded mitochondrial multienzyme complex consisting of pyruvate dehydrogenase (PDH, E1), dihydrolipoamide S-acetyltransferase (DLAT, E2), and dihydrolipoamide dehydrogenase (DLD, E3). The E3 subunit of PDC is shared with branch chain keto acid dehydrogenase complex (BCKDC) and alpha-ketoglutarate dehydrogenase complex. PDC mainly catalyzes the oxidation of pyruvate to acetyl-CoA and CO_2, linking glycolysis and the TCA cycle. The E1 enzyme is a heterotetramer of two alpha and two beta subunits. E1 alpha 1 subunit encoded by the *PDHA1* gene contains the E1 active site, and plays a key role in the function of the PDC. Mutations in *PDHA1* are associated with pyruvate dehydrogenase E1-alpha deficiency and X-linked Leigh syndrome. Mutations in other PDC subunits are also disease associated, including pyruvate dehydrogenase deficiency primary lactic acidosis and maple syrup urine disease in infancy and early childhood. PDC activity is regulated by product inhibition by NADH, which competes with NAD^+ for E3 binding; and by acetyl CoA, which competes with CoA for E2 binding. Several analogues of pyruvate, including fluoropyruvate and bromopyruvate, have been reported to inhibit PDC. However, these molecules also inhibit other pyruvate related enzymes such as pyruvate carboxylase (PC) and LDH and/or glycolytic enzymes (including GAPDH and hexokinase). No specific small molecule inhibitor of PDC has been described.

It has been reported that PDC can use α-KB as an alternative substrate [13]. We confirmed the direct binding of α-KB to PDC using DARTS (Figure 2C). To investigate the mechanism by which α-KB perturbs pyruvate oxidation as an alternative substrate, we performed PDC enzyme kinetics analysis. In contrast to pyruvate, which exhibits non-Michaelis-Menten kinetics (Hill coefficient $h = 1.48 \pm 0.096$) – similar to the *E. coli* enzyme as reported [14] – α-KB shows little cooperativity ($h = 1.05 \pm 0.084$) with similar apparent K_{half} but decreased V_{max} (Figure 2E). Presence of an excess of α-KB results in decreased pyruvate oxidation by PDC (Figure 2D) and

loss of cooperativity (Figure 2F). However, inhibition by α-KB is abrogated and rate of pyruvate oxidation is restored when pyruvate is provided in high concentrations. This is consistent with the model in which α-KB perturbs pyruvate oxidation as a competitive alternative substrate for PDC (Figure 2F).

In contrast, α-KB does not detectably inhibit the reduction of pyruvate by LDH (Figure S2B-C) for which α-KB is also a substrate (Figure S2D). The K_{half} of LDH for α-KB (3.92 mM) is ~50x higher than that for pyruvate (0.076 mM) (Figure S2E), supporting that pyruvate exhibits significantly higher affinity on LDH than α-KB. Additionally, α-KB does not protect PC from protease digestion in DARTS assay, suggesting that PC does not use α-KB as a substrate in vivo (Figure S2F). These results indicate that α-KB does not broadly affect all pyruvate-dependent reactions but only selectively inhibits pyruvate oxidation through PDC. In addition to PDC, BCKDC is able to oxidize α-KB [6]. However, α-KB does not alter BCKDC-driven respiration, as when individual branched-chain alpha-keto acids are offered as a substrate, mitochondrial respiration is not inhibited by α-KB (Figure S2G).

To assess the functional significance of α-KB on pyruvate oxidation in intact cells, we measured cellular respiration. α-KB treatment partially but significantly decreases ATP-linked and maximal respiration, whereas the complex I inhibitor rotenone completely abolishes respiration (Figure S2H). This partial inhibition by α-KB is expected since α-KB does not directly inhibit complex I, and only specifically decreases pyruvate oxidation while sparing other NADH-generating enzymes such as α-KG dehydrogenase.

In eukaryotes, PDH is tightly regulated by pyruvate dehydrogenase kinase (PDK) and pyruvate dehydrogenase phosphatase, which inactivates and activates the enzyme, respectively [15]. Interestingly, phosphorylation of PDH is decreased upon α-KB treatment (Figure S2I), indicating that more PDH is in its unphosphorylated, active form. This would be expected based on the negative feedback on PDK as α-KB treatment decreases acetyl-CoA (Figure 3A), which is an

allosteric activator of PDK. Importantly, this suggests that the inhibition of pyruvate oxidation by α-KB occurs independently of PDH phosphorylation and supports the mechanism of α-KB as a competitive alternative substrate of the PDH.

In agreement with the inhibitory effect of α-KB on pyruvate oxidation, we found that α-KB treatment decrease the respiration of *C. elegans* as well, similar to the scenario with PDH knockdown (Figure 2G and Figure S2J). To determine the significance of pyruvate oxidation to the longevity by α-KB, we measured the lifespan of PDH RNAi adult *C. elegans* given α-KB. PDH RNAi animals live longer than control RNAi animals (Figure 2H), and α-KB does not further extend the lifespan of PDH RNAi worms (Figure 2H), consistent with the longevity effect of α-KB being dependent on pyruvate oxidation.

α-KB rewires mitochondrial substrate utilization through interruption of pyruvate oxidation

The mitochondrion is a pivotal organelle for core metabolic pathways, including TCA cycle, ETC, and lipid metabolism. Various substrates, including pyruvate, glutamine, and lipids, can be utilized for mitochondrial metabolism. Upon nutrient or pathological stress, such as dietary restriction or cancer, substrate utilization by the mitochondria can be drastically altered [16]. PDC is the gatekeeper enzyme controlling pyruvate entry into the TCA cycle. Upon disruption of pyruvate oxidation, cells would be expected to utilize less glucose and increase utilization of alternative substrates for mitochondrial metabolism. In addition to PDC, MPC also regulates pyruvate oxidation by controlling substrate import. To confirm the effects of α-KB on pyruvate oxidation in cells, we performed metabolomics analysis. As would be expected of PDC inhibition, the abundance of acetyl-CoA and citrate was significantly decreased in α-KB treated cells (Figure 3A). Furthermore, metabolomics flux analysis using [U-$^{13}C_6$]glucose shows a

significant decrease in glucose-derived citrate and other TCA cycle intermediates in α-KB treated cells (Figure 3B-C), supporting an inhibitory effect of α-KB on the oxidation of glucose-derived pyruvate. Meanwhile, the abundance of glucose-derived (M3) lactate was not altered by α-KB treatment, whereas the abundance of glucose-derived (M3) alanine and serine was significantly increased (Figure S3A). The overall level of alanine also increased significantly upon α-KB treatment (Figure S3B). This increase in alanine and serine may at least partially contribute to the increase in α-KG, as the reactions that generate alanine and serine simultaneously converts glutamate to α-KG (Figure S3B). In contrast, the amount of leucine/isoleucine and valine was not changed upon α-KB treatment, suggesting that the oxidation of branch-chain alpha-keto acids is not affected (Figure S3B). Together the data indicate that α-KB treatment prevents the entry of glucose-derived pyruvate into the TCA cycle without affecting the conversion of pyruvate into lactate, increases transaminase conversion of pyruvate to alanine, and increases glucose flux into serine synthesis. This further supports that α-KB specifically interrupts PDH as an alternative substrate, but not LDH or alanine transaminase (ALT). By comparison, when pyruvate transportation into the mitochondria is abolished upon MPC inhibition, both total and glucose-derived alanine decreases (Figure S3A and S3C)[17], indicating that α-KB induces distinct metabolic states from MPC disruption.

To further confirm that the metabolic alterations upon α-KB treatment are primarily due to disruption of pyruvate oxidation, we knocked down DLAT, the E2 subunit of PDC, and found that both the total and glucose-derived citrate was decreased, similar to α-KB treatment (Figures 3D and S3C). Notably, both total and glucose-derived alanine was increased upon DLAT knockdown (Figure S3D-E), again consistent with α-KB treatment and different from MPC inhibition. In addition, principle component analysis (PCA) shows that isotopomer distributions induced by DLAT knockdown are similar to those resulting from α-KB treatment, and the magnitude of α-KB-induced metabolomics alterations is decreased in DLAT knockdown cells as

evidenced by isotopomer distribution, glucose-fractional contribution, and relative abundance of metabolites (Figure 3E and data not shown). In contrast, α-KB-induced metabolic alterations are unabated in LDHβ knockdown cells (Figure S3F and data not shown).

It is well documented that disruption of PDC induces distinct changes in glutamine metabolism compared to MPC perturbation by using [U-$^{13}C_5$]glutamine tracer [17]. [U-$^{13}C_5$]glutamine can be converted to M5 citrate through reductive carboxylation or to M4 citrate through oxidation. Additionally, [U-$^{13}C_5$]glutamine is oxidized and converted back to pyruvate through the malic enzyme reaction. The pyruvate derived from [U-$^{13}C_5$]glutamine can further go through PDC and generate labeled acetyl-CoA, which then combines with oxaloacetate to form M6 citrate. Alternatively, the glutamine-derived pyruvate can be converted to M3 lactate or alanine. M6 citrate is the most significantly increased isotopomer of citrate in MPC-knockdown cells, whereas M5 citrate is the most significantly increased species upon PDC inhibition. Our metabolomics analysis with [U-$^{13}C_5$]glutamine supports the hypothesis that PDC is the main target underlying α-KB's inhibition of pyruvate oxidation. Both M5 and M6 citrate increased significantly upon α-KB treatment (Figure 3F). Notably, the increase of M5 citrate is significantly higher than that of M6 citrate, suggesting that α-KB treatment, like hypoxia associated PDC inhibition, majorly increases reductive carboxylation in the TCA cycle [18,19]. On the contrary, M6 citrate is the major increase in UK5099-treated cells (Figure 3F), which is consistent with the previous report [17]. This supports that PDC is the primary target for α-KB in cells. The abundance of fully labeled succinate, fumarate, α-KG, and malate increased significantly in α-KB-treated cells (Figure 3G), suggesting TCA cycle anaplerosis from increased glutaminolysis in α-KB treated cells. Additionally, M3 alanine is increased upon α-KB treatment (Figure S3G), indicating a higher flux of glutamine oxidation and conversion back to pyruvate through the malic enzyme.

Consistent with glucose and glutamine tracer results, we showed that glutamine contribution to lipogenic acetyl-CoA pool was significantly increased while the contribution from glucose was

largely decreased. This further supports that pyruvate oxidation is disrupted by α-KB treatment (Figure 3H).

Our metabolomics analysis indicates that α-KB treatment causes an increased flux of glutamine into the TCA cycle. A prediction of this finding is that the decreased pyruvate oxidation by α-KB would result in an increased reliance on glutamine in α-KB treated cells. Indeed, combined treatment with α-KB and a glutaminase inhibitor synergistically inhibits cell growth (Figure S3H).

In addition to glycolysis, β-oxidation provides acetyl-CoA to fuel into TCA cycle. To investigate whether β-oxidation serves as an compensatory pathway for TCA cycle upon disruption of pyruvate oxidation, we analyzed β-oxidation in α-KB-treated cells by utilizing the [U-$^{13}C_{16}$]palmitate tracer. α-KB treatment increases β-oxidation flux into the TCA cycle, as evidenced by the significant increase in M2 citrate as well as increased label incorporation into other TCA cycle intermediates (Figure 3I-J).

AMPK is required for lifespan increase by α-KB

Since α-KB perturbs pyruvate oxidation and extends lifespan, and AMPK is a major energy sensor and mediator of longevity [20], we asked whether the lifespan extension by α-KB is dependent on AMPK. We found that α-KB does not extend the lifespan of *aak-2* mutant worms (Figure 4A), supporting the involvement of AMPK in α-KB longevity. Lifespan increase by α-KB also requires *daf-16* (Figure 4B), which act downstream of *aak-2* in longevity regulation [21]; in contrast, *daf-2*, which regulates *daf-16* independently of *aak-2*, is not required for the longevity effect of α-KB (Figure 4C), further supporting that α-KB extends lifespan in an AMPK-dependent manner. Since induction of the mitochondrial unfolded protein response (UPR^{mt}) has recently been implicated in the longevity associated with mitochondrial perturbations [5,22,23], we tested whether the longevity effect of α-KB may involve UPR^{mt}. α-KB does not induce the UPR^{mt}

marker HSP60 (Figure S4C), and α-KB extends the lifespan of *C. elegans* with knockdown of UBL-5 (Figure 4D), which is required for induction of the UPR^{mt}, suggesting that UPR^{mt} is not required for the longevity effect of α-KB. This is consistent with the idea that UPR^{mt} acts independently of AMPK in longevity [23]. Importantly, phosphorylated AMPK (encoded by the *C. elegans* orthologue *aak-2*) is increased in α-KB treated worms (Figure 4E) as well as in H9C2 cells (Figure 4F), consistent with α-KB acting upstream of AMPK in longevity signaling.

α-KB activates AMPK by disruption of pyruvate oxidation

Pyruvate oxidation is critical for energy metabolism, as it provides substrate (NADH) for ETC and AMPK is controlled by cellular energy metabolism through an upstream kinase, LKB1. Therefore, it is plausible that α-KB activates AMPK through inhibition of pyruvate oxidation and is dependent on LKB1. Indeed, knockdown of PDC subunits DLAT (E2) or PDHB (E1 component subunit beta) each activates AMPK and abolishes further AMPK activation by α-KB (Figure 4G), whereas AMPK activation by α-KB is normal in LDH or PC knockdown cells (Figure S4A-B). In addition, α-KB no longer activates AMPK in LKB1-null cells (Figure 4H). Plus, AMPK is activated in PDH RNAi *C. elegans* (Figure 4E). Taken together, our results support the model in which α-KB activates AMPK through inhibition of pyruvate oxidation.

AMPK activation has been reported to be beneficial in various disease models, including Alzheimer's disease [24]. Therefore, we asked whether α-KB could relieve the proteotoxic stress in a *C. elegans* Alzheimer's disease model wherein amyloid-beta toxicity causes progressive, age-dependent paralysis [25]. Remarkably, α-KB supplementation delays amyloid-beta induced paralysis (Figure 4I); importantly, α-KB does not protect AAK-2 knockdown *C. elegans* in this model (Figure 4I), consistent with the mechanism involving pyruvate oxidation and subsequent

AMPK activation. The results suggest that α-KB induces AMPK activation in *C. elegans* and could be exploited for aging-related disease intervention.

SUMMARY

We show that an unfamiliar metabolite, α-KB, extends lifespan of adult *C. elegans*. This extension is likely through a direct inhibitory effect of α-KB on pyruvate oxidation and consequent activation of AMPK. Although it has been suggested that α-KB disturbs pyruvate oxidation in vitro [13,26], the physiological and biological significance of this effect on pyruvate metabolism has not been studied. Our report shows that α-KB treatment increases lifespan expectancy by acting as a competitive alternative substrate of PDC. The inhibitory effect of α-KB on pyruvate oxidation is specific, as our results suggest that pyruvate reactions through LDH, PC, and ALT are not inhibited by α-KB treatment. Through its inhibition of PDH, α-KB treatment rewires mitochondrial substrate utilization. The entry of glucose-derived pyruvate into TCA cycle is perturbed upon α-KB treatment while increased glutamine and lipid are utilized by the mitochondria. Altered mitochondrial substrate utilization is associated with numerous pathological conditions, including obesity and diabetes [27,28]. Our finding that α-KB alters mitochondrial metabolism provides novel direction for the treatment of mitochondrial metabolism diseases.

Our results indicate that α-KB exhibits a comparable affinity as pyruvate to PDC, and this suggests the possibility for α-KB to be utilized as a major endogenous PDH substrate. Moreover, when PDC switches to use α-KB as its major substrate, due to the lower efficacy of α-KB, the overall activity of PDC is limited, mitochondrial metabolism is rewired, and AMPK is activated. This points to the possibility that alternative endogenous substrates for pivotal metabolic enzymes, such as PDC, are able to determine the activity of these enzymes and yield

profound effects on the endogenous regulatory systems of signaling and aging. In addition, it is possible that these alternative substrates are employed by the organism under stress, and further studies on alternative substrates may shed light on novel anti-aging interventions. Perhaps reminiscent of the dual effects of mitochondrial ETC inhibition in longevity and disease, although severe PDC deficiency has been linked to neuronal degeneration, cancer, and glucose intolerance [29], moderate inhibition of PDC can bestow health benefits without adversely affecting normal organismal function.

Energy metabolism and AMPK are intimately connected with both aging and health. Metformin, the plant-derived, most widely used anti-diabetic biguanide whose mechanisms include inhibition of mitochondrial complex I and activation of AMPK, has been shown to exhibit beneficial effects against aging and cancer. Our study demonstrates that an endogenous longevity small molecule can also successfully relieve aging-dependent degenerations through AMPK activation, supporting the idea that aging-related diseases can be countered by regulation of longevity pathways.

Figure Legends

Figure 1. α-KB increases the lifespan of adult *C. elegans*.

(A) Structure of α-KB.

(B) α-KB extends the lifespan of adult worms, mean lifespan (days of adulthood) with vehicle treatment (m_{veh}) = 14.1 (n = 111 animals tested), $m_{\alpha\text{-KB}}$ = 22.4 (n = 66), $p < 0.0001$ (log-rank test).

(C) Dose–response curve of the α-KB effect on longevity.

Figure 2. α-KB perturbs pyruvate oxidation.

(A-B) Isolated mitochondria from mouse liver are offered with different respiratory substrates. Upon α-KB treatment (500 μM), both state 3 (A) and state 3u (B) respiration is decreased when pyruvate (Pyr) and methyl pyruvate (Me-pyr) are utilized as substrates (∗∗$p < 0.01$, ∗∗∗$p < 0.001$). Unpaired t test, two-tailed, two-sample unequal variance is used. Mean ± s.d. is plotted.

(C) DARTS identifies PDH as an α-KB-binding protein complex. α-KB does not bind to ETC complex I; NQO1 and NDUFB8 are subunits of complex I. U87 cell lysates were used. Similar results were obtained with HEK293 cells (data not shown).

(D) Inhibition of PDC activity by α-KB. Pyruvate (1 mM) is provided as substrate.

(E) Allosteric sigmoidal kinetics of pyruvate and α-KB on PDC, by nonlinear regression least-squares fit. The V_{max} and K_{half} values for pyruvate vs. α-KB are 0.004 vs. 0.001 and 54.05 vs. 56.13, respectively.

(F) α-KB acts as a competitive alternative substrate to perturb pyruvate oxidation and decrease NADH generation. PDC activity is measured based on the synthesis rate of NADH.

(G) Decreased oxygen consumption rate (OCR) in α-KB-treated worms ($p < 0.05$; by t-test, two-tailed, two-sample unequal variance) for the entire time.

(H) α-KB cannot extend the lifespan of PDHB-1 knockdown worms. Control, m_{veh} = 19.5 (n = 94), $m_{α\text{-}KB}$ = 21.8 (n = 88), $p < 0.0001$ (log-rank test); *pdhb-1* RNAi, m_{veh} = 22.5 (n = 81), $m_{α\text{-}KB}$ = 19.8 (n = 84), $p < 0.0001$ (log-rank test).

Figure 3. α-KB treatment alters mitochondrial substrate utilization and activates AMPK.

(A) Relative abundance of citrate of acetyl-CoA.

(B) Citrate mass isotopomer distribution (MID) upon α-KB treatment resulting from culture with [U-$^{13}C_6$]glucose (UGlc).

(C) Percentage of fully labeled metabolites derived from [U-$^{13}C_6$]glucose (UGlc).

(D) Citrate MID upon DLAT knockdown resulting from culture with [U-$^{13}C_6$]glucose (UGlc).

(E) Principle component analysis using isotopomer distribution from UGlc to all measured metabolites in DLAT-knockdown and α-KB-treated cells.

(F) Citrate mass isotopomer distribution (MID) upon α-KB or UK5099 (10 μM) treatment resulting from culture with [U-$^{13}C_5$]glutamine (UGln).

(G) Percentage of fully labeled metabolites derived from [U-13C5]glutamine (UGln).

(H) Contribution of UGln and UGlc to lipogenic AcCoA as determined by isotopomer enrichment modeling.

(I) Relative abundance of M2 citrate upon α-KB treatment resulting from culture with [U-$^{13}C_{16}$]palmitate conjugated to BSA (UPalm).

(J) Percentage of fully labeled metabolites derived from [U-$^{13}C_{16}$]palmitate conjugated to BSA (UPalm).

Unpaired t test, two-tailed, two-sample unequal variance was used for (A)-(D) and (F)-(I) ($****p < 0.0001$, $***p < 0.001$, $**p < 0.01$, $*p < 0.05$). Mean ± SD is plotted. 3.2 mM α-KB was used in (A)-(I).

Figure 4. α-KB extends lifespan and ameliorate aging-dependent symptoms through AMPK and disruption of pyruvate oxidation.

(A) α-KB does not extend (and, in fact, slightly reduces) the lifespan of *aak-2(gt33)* adult worms, m_{veh} = 15.9 (n = 120), $m_{\alpha\text{-KB}}$ = 15.1 (n = 138), p = 0.0029 (log-rank test).

(B) α-KB does not extend the lifespan of *daf-16(mu86)* adult worms, m_{veh} = 15.5 (n = 97), $m_{\alpha\text{-KB}}$ = 16.0 (n = 99), p = 0.1482 (log-rank test).

(C) α-KB further extends the lifespan of *daf-2(e1370)* adult worms, m_{veh} = 37.0 (n = 100), $m_{\alpha\text{-KB}}$ = 47.0 (n = 95), p < 0.0001 (log-rank test).

(D) α-KB extends the lifespan of adult worms with UBL-5 knockdown. Control, m_{veh} = 16.0 (n = 67), $m_{\alpha\text{-KB}}$ = 18.5 (n = 71), p < 0.0001 (log-rank test); *ubl-5* RNAi, m_{veh} = 16.2 (n = 68), $m_{\alpha\text{-KB}}$ = 18.4 (n = 63), p < 0.0001 (log-rank test).

(E) α-KB treatment or PDHB-1 knockdown increases phosphorylated AMPK in adult C. *elegans*.

(F) AMPK signaling is activated in α-KB-treated cells. Similar results were obtained in multiple cell lines, including H9C2 (shown), U87 and HAP1 cells (not shown).

(G) α-KB treatment does not further activate AMPK in PDC-knockdown H9C2 cells.

(H) α-KB does not activate AMPK in HeLa cells, which are deficient in the upstream kinase LKB1.

(I) α-KB delays paralysis in the $A\beta_{1\text{-}42}$ expressing GMC101 worms, but does not reduce amyloid-beta toxicity in AAK-2 knockdown animals. Control, m_{veh} = 2.5 (n = 248), $m_{\alpha\text{-KB}}$ = 3.5 (n = 150), p < 0.0001 (log-rank test); *aak-2* RNAi, m_{veh} = 2.6 (n = 281), $m_{\alpha\text{-KB}}$ = 2.7 (n = 231), p = 0.7106 (log-rank test).

References

1 Longo, V. D. *et al.* Interventions to Slow Aging in Humans: Are We Ready? *Aging Cell* **14**, 497-510, doi:10.1111/acel.12338 (2015).

2 Lopez-Otin, C., Galluzzi, L., Freije, J. M., Madeo, F. & Kroemer, G. Metabolic Control of Longevity. *Cell* **166**, 802-821, doi:10.1016/j.cell.2016.07.031 (2016).

3 Chin, R. M. *et al.* The metabolite alpha-ketoglutarate extends lifespan by inhibiting ATP synthase and TOR. *Nature* **510**, 397-401, doi:10.1038/nature13264 (2014).

4 Zhang, H. *et al.* NAD(+) repletion improves mitochondrial and stem cell function and enhances life span in mice. *Science* **352**, 1436-1443, doi:10.1126/science.aaf2693 (2016).

5 Mouchiroud, L. *et al.* The NAD(+)/Sirtuin Pathway Modulates Longevity through Activation of Mitochondrial UPR and FOXO Signaling. *Cell* **154**, 430-441, doi:10.1016/j.cell.2013.06.016 (2013).

6 Paxton, R., Scislowski, P. W., Davis, E. J. & Harris, R. A. Role of branched-chain 2-oxo acid dehydrogenase and pyruvate dehydrogenase in 2-oxobutyrate metabolism. *Biochem J* **234**, 295-303 (1986).

7 Sullivan, L. B. *et al.* Supporting Aspartate Biosynthesis Is an Essential Function of Respiration in Proliferating Cells. *Cell* **162**, 552-563, doi:10.1016/j.cell.2015.07.017 (2015).

8 Cabreiro, F. & Gems, D. Worms need microbes too: microbiota, health and aging in Caenorhabditis elegans. *EMBO Mol Med* **5**, 1300-1310, doi:10.1002/emmm.201100972 (2013).

9 Brand, M. D. & Nicholls, D. G. Assessing mitochondrial dysfunction in cells. *Biochem J* **435**, 297-312, doi:10.1042/BJ20110162 (2011).

10 Bricker, D. K. *et al.* A mitochondrial pyruvate carrier required for pyruvate uptake in yeast, Drosophila, and humans. *Science* **337**, 96-100, doi:10.1126/science.1218099 (2012).

11 Halestrap, A. P. The mitochondrial pyruvate carrier. Kinetics and specificity for substrates and inhibitors. *Biochem J* **148**, 85-96 (1975).

12 Lomenick, B. *et al.* Target identification using drug affinity responsive target stability (DARTS). *Proc Natl Acad Sci U S A* **106**, 21984-21989, doi:10.1073/pnas.0910040106 (2009).

13 Kanzaki, T., Hayakawa, T., Hamada, M., Fukuyoshi, Y. & Koike, M. Mammalian alpha-keto acid dehydrogenase complexes. IV. Substrate specificities and kinetic

properties of the pig heart pyruvate and 2-oxyoglutarate dehydrogenase complexes. *J Biol Chem* **244**, 1183-1187 (1969).

14 Biswanger, H. & Henning, U. Regulatory properties of the pyruvate-dehydrogenase complex from Escherichia coli. Positive and negative cooperativity. *Eur J Biochem* **24**, 376-384 (1971).

15 Linn, T. C., Pettit, F. H., Hucho, F. & Reed, L. J. Alpha-keto acid dehydrogenase complexes. XI. Comparative studies of regulatory properties of the pyruvate dehydrogenase complexes from kidney, heart, and liver mitochondria. *Proc Natl Acad Sci U S A* **64**, 227-234 (1969).

16 Peters, S. J. & Leblanc, P. J. Metabolic aspects of low carbohydrate diets and exercise. *Nutr Metab (Lond)* **1**, 7, doi:10.1186/1743-7075-1-7 (2004).

17 Vacanti, N. M. *et al.* Regulation of substrate utilization by the mitochondrial pyruvate carrier. *Mol Cell* **56**, 425-435, doi:10.1016/j.molcel.2014.09.024 (2014).

18 Kim, J. W., Tchernyshyov, I., Semenza, G. L. & Dang, C. V. HIF-1-mediated expression of pyruvate dehydrogenase kinase: a metabolic switch required for cellular adaptation to hypoxia. *Cell Metab* **3**, 177-185, doi:10.1016/j.cmet.2006.02.002 (2006).

19 Papandreou, I., Cairns, R. A., Fontana, L., Lim, A. L. & Denko, N. C. HIF-1 mediates adaptation to hypoxia by actively downregulating mitochondrial oxygen consumption. *Cell Metab* **3**, 187-197, doi:10.1016/j.cmet.2006.01.012 (2006).

20 Lee, H. *et al.* The Caenorhabditis elegans AMP-activated protein kinase AAK-2 is phosphorylated by LKB1 and is required for resistance to oxidative stress and for normal motility and foraging behavior. *J Biol Chem* **283**, 14988-14993, doi:10.1074/jbc.M709115200 (2008).

21 Greer, E. L., Banko, M. R. & Brunet, A. AMP-activated protein kinase and FoxO transcription factors in dietary restriction-induced longevity. *Ann N Y Acad Sci* **1170**, 688-692, doi:10.1111/j.1749-6632.2009.04019.x (2009).

22 Durieux, J., Wolff, S. & Dillin, A. The cell-non-autonomous nature of electron transport chain-mediated longevity. *Cell* **144**, 79-91, doi:10.1016/j.cell.2010.12.016 (2011).

23 Houtkooper, R. H. *et al.* Mitonuclear protein imbalance as a conserved longevity mechanism. *Nature* **497**, 451-457, doi:10.1038/nature12188 (2013).

24 Vingtdeux, V. *et al.* AMP-activated protein kinase signaling activation by resveratrol modulates amyloid-beta peptide metabolism. *J Biol Chem* **285**, 9100-9113, doi:10.1074/jbc.M109.060061 (2010).

25 McColl, G. *et al.* Utility of an improved model of amyloid-beta (Abeta(1)(-)(4)(2)) toxicity in Caenorhabditis elegans for drug screening for Alzheimer's disease. *Mol Neurodegener* **7**, 57, doi:10.1186/1750-1326-7-57 (2012).

26 Jones, S. M. & Yeaman, S. J. Oxidative decarboxylation of 4-methylthio-2-oxobutyrate by branched-chain 2-oxo acid dehydrogenase complex. *Biochem J* **237**, 621-623 (1986).

27 Gaster, M., Rustan, A. C., Aas, V. & Beck-Nielsen, H. Reduced lipid oxidation in skeletal muscle from type 2 diabetic subjects may be of genetic origin: evidence from cultured myotubes. *Diabetes* **53**, 542-548 (2004).

28 Kim, J. Y., Hickner, R. C., Cortright, R. L., Dohm, G. L. & Houmard, J. A. Lipid oxidation is reduced in obese human skeletal muscle. *Am J Physiol Endocrinol Metab* **279**, E1039-1044 (2000).

29 Stacpoole, P. W. The pyruvate dehydrogenase complex as a therapeutic target for age-related diseases. *Aging Cell* **11**, 371-377, doi:10.1111/j.1474-9726.2012.00805.x (2012).

Figure 1

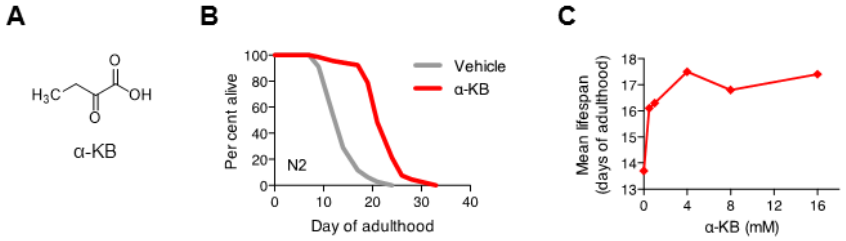

Figure 2

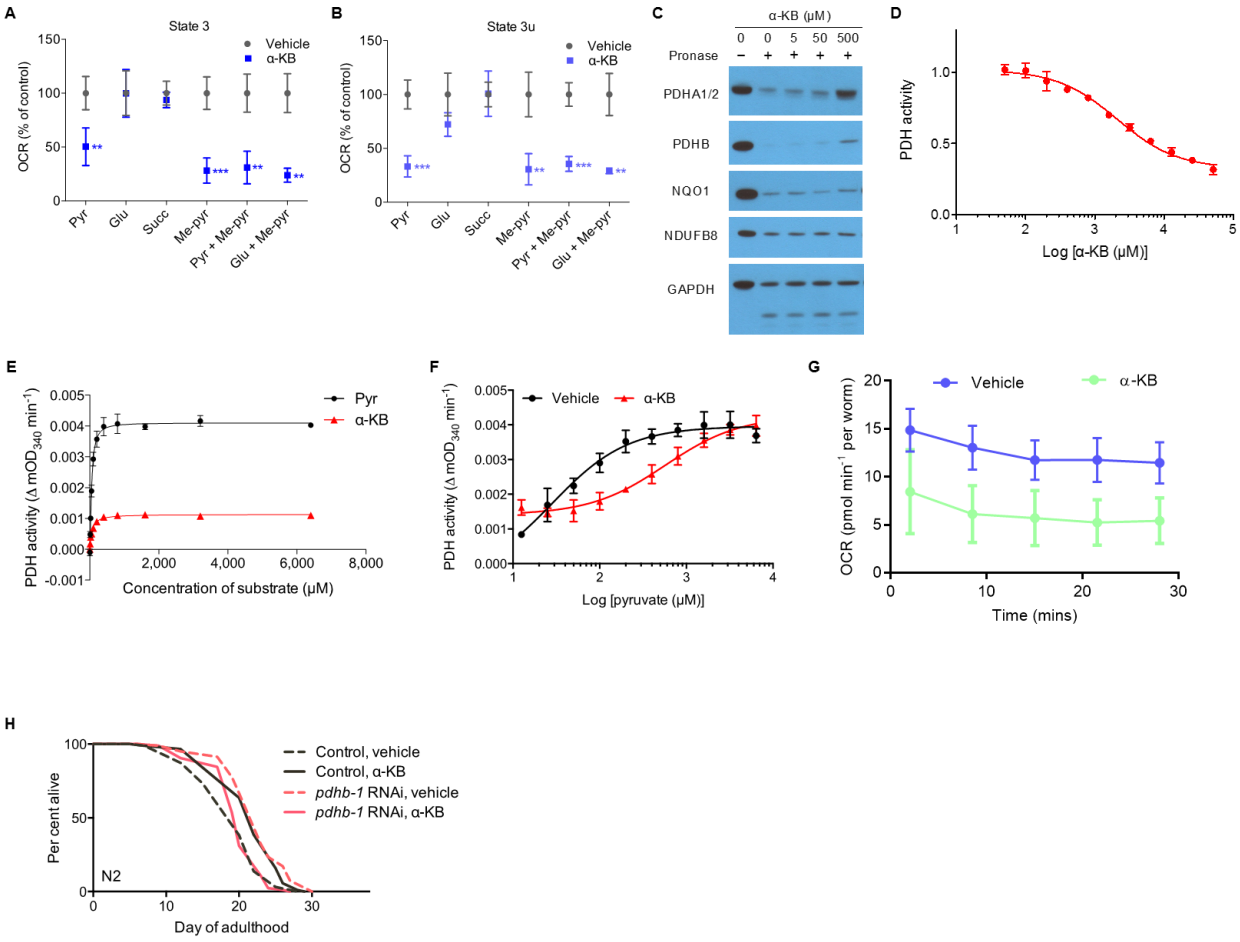

Figure 3

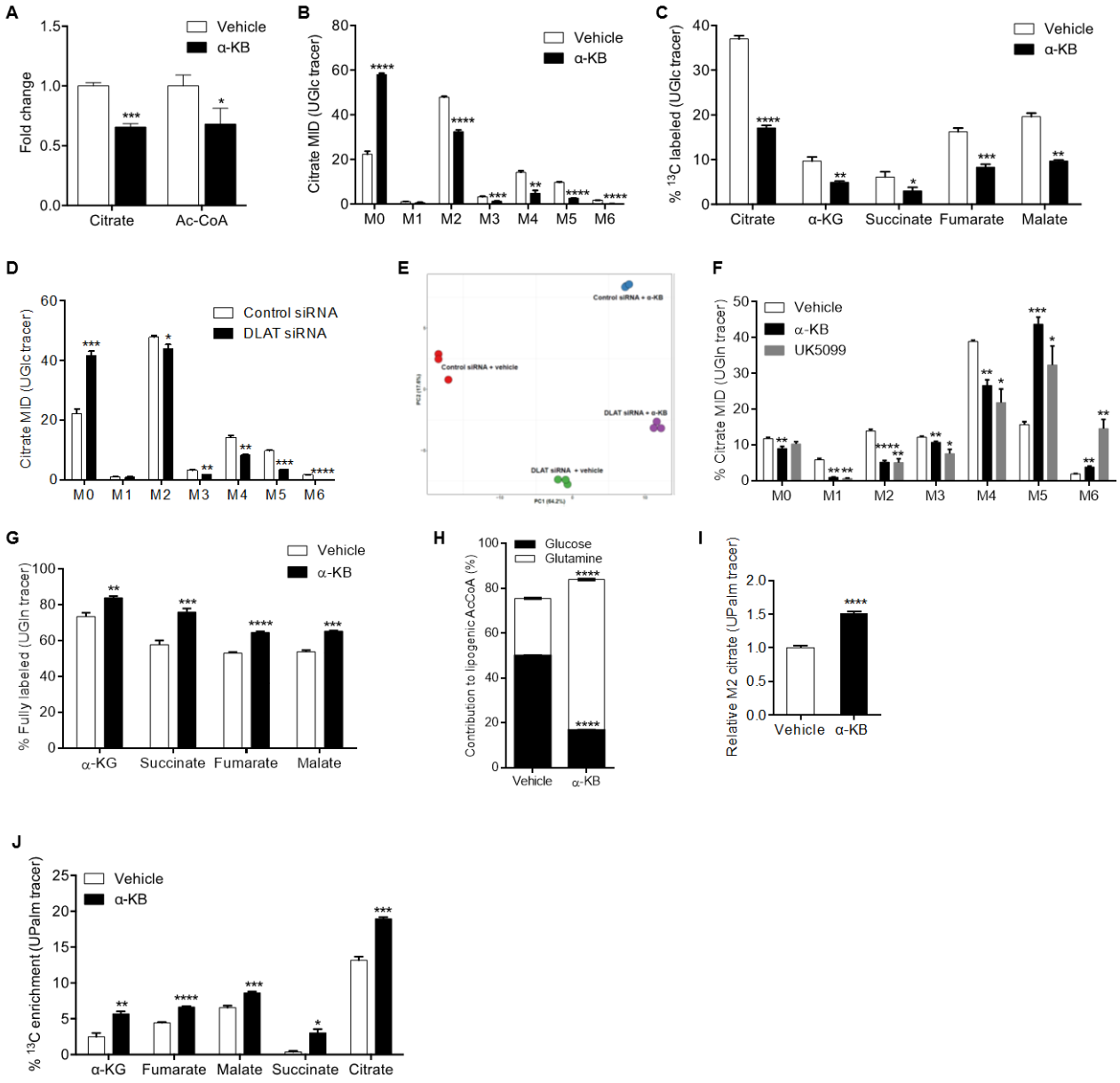
A
Fold change
Vehicle
α-KB
Citrate
Ac-CoA
B
Citrate MID (UGlc tracer)
M0 M1 M2 M3 M4 M5 M6
C
% 13C labeled (UGlc tracer)
Citrate α-KG Succinate Fumarate Malate
D
Citrate MID (UGlc tracer)
Control siRNA
DLAT siRNA
E
Control siRNA + α-KB
Control siRNA + vehicle
DLAT siRNA + α-KB
DLAT siRNA + vehicle
F
% Citrate MID (UGln tracer)
UK5099
G
% Fully labeled (UGln tracer)
α-KG Succinate Fumarate Malate
H
Contribution to lipogenic AcCoA (%)
Glucose
Glutamine
I
Relative M2 citrate (UPalm tracer)
J
% 13C enrichment (UPalm tracer)
α-KG Fumarate Malate Succinate Citrate

Figure 4

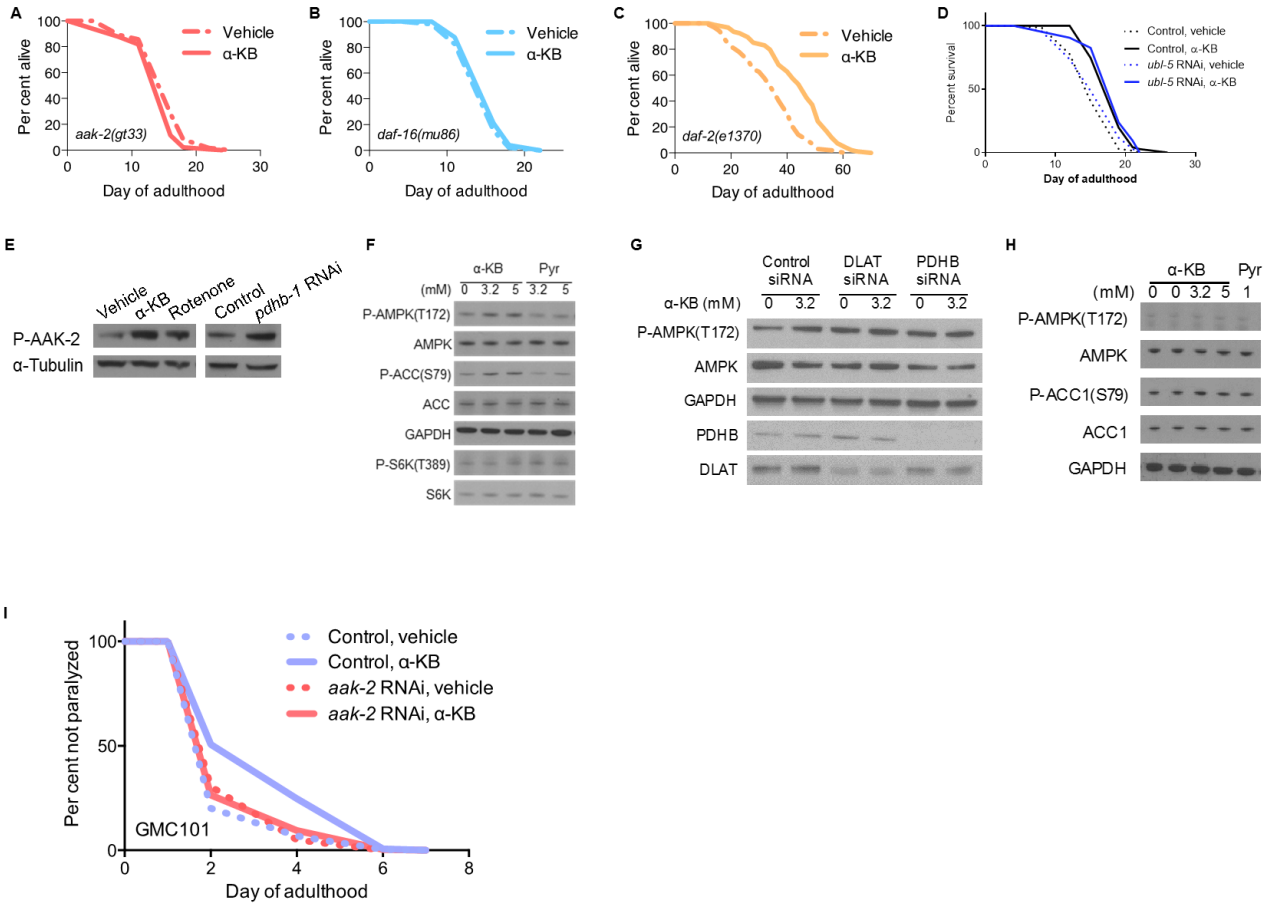
A
Per cent alive
Vehicle
α-KB
aak-2(gt33)
Day of adulthood
B
Per cent alive
Vehicle
α-KB
daf-16(mu86)
Day of adulthood
C
Per cent alive
Vehicle
α-KB
daf-2(e1370)
Day of adulthood
D
Percent survival
Control, vehicle
Control, α-KB
ubl-5 RNAi, vehicle
ubl-5 RNAi, α-KB
Day of adulthood
E
Vehicle
α-KB
Rotenone
Control
pdhb-1 RNAi
P-AAK-2
α-Tubulin
F
α-KB
Pyr
(mM) 0 3.2 5 3.2 5
P-AMPK(T172)
AMPK
P-ACC(S79)
ACC
GAPDH
P-S6K(T389)
S6K
G
Control siRNA
DLAT siRNA
PDHB siRNA
α-KB (mM) 0 3.2 0 3.2 0 3.2
P-AMPK(T172)
AMPK
GAPDH
PDHB
DLAT
H
α-KB
Pyr
(mM) 0 0 3.2 5 1
P-AMPK(T172)
AMPK
P-ACC1(S79)
ACC1
GAPDH

I
Per cent not paralyzed
Control, vehicle
Control, α-KB
aak-2 RNAi, vehicle
aak-2 RNAi, α-KB
GMC101
Day of adulthood

Supplemental Figures

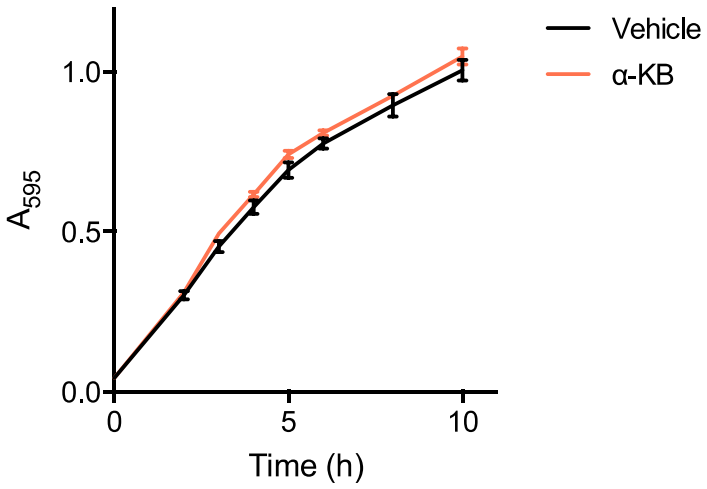

Figure S1, related to Figure 1. α-KB increases the lifespan of adult *C. elegans*.

α-KB does not alter the growth rate of the OP50 *E. coli*. OP50 is the standard laboratory food source for nematodes. α-KB (4 mM) or vehicle (H_2O) was added to standard LB media and the pH was adjusted to 6.6 by the addition of NaOH. Bacterial cells from the same overnight OP50 culture were added to the LB ± α-KB mixture at a 1:40 dilution, and then placed in the 37 ^{o}C incubator shaker at 300 r.p.m. The absorbance at 595 nm was read at 1 h time intervals to generate the growth curve.

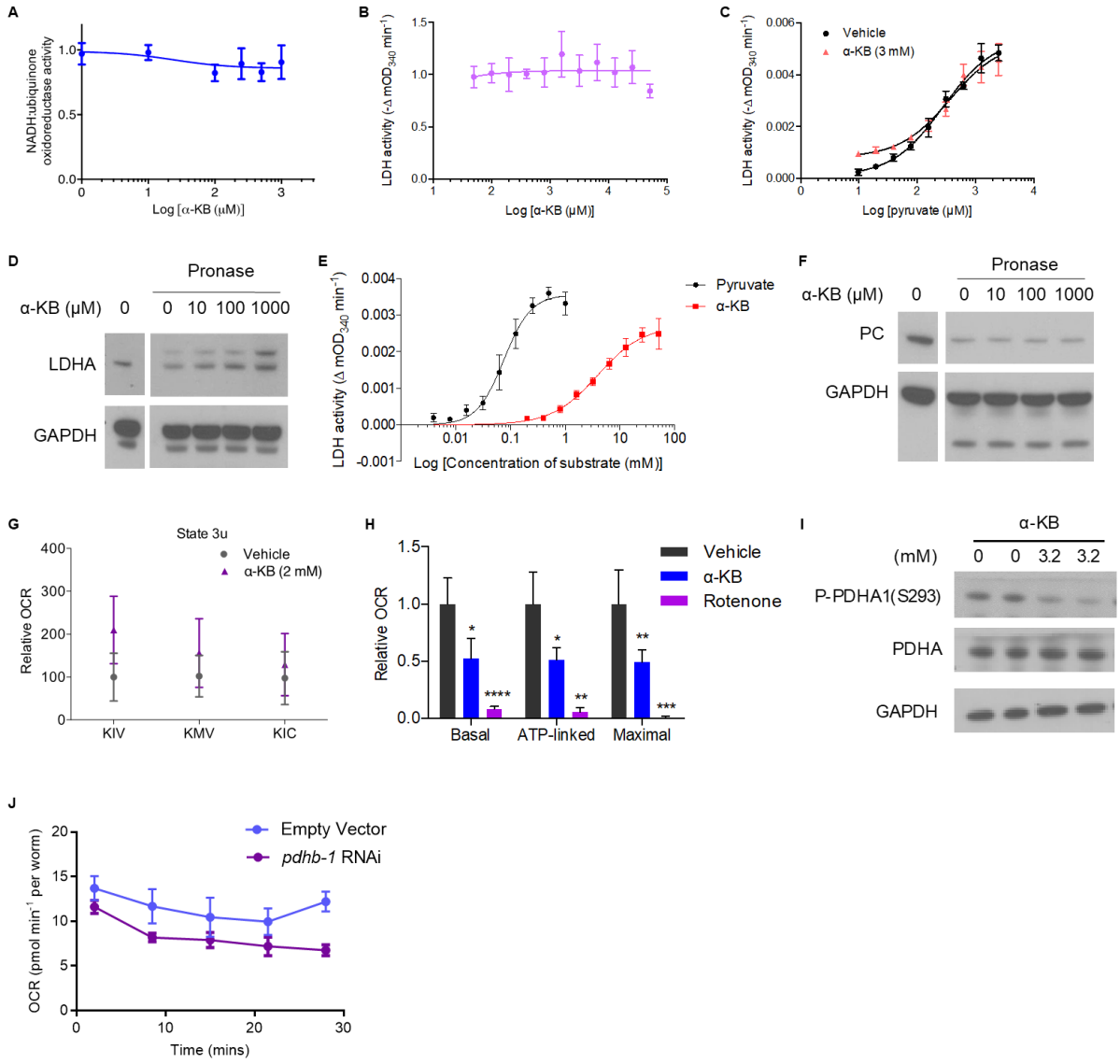

Figure S2, related to Figure 2. α-KB perturbs pyruvate oxidation.

(A) α-KB does not inhibit complex I activity.

(B) α-KB does not decrease LDH activity in converting pyruvate to lactate. Pyruvate (1 mM) is provided as substrate.

(C) α-KB does not act as a competitive alternative substrate for pyruvate on LDH and does not decrease NADH consumption rate. LDH activity is measured based on the consumption rate of NADH.

(D) DARTS showing α-KB binding to LDH.

(E) Allosteric sigmoidal curves of pyruvate vs. α-KB on LDH, by nonlinear regression least-squares fit. The V_{max} and K_{half} values for pyruvate vs. α-KB are 0.0036 vs. 0.0027 and 0.076 vs. 3.92, respectively. LDH activity is measured based on the consumption rate of NADH. Mean ± s.d. is plotted.

(F) DARTS showing α-KB does not bind to PC.

(G) Isolated mitochondria from mouse liver are offered with different respiratory substrates. Upon α-KB, states 3u mitochondrial respiration is not inhibited when 5 mM KIC, 10 mM KIV, or 10 mM KMV is utilized as substrates together with 10 mM malate.

(H) Basal respiration, ATP-linked respiration (oligomycin-insensitive respiration) and maximum respiration (FCCP-induced respiration) upon α-KB (5 mM) or rotenone (1 μM) treatment; $****p < 0.0001$, $**p < 0.01$, $*p < 0.05$. Unpaired t test, two-tailed, two-sample unequal variance was used.

(I) The level of phosphor-PDHA1 is decreased upon α-KB treatment in H9C2 cells.

Mean ± s.d. is plotted.

(J) pdhb-1 RNAi worms have lower oxygen consumption compared to control, $p < 0.05$ (t-test, two-tailed, two-sample unequal variance) for the entire time; similar to α-KB-treated worms shown in Fig. 2G.

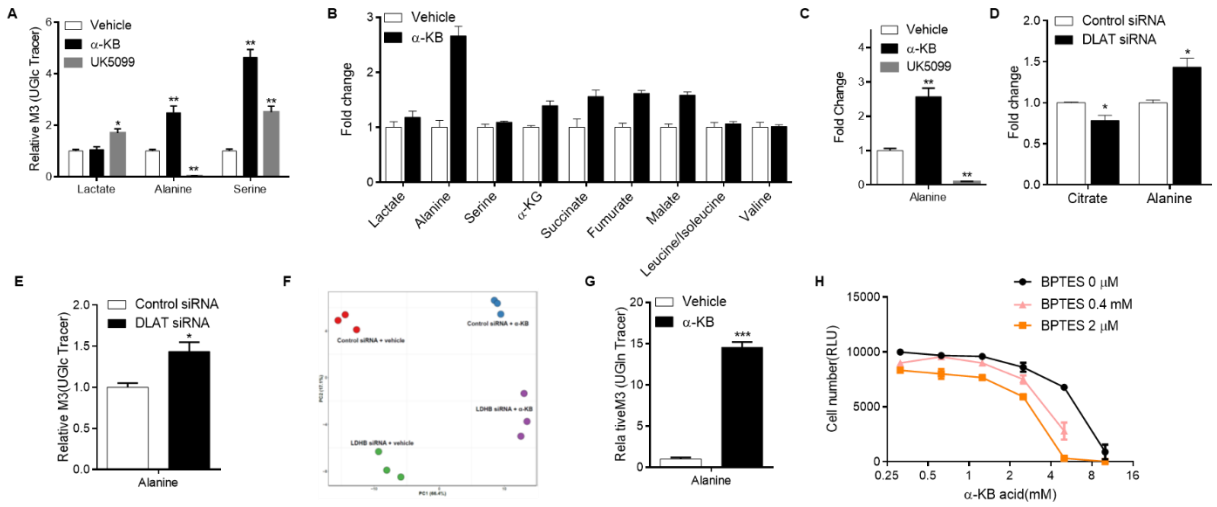

Figure S3, related to Figure 3. α-KB treatment alters mitochondrial substrate utilization and activates AMPK.

(A) Relative abundance of M3 lactate, alanine, and serine in cells with α-KB or UK5099 (10 μM) treatment resulting from culture with UGlc.

(B) Relative abundance of lactate, alanine, and serine in cells with α-KB treatment.

(C) Relative abundance of alanine in cells with α-KB or UK5099 (10 μM) treatment resulting from culture with UGlc.

(D) DLAT-knockdown cells exhibit decreased citrate and increased alanine.

(E) Relative abundance of M3 alanine in DLAT-knockdown cells resulting from culture with UGlc.

(F) Principle component analysis using isotopomer distribution from UGlc to all measured metabolites in LDHB-knockdown and α-KB-treated cells.

(G) Relative abundance of M3 lactate and alanine in cells treated with α-KB resulting from culture with UGln.

(H) α-KB synergistically inhibits cell growth with BPTES, a known glutaminase inhibitor [1].

Unpaired t test, two-tailed, two-sample unequal variance was used for (A)-(D) and (F)-(I) (****p < 0.0001, ***p < 0.001, **p < 0.01, *p < 0.05). Mean ± SD is plotted. 3.2 mM α-KB was used in (A)-(H).

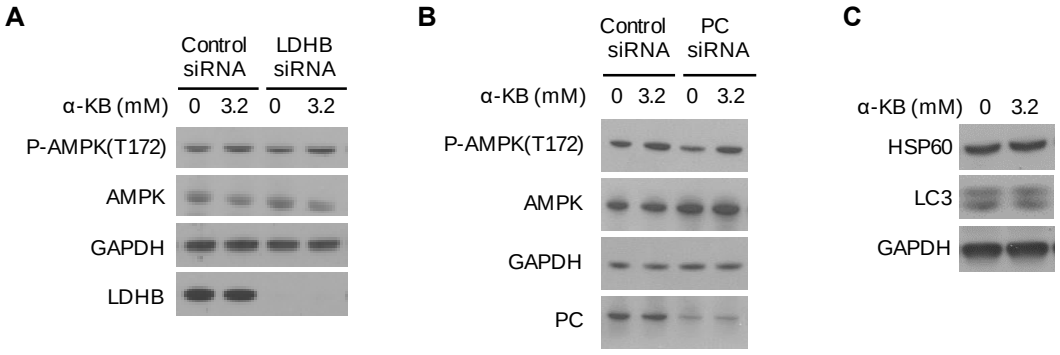

Figure S4, related to Figure 4. α-KB extends lifespan and ameliorate aging-dependent symptoms through AMPK and disruption of pyruvate oxidation.

(A) LDHB (lactate dehydrogenase B chain) knockdown does not abolish α-KB activation of AMPK. H9C2 cells were used.

(B) PC knockdown does not abolish α-KB activation of AMPK. H9C2 cells were used.

(C) α-KB does not modulate HSP60 or LC3.

Supplemental Experimental Procedures

Nematode strains

The following strains were used (strain, genotype): Bristol N2, wild type; TG38, *aak-2(gt33)*X; DA1116, *eat-2(ad1116)*II; CB1370, *daf-2(e1370)*III; CF1038, *daf-16(mu86)*; skn-1*(zu67)*. All strains were obtained from the *Caenorhabditis* Genetics Center (CGC).

Lifespan analysis

Lifespan assays were conducted as described [2] at 20 ^{o}C on solid nematode growth media (NGM) using standard protocols and were replicated in at least two independent experiments.

All lifespan data are available in Extended Data Table 1, including sample sizes. The sample size was chosen on the basis of standards done in the field in published manuscripts. No statistical method was used to predetermine the sample size. Animals were assigned randomly to the experimental groups. Worms that ruptured, bagged (that is, exhibited internal progeny hatching), or crawled off the plates were censored. Lifespan data were analyzed using GraphPad Prism; *P* values were calculated using the log-rank (Mantel–Cox) test.

Statistical analyses

All experiments were repeated at least two times with identical or similar results. Data represent biological replicates. Appropriate statistical tests were used for every figure. Data meet the assumptions of the statistical tests described for each figure. Mean ± s.d. is plotted in all figures unless stated otherwise.

Assay for *C. elegans* paralysis in Alzheimer's disease model

The GMC101 *C. elegans* strain [3] expresses the full length human amyloid-beta 1-42 protein in the body wall muscle cells, leading to a fully-penetrant age-progressive paralysis. Worms were age-synchronized by performing a timed egg lay for 3 h with ~100 gravid adults and the eggs placed in a 20 °C incubator. Once the eggs had developed to the L4 stage at 42 h post egg lay, they were picked onto NGM treatment plates containing 49.5 µM 5-fluoro-2'-deoxyuridine (FUDR, Sigma F0503) to prevent progeny production and either α-KB (2 mM) or vehicle (water) control. Worms were then shifted to 30°C to induce amyloid-beta aggregation and paralysis. Worms were assessed for paralysis daily, beginning on the second day of treatment, by the failure to perform whole body bends and to significantly move forward and backward upon gentle prodding with a platinum wire. Most paralyzed worms could still move their heads and part of their body. All worms were transferred to fresh treatment plates on day 4.

Measurement of mitochondrial respiration

Mitochondria were isolated from mouse liver as described [2]. The final mitochondrial pellet was resuspended in 30 µl of MAS buffer (70 mM sucrose, 220 mM mannitol, 10 mM KH_2PO_4, 5 mM $MgCl_2$, 2 mM HEPES, 1 mM EGTA, and 0.2% fatty acid free BSA, pH 7.2).

Mitochondrial respiration was measured by running coupling and electron flow assays. For the coupling assay, MAS buffer supplemented with10 mM succinate and 2 µM rotenone, or 10 mM pyruvate and 2 mM malate (with or without 20 mM methyl pyruvate), or 10 mM glutamate and 10 mM malate (with or without 20 mM methyl pyruvate), or 10 mM methyl pyruvate and 2mM malate. Mitochondria in complete MAS buffer were seeded into a XF24 Seahorse plate by

centrifugation at 2,000*g* for 20 min at 4 °C. Just before the assay, the mitochondria were supplemented with complete MAS buffer for a total of 500 µl (with Vehicle or α-KB), and warmed at 37 °C for 30 min before starting the OCR measurements. Mitochondrial respiration begins in a coupled state 2; state 3 is initiated by 2 mM ADP; state 4o (oligomycin insensitive, that is, complex V independent) is induced by 2.5 µM oligomycin; and state 3u (FCCP-uncoupled maximal respiratory capacity) by 4 µM FCCP. Finally, 1.5 µg/mL antimycin A was injected at the end of the assay.

For the electron flow assay, the MAS buffer was supplemented with 10 mM sodium pyruvate, 2 mM malate and 4 µM FCCP, and the mitochondria are seeded the same way as described for the coupling assay. After basal readings, the sequential injections were as follows: 2 µM rotenone (complex I inhibitor), 10 mM succinate (complex II substrate), 4 µM antimycin A (complex III inhibitor), and 10 mM/100 µM ascorbate/tetramethylphenylenediamine (complex IV substrate).

Measurement of oxygen consumption rates (OCR)

OCR measurements were made using a Seahorse XF-24 analyzer (Seahorse Bioscience). H9C2 Cells were seeded in Seahorse XF-24 cell culture microplates in DMEM media supplemented with 10% FBS and 10 mM glucose, and incubated at 37 °C and 5% CO_2 overnight. Treatment with designated compounds was for 2 h. Cells were washed in unbuffered DMEM medium (pH 7.4, 10 mM glucose) just before measurements, and maintained in this buffer with indicated concentrations of α-KB. OCR was measured three times under basal conditions and normalized to protein concentration per well.

Measurement of OCR in living *C. elegans* was carried out as follows. Wild-type day 1 adult N2 worms were placed on NGM plates containing 4 mM α-KB or H2O (vehicle control). OCR was

assessed on day 2 of adulthood. On day 2 of adulthood, worms were collected and washed four times with M9 to rid the samples of bacteria, and then the animals were in Seahorse XF-24 cell culture microplates (Seahorse Bioscience, V7-PS) in 200 µl M9 at ~100 worms per well. Oxygen consumption rates were measured seven times under basal conditions and normalized to the number of worms counted per well. The experiment was repeated twice. Statistical analysis was performed using Microsoft Excel (t-test, two-tailed, two-sample unequal variance).

Complex I (NADH:ubiquinone oxidoreductase) assay

NADH:ubiquinone oxidoreductase activity was measured using MitoTox™ Complex I OXPHOS Activity Microplate Assay (Abcam, ab109903) according to manufacturer's instructions.

Pyruvate dehydrogenase (PDH) and lactate dehydrogenase (LDH) enzyme activity assays

The enzyme activities were measured as described [4,5] using purified porcine heart PDH (Sigma, P7032-25UN) and purified rabbit LDH (Promega, G9071). 10 mM NaF is included to exclude the effect of enzyme phosphorylation for PDH assay.

Metabolic profile analysis

Cells were cultured for 24 h, rinsed with PBS, and medium containing [U-$^{13}C_6$]glucose, [U-$^{13}C_5$]glutamine, or [U-$^{13}C_{16}$]palmitate added. After 24 h culture, cells were rinsed with ice-cold 150 mM NH_4AcO (pH 7.3) followed by addition of 400 µL cold methanol and 400 µL cold water. Cells were scraped off, transferred to an Eppendorf tube, and 10 nmol norvaline as well as 400 µL chloroform added to each sample. For the metabolite extraction, samples were vortexed for

5 min on ice, spun down, and the aqueous layer transferred into a glass vial and dried. Metabolites were resuspended in 70% ACN, and 5 µL sample loaded onto a Phenomenex Luna 3u NH2 100A (150 x 2.0 mm) column. The chromatographic separation was performed on an UltiMate 3000RSLC (Thermo Scientific) with mobile phases A (5 mM NH4AcO, pH 9.9) and B (ACN) and a flow rate of 300 µL/ min. The gradient ran from 15% A to 95% A over 18 min, 9 min isocratic at 95% A, and re-equilibration for 7 min. Metabolite detection was achieved with a Thermo Scientific Q Exactive mass spectrometer run in polarity switching mode (+3.0 kV / −2.25 kV). TraceFinder 3.1 (Thermo Scientific) was used to quantify metabolites as area under the curve using retention time and accurate mass measurements (≤ 3 ppm). Relative amounts of metabolites were calculated by summing up all isotopomers of a given metabolite and were normalized to internal standard and cell number. Natural occurring ^{13}C was accounted for as described in (Yuan et al., 2008).

Cell Culture

H9C2 cells were cultured in glucose-free DMEM (Life technologies, 11966-025) supplemented with 10% fetal bovine serum (FBS) and 10 mM glucose. H9C2 cells were cultured at 37°C and 5% CO2. Cells were transfected with indicated siRNA using DharmaFECT 1 Transfection Reagent by following the manufacturer's instructions. Knockdown efficiency was confirmed by Western blotting.

RNAi in *C. elegans*

RNAi in C. elegans was accomplished by feeding worms HT115 (DE3) bacteria expressing target-gene double-stranded RNA (dsRNA) from the pL4440 vector. dsRNA production was

induced overnight on plates containing 1 mM isopropyl-b-D-thiogalactoside (IPTG). All RNAi feeding clones were obtained from the *C. elegans* ORF-RNAi Library (Thermo Scientific/Open Biosystems) unless otherwise stated. In lifespan experiments, we used RNAi to inactivate AAK-2, UBL-5 and PDHB-1 in mature animals in the presence or absence of exogenous a-KB. The concentration of a-KB used in these experiments (4 mM) was empirically determined to be most beneficial for wild-type animals (Figure 1C).

Assay for AMPK pathway activity in *C. elegans*

Wild-type N2 were grown at 20 °C from the L1 stage until L4. L4 worms were transferred onto NGM plates (55-mm diameter) with vehicle (water), 4mM α-KB, pdhb-1 RANi bacteria. After one-day treatment, adult worms were washed from three plates using M9 buffer, followed by centrifuging at 1400 rpm for 1 min. After removing the supernatant, the worms were frozen in ~ 25 µl M9 buffer quickly in liquid nitrogen. Then the worm samples were stored at −80 °C. Before western blotting analysis, worms were thaw on ice and mixed with 2× sample loading buffer (50 mM Tris-Cl, pH 6.8, 2 mM EDTA, 4% glycerol, 4% SDS, bromophenol blue, 1X PIC) and sonicated at 50 sonics at 40 °C for 3 min and then boiled at 95 °C for 6 min. Cool samples on ice before load in 4-12% Bis-Tris gel. AMPK pathway activity in C. elegans treated with α-KB or pdhb-1 knockdown was determined by the levels of phosphorylation of AMPK (T172) [6]. Specific antibodies used: P-AMPKα T172 (Cell Signaling, 2535S), α-Tubulin (Sigma, T6199).

Assay for AMPK and mammalian TOR (mTOR) pathway activity

AMPK and mTOR pathway activity in cells treated with α-KB was determined by the levels of phosphorylation of AMPK (T172), AAC (S79), and S6K (T389). Specific antibodies used:

phospho (P)-S6K T389 (Cell Signaling, 9234), S6K (Cell Signaling, 9202S), P-AMPKα T172 (Cell Signaling, 2535S), AMPKα (Cell Signaling, 2532S), P-ACC S79 (Cell Signaling, 3661S), ACC (Cell Signaling, 3662S), GAPDH (Santa Cruz Biotechnology, 25778), DLAT (Thermofisher, PA5-29043), DLD (Thermofisher, PA5-27364), P-PDHA (Novus, NB110-93479), LDHA(Cell Signaling, 2012S), LDHB(Abcam, ab53292), PC(Abcam, ab126707), PKM1/2(Cell Signaling, 3186s), and PDHA (Cell Signaling, 2784S).

Assay for cellular growth

H9C2 cells were seeded in 96-well plates at 2 x 10^3 cells per well and treated with indicated compound for 2 day. Cell number was measured using the CellTiter-Glo luminescent ATP assay (Promega, G7572); luminescence was read using Analyst HT (Molecular Devices).

Assay for NAD^+/NADH

NAD^+/NADH level is measured by NAD/NADH-Glo™ Assay (Promega, G9071) with adapted protocol as described [4].

Isotopomer enrichment modeling

Isotopomer enrichment modeling was performed as described[7].

Supplemental References

1 Robinson, M. M. *et al.* Novel mechanism of inhibition of rat kidney-type glutaminase by bis-2-(5-phenylacetamido-1,2,4-thiadiazol-2-yl)ethyl sulfide (BPTES). *Biochem J* **406**, 407-414, doi:10.1042/BJ20070039 (2007).

2 Chin, R. M. *et al.* The metabolite alpha-ketoglutarate extends lifespan by inhibiting ATP synthase and TOR. *Nature* **510**, 397-401, doi:10.1038/nature13264 (2014).

3 McColl, G. *et al.* Utility of an improved model of amyloid-beta (Abeta(1)(-)(4)(2)) toxicity in Caenorhabditis elegans for drug screening for Alzheimer's disease. *Mol Neurodegener* **7**, 57, doi:10.1186/1750-1326-7-57 (2012).

4 Sullivan, L. B. *et al.* Supporting Aspartate Biosynthesis Is an Essential Function of Respiration in Proliferating Cells. *Cell* **162**, 552-563, doi:10.1016/j.cell.2015.07.017 (2015).

5 Hinman, L. M. & Blass, J. P. An NADH-linked spectrophotometric assay for pyruvate dehydrogenase complex in crude tissue homogenates. *J Biol Chem* **256**, 6583-6586 (1981).

6 Lee, H. *et al.* The Caenorhabditis elegans AMP-activated protein kinase AAK-2 is phosphorylated by LKB1 and is required for resistance to oxidative stress and for normal motility and foraging behavior. *J Biol Chem* **283**, 14988-14993, doi:10.1074/jbc.M709115200 (2008).

7 Williams, K. J. *et al.* An essential requirement for the SCAP/SREBP signaling axis to protect cancer cells from lipotoxicity. *Cancer Res* **73**, 2850-2862, doi:10.1158/0008-5472.CAN-13-0382-T (2013).

CHAPTER 5

Conclusions

This dissertation has presented several novel endogenous longevity compounds, including α-ketoglutarate (α-KG)[1], 2-hydroxyglutarate (2-HG)[2], and α-ketobutyrate (α-KB). To explore the anti-aging mechanisms of these compounds, we combined analyses of target identification[3], metabolomics, bioenergetics, as well as epistasis using both *C. elegans* and mammalian cells. These approaches allowed us to identify and validate the functional targets and downstream metabolic signaling pathways acted upon by of these compounds.

We first discovered that α-KG is a novel and potent longevity compound. By applying DARTS (drug affinity response target stability)[3], we identified ATP5B, a subunit of the F1 component of ATP synthase, as a novel target for this metabolite. The inhibitory effect of α-KG on ATP synthase was further validated in purified enzyme activity assays, cells, and *C. elegans*. We next found that TOR is a downstream signaling target for the longevity effects of α-KG. It is likely that α-KG inhibits TOR through ATP synthase inhibition, as TOR signaling is modulated by energy metabolism and is inhibited upon dietary restriction (DR). Interestingly, we found that the longevity effect of α-KG overlaps with DR and endogenous α-KG accumulates upon DR in *C. elegans*. Consistently, a recent study reported that α-KG accumulates in starved mice[4]. These results suggest that α-KG may serve as a bridge signaling to connect DR, TOR, and lifespan extension.

2-HG is a well-known oncometabolite that becomes accumulated in IDH mutant tumors and facilitates tumor transformation[5]. Unexpectedly, we discovered that 2-HG, similar to α-KG,

extends lifespan in *C. elegans* via inhibition of 2-HG ATP synthase and TOR. The inhibitory effect of 2-HG on ATP synthase causes a bioenergetics deficiency in IDH mutant cells and inhibits cellular growth. Importantly, 2-HG accumulation makes these cells highly sensitive to glucose deprivation, which may be exploited by metabolic intervention for IDH mutant tumors.

Finally, we present one additional longevity metabolite, α-KB. As a competitive alternative substrate of pyruvate dehydrogenase, the metabolite α-KB specifically interrupts complex I-dependent respiration, rewires pyruvate metabolism, activates AMPK signaling, and extends lifespan in *C. elegans*. Importantly, we found that α-KB delays the onset of paralysis induced by proteotoxic stress, indicating that α-KB could potentially be useful as a treatment for neurodegeneration. This study provides an example of the profound effects that endogenous alternative substrates for key metabolic enzymes can exert on metabolism and downstream signaling pathways. There is an abundance of metabolites that can serve as alternative substrates to various enzymes, and their biological significance has not been fully studied. It will be interesting to further explore their potential effects in aging and aging-related symptoms, as well as other physiological processes and diseases.

Our results build upon previous studies indicate that metabolites are not merely substrates for enzymes but can also serve as pivotal signaling metabolites that regulate various physiological processes and influence cellular and organismal health. Consistently, there is increasing evidence showing that metabolites play crucial roles in diseases and aging[1,6-8]. The development of metabolomics and target identification techniques has enabled accurate mechanistic studies on metabolites and revealed unappreciated biological networks acted on by metabolites. The longevity effects of metabolites are not likely to be fortuitous. Indeed, our results and results from other groups indicate that α-KG accumulates upon dietary restriction[1,4] and may serve as an endogenous signal for starvation stress. Together these results suggest

that it is possible to identify novel endogenous pathways to counteract detrimental effects of aging.

The elderly population has been continually increasing globally, and society desperately needs new means of tackling the burdens of aging and aging-related diseases[9]. Pharmacological perturbation of aging is one of the best strategies for us to improve the life quality of the older population. However, safety issues have largely impeded the development of anti-aging compounds. For instance, long-term treatment of rapamycin, a compound with proven longevity-promoting activity in mice, causes unexpected side effects, including hyperlipidemia, in patients[10]. Moreover, rapamycin's activity as an immune suppressant could also be detrimental to older individuals with an already weakened immune system, potentially making them more susceptible to cancer and infectious diseases. Our studies have uncovered several prominent candidates for anti-aging drug development. We speculate that these compounds are safe to be used as supplements as they are endogenous metabolites unlikely to be toxic at the does necessary for anti-aging activity, and α-KG already has a history of use as a supplement in humans. Although we have only tested the longevity effects of these compounds in *C. elegans*, their pro-longevity activities are likely to also benefit humans as the mechanisms by which they extend lifespan are conserved in mammals and we have validated their molecular bioactivities and mechanisms in human cell lines. Notably, our studies indicate that these longevity compounds may be exploited as intervention for aging-related symptoms. For instance, we and other groups have shown that α-KG inhibits tumor cell growth, interrupts tumor angiogenesis in xenograft cancer models[2,11,12], and decreases the arterial stiffening which occurs in aged mice[13].

The goal of aging research is to discover and develop safe and potent compounds as interventions for aging and aging-related diseases. To fulfill this aim, we and other researchers will continue to identify novel anti-aging metabolites, explore the effects of longevity compounds

in aging-related symptoms, as well as test combination effects of these novel longevity compounds for delaying aging and the prevention and treatment of age-related diseases.

References

1 Chin, R. M. *et al.* The metabolite alpha-ketoglutarate extends lifespan by inhibiting ATP synthase and TOR. *Nature* **510**, 397-401, doi:10.1038/nature13264 (2014).

2 Fu, X. *et al.* 2-Hydroxyglutarate Inhibits ATP Synthase and mTOR Signaling. *Cell Metab* **22**, 508-515, doi:10.1016/j.cmet.2015.06.009 (2015).

3 Lomenick, B. *et al.* Target identification using drug affinity responsive target stability (DARTS). *P Natl Acad Sci USA* **106**, 21984-21989, doi:10.1073/pnas.0910040106 (2009).

4 Lin, A. L., Zhang, W., Gao, X. & Watts, L. Caloric restriction increases ketone bodies metabolism and preserves blood flow in aging brain. *Neurobiol Aging* **36**, 2296-2303, doi:10.1016/j.neurobiolaging.2015.03.012 (2015).

5 L, M. G., Boulay, K., Topisirovic, I., Huot, M. E. & Mallette, F. A. Oncogenic Activities of IDH1/2 Mutations: From Epigenetics to Cellular Signaling. *Trends Cell Biol*, doi:10.1016/j.tcb.2017.06.002 (2017).

6 Flavahan, W. A. *et al.* Insulator dysfunction and oncogene activation in IDH mutant gliomas. *Nature* **529**, 110-114, doi:10.1038/nature16490 (2016).

7 Chouchani, E. T. *et al.* Ischaemic accumulation of succinate controls reperfusion injury through mitochondrial ROS. *Nature* **515**, 431-435, doi:10.1038/nature13909 (2014).

8 Mouchiroud, L. *et al.* The NAD(+)/Sirtuin Pathway Modulates Longevity through Activation of Mitochondrial UPR and FOXO Signaling. *Cell* **154**, 430-441, doi:10.1016/j.cell.2013.06.016 (2013).

9 de Cabo, R., Carmona-Gutierrez, D., Bernier, M., Hall, M. N. & Madeo, F. The search for antiaging interventions: from elixirs to fasting regimens. *Cell* **157**, 1515-1526, doi:10.1016/j.cell.2014.05.031 (2014).

10 Sarbassov, D. D. *et al.* Prolonged rapamycin treatment inhibits mTORC2 assembly and Akt/PKB. *Mol Cell* **22**, 159-168, doi:10.1016/j.molcel.2006.03.029 (2006).

11 Matsumoto, K. *et al.* Antitumor effects of 2-oxoglutarate through inhibition of angiogenesis in a murine tumor model. *Cancer Sci* **100**, 1639-1647, doi:10.1111/j.1349-7006.2009.01249.x (2009).

12 Tennant, D. A. & Gottlieb, E. HIF prolyl hydroxylase-3 mediates alpha-ketoglutarate-induced apoptosis and tumor suppression. *J Mol Med (Berl)* **88**, 839-849, doi:10.1007/s00109-010-0627-0 (2010).

13 Niemiec, T. *et al.* Alpha-ketoglutarate stabilizes redox homeostasis and improves arterial elasticity in aged mice. *J Physiol Pharmacol* **62**, 37-43 (2011).